Electromagnetic form factors of hadrons

by

Vaughn Stephen Zidell

A Dissertation Submitted to the

Graduate Faculty in Partial Fulfillment of

The Requirements for the Degree of

DOCTOR OF PHILOSOPHY

Department: Physics
Major: Elementary Particle Physics

Approved:

Signature was redacted for privacy.

In Charge of Major Work

Signature was redacted for privacy.

For the Major Department

Signature was redacted for privacy.

For the Graduate College

Iowa State University
Ames, Iowa

1975

TABLE OF CONTENTS

I. INTRODUCTION

The Dirac theory of the spin 1/2 point-particle predicts that the electron should possess a magnetic moment of magnitude $e\hbar/2m_e c$. Actual measurements reveal a tiny discrepancy on the order of $\alpha/2\pi$, where $\alpha=1/137.036$ is the fine structure constant. This deviation from Dirac point-particle behaviour is accounted for in the context of quantum electrodynamics by higher-order processes involving the emission and reabsorption of virtual photons by the bare electron. These virtual photons are imagined to form a sort of cloud around the bare electron and consequently to generate its spatial structure. Measurements suggest (1) that this structure extends into space a distance on the order of one-hundredth of a fermi. For all practical purposes, then, an electron can be treated as a structureless Dirac point-particle.

For hadrons the situation is quite different. For example, the proton's total magnetic moment, $(e\hbar/2m_p c)(1+\mu_p)$, includes an anomalous part, $\mu_p=1.792782$, giving rise to a contribution on the order of the Dirac moment itself. Such a large deviation cannot be considered the result of corrections of order $\alpha/2\pi$. Equally mysterious from the standpoint of pure quantum electrodynamics is the neutron. According to this theory a neutral point-particle has no magnetic moment. However, measurements of the neutron's magnetic dipole moment in nuclear magnetic resonance experiments have shown its value to be $(e\hbar/2m_n c)\mu_n$, where $\mu_n=-1.913148$ is the anomalous magnetic moment of the neutron.

The earliest explanation of this discrepancy from Dirac point-particle behaviour was given by pseudoscalar meson field theory (2). The idea is that a virtual photon used to probe the proton structure can interact with both the bare Dirac proton and with the cloud of virtual, strongly interacting mesons which presumably are being continuously emitted and reabsorbed by the proton. This cloud is assumed to produce a complicated distribution of charge and current density which increases the proton's intrinsic magnetic moment above the value, $e\hbar/2m_p c$, expected on the basis of Dirac theory.

The first experiments to detect the existence of such an extended structure in the proton were made by Hofstadter et al. (3). Calculations of the proton's structure based on the meson model, however, have led only to qualitative success in understanding Hofstadter's results. Neither the anomalous moment of the radius of the proton has been satisfactorily explained (4).

Since fundamental theories for the interaction of mesons and nucleons have not yet led to reliable, self-consistent quantitative calculations of electromagnetic structure, information about the structure of the hadron is obtained from the phenomenological analysis of two types of experiments:

(1.) Electron-hadron elastic scattering,

(2.) Electron-positron annhilation into hadron-antihadron pairs.

Hofstadter's experiment, electron-proton elastic scattering, is an example of the first of these experiments, and pion pair production in electron-positron colliding beam experiments is an example of the second type. The relevant kinematical variable for both of these processes

is the four-momentum transfer, q, which can be either a space-like ($q^2>0$) or a time-like ($q^2<0$) Lorentz four-vector depending on which channel the interaction occurs in.

In the case of electron-proton scattering only two functions of space-like q^2 are required to completely characterize the process in the one-photon-exchange limit (i.e., in the case where only a single virtual photon is exchanged between the electron and proton). These are called the electric (E) and magnetic (M) form factors of the proton (p), $G_E^p(q^2)$ and $G_M^p(q^2)$, respectively. The experimental data describing the momentum space distribution of the proton charge and magnetization density are summarized by the dipole law,

$$G_E^p(q^2) = [1 + (q^2/0.71)]^{-2}, \tag{1.1}$$

and the form factor scaling law,

$$G_M^p(q^2) = (1 + \mu_p)G_E^p(q^2). \tag{1.2}$$

The dipole law receives its name from the existence of the double pole at $q^2=-0.71$ $(GeV/c)^2$, and the scaling law from the constant ratio of the form factors from which one may be obtained by scaling the other. As discussed in Appendix A, the Fourier transforms of these functions are related to the charge and magnetization density of the proton in coordinate space. In this sense, the dipole and scaling laws suggest that the charge and magnetic moment density of the proton fall off exponentially with distance. Furthermore, the asymptotic behaviour

of the form factors suggests that the proton is a composite, not an elementary particle (see Appendix A for a further discussion of these points).

In the case of electron-positron annhilation into a charged pion-antipion pair, the spinless nature of the pion requires only a single form factor for a complete description of its electromagnetic structure. Since $q^2<0$, this is a time-like form factor. The experimental data indicates the existence of a distinct Breit-Wigner-like resonance peak in the form factor at a fairly definite value of q^2. In the vicinity of this peak the pion form factor, $f^{\gamma\pi}(q^2)$, is well-described by the function

$$|f^{\gamma\pi}(q^2)|^2 = \frac{m_\rho^2}{(q^2+m_\rho^2)^2 + m_\rho^2\Gamma_\rho^2},$$

where m_ρ^2 is the (mass)^2 of the ρ meson and Γ_ρ its width. The exact manner in which this meson comes into the picture will be discussed later in connection with the vector meson dominance model.

The standard theoretical approach to the problem of electromagnetic structure begins with dispersion relations (5). Let $G(q^2)$ be the charge form factor of a given hadron, H, and let μ represent the threshold of the least massive channel into which H can decay. In the dispersion theory treatment, $G(q^2)$ is assumed to be analytic everywhere in the complex q^2-plane except for simple poles on the unphysical sheet and along a branch cut from $-\mu^2$ to $-\infty$. If it is also assumed that $G(q^2)$

vanishes as $|q^2| \to \infty$, then as a consequence of these conditions, $G(q^2)$ must satisfy an unsubtracted dispersion relation,

$$G(q^2) = \frac{1}{\pi} \int_{-\mu^2}^{-\infty} \frac{\mathrm{Im}[G(s^2)]}{q^2 - s^2} \, ds^2, \tag{1.3}$$

which defines the form factor uniquely in terms of an integral over the spectral function, $\mathrm{Im}[G(s^2)]$ (6). The integration variable, s^2, represents the $(\text{mass})^2$ of the various intermediate states through which the photon-hadron interaction occurs.

The spectral function is calculated using the unitarity property of the S-matrix. The calculation shows that it may be written as a sum over all the strongly-interacting intermediate states consistent with energy-momentum conservation and the conserved quantum numbers of the strong interaction. The determination of the spectral function thus requires a complete knowledge of all the basic interactions mediating the electron-hadron scattering process. This is a formidible problem as the number of such states is unlimited.

Using experimental data it is possible to at least place constraints on the functional form of the spectral function. First of all, the form factor is normalized at $q^2=0$ to the charge of the hadron, Q_H. So there exists the sum rule

$$Q_H = \frac{1}{\pi} \int_{-\mu^2}^{-\infty} \frac{\mathrm{Im}[G(s^2)]}{-s^2} \, ds^2.$$

Secondly, the dipole law, Eq. (1.1), indicates that the form factors of the nucleon decrease at least as fast as q^{-4} for large q^2. This condition may be imposed on Eq. (1.3) by using the identity

$$\frac{1}{q^2-s^2} = \frac{1}{q^2} - \frac{s^2}{q^2(q^2-s^2)}$$

with the result that

$$G(q^2) = \frac{1}{\pi}\int_{-\mu^2}^{-\infty} \frac{\mathrm{Im}[G(s^2)]}{q^2}\, ds^2 + \frac{1}{\pi}\int_{-\mu^2}^{-\infty} \frac{s^2\mathrm{Im}[G(s^2)]}{q^2(q^2-s^2)}\, ds^2. \qquad (1.4)$$

Now, if an asymptotic behaviour of the form

$$\lim_{q^2\to\infty} q^4 G(q^2) = 0$$

is imposed, then from Eq. (1.4) there follows the two "dispersion sum rules" (7),

$$\int_{-\mu^2}^{-\infty} \mathrm{Im}[G(s^2)]ds^2 = 0,$$

$$\int_{-\mu^2}^{-\infty} s^2\mathrm{Im}[G(s^2)]ds^2 = 0, \qquad (1.5)$$

both of which place mathematical limitations on the form of $\mathrm{Im}[G(s^2)]$.

More generally, if the form factor goes to zero more rapidly than the dipole, then

$$\lim_{q^2\to\infty} q^{2n}G(q^2) = 0$$

implies the set of sum rules,

$$\int_{-\mu^2}^{-\infty} s^{2N-2}\,\mathrm{Im}[G(s^2)]\,ds^2 = 0;\ N=1,2,3,\ldots n. \qquad (1.6)$$

To go further in the analysis the assumption of vector meson dominance (8) is usually made. This is a model for photon-hadron interactions in which it is assumed that the photon couples dominantly only to neutral vector mesons bearing the same quantum numbers, $J^{PC}=1^{--}$, as the photon and that the vector mesons in turn interact strongly with the hadron (the experimental values of the masses, widths, thresholds and photon-couplings of these vector mesons are given in Table 1). The simplicity of the vector dominance model is due to the assumption that the unstable vector meson states dominate the photon-hadron interaction; that is, that uncorrelated pions, kaons, nucleon-antinucleon pairs, etc., make only negligible contributions to the intermediate states. Mathematically this assumption means that the vector meson singularities of $\mathrm{Im}[G(s^2)]$ should dominate the form factor. In electron scattering experiments, the form factors are required for $q^2>0$, which is presumably

Table 1. Experimental Data on the Neutral Vector Mesons

	Mass[a]	Width	Threshold	γ_V
ρ	0.770 ±0.010	0.150 ±0.010	0.27914	2.6±0.2
ω	0.7827±0.0006	0.010 ±0.004	0.41410	7.7±0.8
ϕ	1.0197±0.0003	0.0042±0.0002	0.98741	6.2±0.9
ρ'	1.6	0.4	0.5582	5.2
ψ	3.105 ±0.003	$\leq$0.0019		
ψ'	3.695 ±0.004	$\leq$0.0027		

[a]Mass, width and threshold are in units of GeV.

far enough from the vector meson resonance peaks to allow them to be approximated by a delta function,

$$\mathrm{Im}[G(s^2)] = \pi \sum_V a_{VH} \delta(s^2 + m_V^2),$$

where a_{VH} is a coupling constant and m_V the mass of the vector meson, V. The sum is over the established vector meson resonances, ρ, ω, and ϕ. A ρ' may also be present, but the resonance interpretation of the relevant data is still uncertain.

This approximation amounts to ignoring the width of the vector mesons and the cut structure of the integrand of Eq. (1.3); that is, the vector mesons are treated as stable rather than unstable particles. As a result of this approximation the dispersion integral simplifies to the so-called monopole form for the electromagnetic form factors,

$$G(q^2) = \sum_V \frac{a_{VH}}{q^2 + m_V^2}. \tag{1.7}$$

The electromagnetic form factor may be broken up into a part receiving contributions from only the isovector vector mesons,

$$G^V(q^2) = \frac{a_{\rho H}}{q^2 + m_\rho^2},$$

since the ρ is the only established isovector vector-meson which couples to the photon (that is, the ρ meson is a member of an isospin triplet),

and a part receiving contributions from only the isoscalar vector mesons,

$$G^S(q^2) = \frac{a_{\omega H}}{q^2 + m_\omega^2} + \frac{a_{\phi H}}{q^2 + m_\phi^2} .$$

Experimentally, it is known that both obey a q^{-4} dependence at high q^2. The sum rules given in Eqs. (1.5) then take the form

$$\begin{aligned} &a_{\omega H} + a_{\phi H} = 0, \\ &a_{\rho H} = 0, \\ &m_\omega^2 a_{\omega H} + m_\phi^2 a_{\phi H} = 0, \\ &m_\rho^2 a_{\rho H} = 0. \end{aligned} \tag{1.8}$$

Since the ρ, ω, and ϕ differ in mass, these sum rules imply $a_{\rho H}=a_{\omega H}=a_{\phi H}=0$, which contradicts the experimental evidence for the existence of non-zero vector meson-hadron couplings.

Attempts to fit the nucleon form factor data using just ρ, ω, and ϕ dominance and monopole propagators (9) have led to good fits to the low energy data at the expense of requiring the ρ mass to be at least 200 MeV smaller than its measured value in leptonic decays. Even when core terms are added as adjustable parameters a good fit using the observed masses of the vector mesons in Eq. (1.7) has never been achieved. As expected from the sum rules, the problem is aggravated at high q^2 due to the rapid fall-off of the data. Monopole propagators

therefore can only be regarded as phenomenological representations of the data. The mass and coupling parameters occurring in the theory cannot be identified with the real masses and couplings of the vector mesons.

For the time-like electromagnetic form factors Eq. (1.7) is usually modified to give a Breit-Wigner resonance at each vector meson mass. In the small-width approximation, $\Gamma_V << m_V$, the electromagnetic form factor becomes

$$G(q^2) = \sum_V \frac{m_V^2}{q^2 + m_V^2 - i m_V \Gamma_V}$$

and gives a good representation of the data for time-like q^2 in the region of the vector meson resonance peaks. However, in addition to being an approximation around the vector meson pole, the Breit-Wigner propagator is defective because it produces poles on all sheets of the scattering amplitude and because the pole position is unrelated to the resonance width. Thus it gives no insight into the dynamical origin of the resonance.

As a consequence of the apparent failure of vector meson dominance in the space-like region, the monopole model has been amended by several authors. It is important to discuss some of these modifications and their success and failure in fitting the nucleon and pseudoscalar form factor data. These modifications fall into five classes:

(1.) Extended Vector Meson Dominance: In addition to the ρ, ω, and ϕ, contributions from additional higher vector mesons like the ρ'

are required. These will modify the sum rule for the isovector couplings and presumably eliminate the contradiction posed by Eq. (1.8). Attempts to fit the data utilize the monopole propagators and treat the mass and couplings of the ρ' as adjustable parameters. The general result (10) has been that a good four-pole fit, with or without core terms and using the experimental ρ, ω, and ϕ masses requires a ρ' mass on the order of 900 MeV. No ρ' has ever been observed in this region. Chan et al. (9), however, have obtained a fair fit to the data (χ^2_F=1.8) in the momentum transfer region less than 1 $(GeV/c)^2$ using a ρ' mass of 1.2 GeV. Such a ρ' may be identified with an $\omega\pi$ enhancement detected in some experiments. Even so, extensions to higher q^2 have resulted in a rapidly deteriorating fit.

(2.) Pole dominance is wrong and contributions from the continuum are needed. In the time-like region it is to be expected that vector meson dominance works well because of the obvious resonances which dominate any continuum background. But why a pole on the unphysical sheet should dominate the dispersion integral in the space-like region is a mystery. There is no a priori justification for vector meson dominance, according to this philosophy, it is merely a simplicity assumption.

Core terms have been included in the three and four-pole fits (11) in order to simulate a continuum contribution. These core terms, though tiny, are crucial to the fit and violate the observed asymptotic dipole behaviour of the form factor. Ball and Parkinson (12) have included contributions from the closed decay channels of the ρ. The resonance

is represented by a relativistic generalization of the Breit-Wigner propagator based on the Frazer-Fulco ansatz. They found that the $N\bar{N}$ state is dominant and that the $\pi\pi$ state is the smallest contribution, leading them to the conclusion that ρ-dominance is not sufficient to explain the nucleon isovector form factor. Other models (13) have been proposed that include corrections to simple pole dominance due to the non-resonant structure, but have not yet been shown to give good agreement with the data.

(3.) Pole dominance is wrong because additional form factors come into the problem. The vector meson-nucleon coupling constants, a_{VH}, have been allowed a monopole momentum dependence (14) designed to simulate dipole-like behaviour when the monopole propagators are retained for the vector meson pieces. Massam and Zichichi (15) use, in addition to a monopole momentum dependence for a_{VH}, SU(3) symmetry and its breaking to relate the various coupling constants and make a one parameter fit to the nucleon form factor data. Their final chi-square per degree of freedom, χ^2_F, is 4.0, so the fit is not satisfactory.

In the vector meson dominance field theory of Kroll, Lee and Zumino (16), the form factors are predicted to obey the form

$$G(q^2) = \sum_V \frac{a_{VH}(q^2)}{q^2 + m_V^2},$$

where $a_{VH}(q^2)$ is proportional to the strong form factor of the vector meson. This obviously allows for a more complicated q^2-dependence, but the a_{VH} cannot be calculated from the theory. Ng (17) has made a

fit to the form factor data using the theory of Kroll, Lee and Zumino and assuming that the vector meson-nucleon vertices obey a monopole momentum dependence. A fit to all the nucleon form factor data over a momentum region up to 4 $(GeV/c)^2$ gave χ^2_F=1.5 for a four parameter fit. However, the assumptions made about the momentum dependence of the strong vector meson-nucleon couplings are thoroughly ad hoc.

A priori it is possible that, in a quark model description, the extra q^2-dependence could come from the vector meson-quark-quark coupling and/or from the spatial extension of the bound state quark wave function (18). However, more knowledge of quark dynamics is necessary before such a hypothesis can be given substance. The implications for the existence of the dipole ρ meson as they relate to the nucleon form factor data have been discussed by Krepps and Moffat (19).

(4.) Generalized Vector Meson Dominance: An arbitrarily large number of higher vector mesons have been included in Veneziano model descriptions (20). In these models the cut in the form factor is approximated by an infinite set of equally spaced poles associated with Regge recurrences on a linearly rising Regge trajectory. These give good "eyeball fits" to selected form factors, but no analysis for all the nucleon form factors has been made. Jengo and Remiddi (21) considered contributions from three recurrences of the ρ-trajectory and found a good eyeball fit to $G_M^p(q^2)$ alone. However, a good fit to a selected form factor is always possible when enough arbitrary parameters are introduced. The authors ignored finite-width effects and contributions from the ω and ϕ, making the analysis quite weak.

(5.) Vector meson dominance with ρ, ω, and ϕ contributions works if the vector meson propagator and the vector meson-nucleon vertex are constructed with the correct analytic properties. Many attempts have been made, nearly all of them have been ad hoc in one way or another. One such attempt (22) involved the use of the relativistic S-wave Breit-Wigner parametrization to obtain

$$G(q^2) = \sum_V \frac{m_V^2}{q^2 + m_V^2 + \Gamma_V \sqrt{q^2 + m_V^2}}$$

with a square-root function to represent the elastic cut in the propagator. Though this propagator has the correct analytic behaviour in that it satisfies a dispersion relation, possesses a resonance at $q^2=-m_V^2$ and yields good eyeball fits to the data, it is not suitable for a description of the ρ meson, for example, because the resonant $\pi\pi$ system forming the ρ meson interacts in a P-wave, not an S-wave, state. Thus the S-wave Breit-Wigner gives rise to a $\pi\pi$ phase shift possessing the wrong threshold behaviour.

Deo and Parida (23) have fit G_M^p using the N/D method of Chew and Mandelstam (24). The P-wave structure of the partial wave amplitudes arising in the dispersion relation method were parametrized using an effective-range formula. The resulting fit, though good, depended on their being a large number of free parameters and on the relative lack of constraint in fitting only one of the four nucleon form factors.

In an attempt to avoid the use of hypothetical higher vector mesons and capitalize on the use of unitarity and analyticity, Renard (25)

constructed propagators including contributions from the inelastic channels that couple to the ρ. These channels give cusp-like effects at their thresholds that simulate the bumps attributed to the higher vector mesons. Renard is able to fit all the data reasonably well (no χ^2 is reported) including the high energy pion and kaon data. The drawbacks to his approach lie in the arbitrary choice he makes for the structure functions and in the ad hoc momentum dependence of the vector meson-nucleon couplings.

None of these modifications of the monopole model is widely accepted due to their arbitrariness. The purpose of this work is to construct a phenomenological model of hadronic form factors based on vector meson dominance and on an unstable particle field theory. The unstable vector meson propagators used in the analysis possess the correct analytic properties to enable a representation of unstable particles; i.e., poles only on the unphysical sheet and a branch cut on the real axis. Furthermore, the resonance width or total decay rate is connected to a function characterizing the dynamical nature of the resonance. This model is then compared to the experimental data on pion, kaon and nucleon electromagnetic form factors, and used to make predictions where experimental data is presently lacking.

In Chapter II the space-like electromagnetic form factors are defined, a model for them constructed, and fits made to the low-energy nucleon, pion and kaon data are analyzed. Unlike fits using monopole propagators, only the ρ, ω, and ϕ are required to achieve a good χ^2 fit to the data. At higher energies a contribution from a heavy isovector-vector meson

is utilized. An interpretation of this meson in terms of known resonances is made. The theory is very sensitive to the mass and half-width of the vector mesons, and these values are close to their experimental counterparts. In addition, the vector meson-nucleon coupling constants determined by this fit satisfy sum rules implying that there exists no direct photon-nucleon coupling. By a χ^2 criterion, the data fits are much better than those obtained using stable particle propagators, suggesting that the instability of the vector mesons is crucial and reinforcing the validity of the vector meson dominance model in the space-like region.

Also in this chapter, the pion and kaon space-like form factors are predicted on the basis of fits to the nucleon data using vector meson universality. The radii of the pion, kaon, and nucleon are calculated and found to be slightly larger than the accepted values.

In Chapter III the time-like electromagnetic form factors are defined. These are obtained by analytic continuation of q^2 from the space-like region. There is no other attempt in the literature to describe the space and time-like electromagnetic form factors of the pion, kaon and nucleon simultaneously with the same set of three vector meson propagators. Good fits to the low-energy pion form factor are obtained only if ρ-ω mixing is included. The fits demonstrate that within the present accuracy of the experimental data, the ρ couples universally to the pion and nucleon so that the identification $f^{\gamma\pi}=2f_1^V$ can be made. Good fits to both the low and high energy pion and kaon form factor data require a contribution from a heavy ρ meson which can easily be

identified with the experimental ρ' at 1.6±0.2 GeV. Furthermore, it is found that the vector meson-pion and vector meson-kaon couplings obey sum rules that suggest there exists no direct photon-pion or photon-kaon interaction.

The pion charge radius calculated on the basis of fits to the pion form factor data give a large value with respect to the accepted value. This discrepancy can be traced to the anomalous threshold behaviour due to the cut structure of the model propagator used in the analysis. When this propagator is modified to incorporate the correct P-wave threshold behaviour, the radius predicted on the basis of a fit to the pion form factor is 0.75±0.05 f., in excellent agreement with the recent controversial result from $e\pi$ scattering: 0.78±0.10 f. However, the P-wave $\pi\pi$ phase shift calculated using the theoretical form factor lies outside the error bars of the data. The disagreement is especially acute at the inelastic threshold, $18\pm3^{\circ}$ compared to $11\pm5^{\circ}$, given by experiment. This suggests that some other mechanism other than vector meson instability may be needed to consistently account for the large pion charge radius. Possibilities include structure in the $\rho\pi\pi$ vertex, contributions from inelastic channels, etc.

Appendix A contains a discussion of the physical interpretation of the electromagnetic form factors as charge and magnetic moment distributions in coordinate space. In Appendix B the theoretical basis for vector meson universality is discussed. Appendices C and D contain a discussion of the initial values of a propagator function, $I_V(q^2)$, and its initial derivatives, and of the computer programs used in the

analysis, respectively. Appendix E contains a brief discussion of work in progress concerning an attempt to modify the vector meson propagator to include structure in the $\rho\pi\pi$ vertex. The work is concluded with a comprehensive bibliography, references (1-166).

II. SPACE-LIKE ELECTROMAGNETIC FORM FACTORS

This chapter begins with a definition of the electromagnetic form factors of hadrons defined for space-like values of the four-momentum transfer. This definition is necessary since an elementary particle may possess strong, weak and gravitational form factors due to its interaction with the corresponding fields, as well as electromagnetic form factors due to its interaction with photons. The experimental methods for measuring these form factors and a discussion of the limits of validity of the form factor data is given in Section B. A vector meson dominance theory of space-like form factors is described in Section C which is based upon propagators possessing analytic properties capable of representing unstable vector mesons. Finally, in Section D the space-like electromagnetic form factors for the proton, neutron, pion and kaon are analyzed using this model and the results are discussed.

A. Definition

Consider a single virtual photon which interacts with a hadron, H, of spin S. In terms of a Feynman graph this process is represented by Fig. 1. In this figure $p=(\bar{p},iE)$ is the incident and $p'=(\bar{p}',iE')$ the final four-momentum of the hadron. Four-momentum is conserved at the photon-hadron vertex so the four momentum carried by the photon is

$$q = p' - p$$

$$q^2 = -(E' - E)^2 + (\bar{p}' - \bar{p})^2 \geq 0.$$

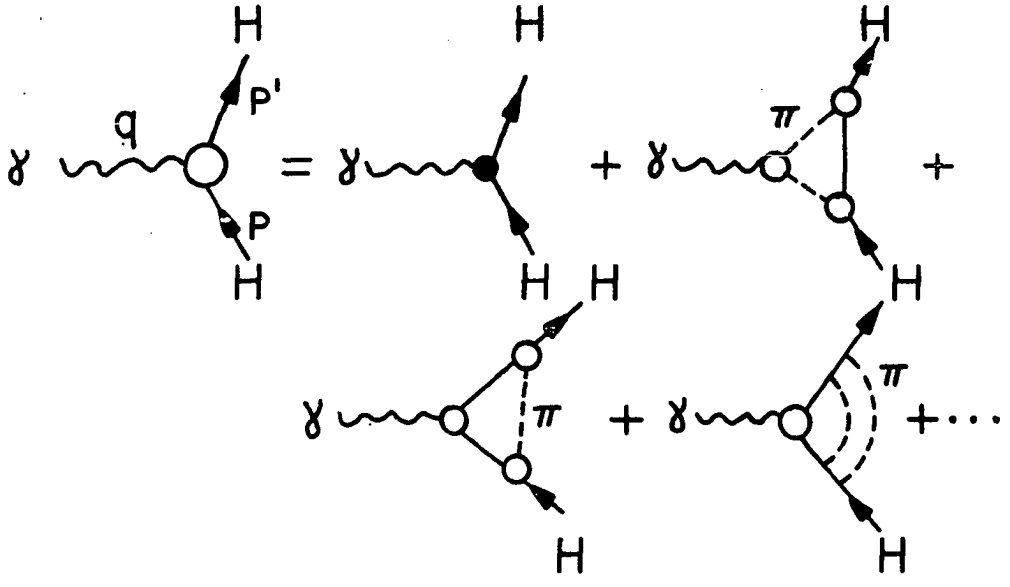

Figure 1. Feynman diagrams for the interaction of a virtual photon, γ, with a hadron, H.

The blob at the vertex in Fig. 1 represents the set of all strongly interacting intermediate states which are involved in the process. For example, there are contributions from uncorrelated pions, pionic resonances, uncorrelated kaons, nucleon-antinucleon pairs, etc. This graph is described by the matrix element

$$j_\mu^{\gamma H}(q) = \langle \bar{p}' | J_\mu^{\gamma H}(0) | \bar{p} \rangle,$$

where $J_\mu^{\gamma H}(x)$ is the hadronic electromagnetic current operator. The x-dependence in the matrix element has been transformed away using space-translation invariance.

There is no way to sum the infinite number of graphs appearing on the right in Fig. 1, so the exact functional form of the electromagnetic current matrix element between hadronic states is unknown. However, since it is a Lorentz four-vector it may be written as a sum of Lorentz covariants for spin S, I_μ^j, multiplied by 2S+1 scalar "form factors" (26), $f_j^{\gamma H}(q^2)$,

$$j_\mu^{\gamma H}(q) = \sum_{j=1}^{2S+1} I_\mu^j(p,p') f_j^{\gamma H}(q^2).$$

In this work only the form factors for particles of spin 0 and spin ½ will be analyzed. Measurements of the form factors of nucleon resonances exist, but are not directly susceptible to the analysis presented in this work. No measurements of elastic form factors of particles of spin greater than 1 (outside of nuclei) exist.

1. Baryon form factors ($S=\frac{1}{2}$)

For any member, H=B, of the $\frac{1}{2}^+$ baryon octet, B={N, Σ, Λ, Ξ}, Lorentz invariance and current conservation require that, for space-like q^2 and for B on the mass shell,

$$j_\mu^{\gamma H}(q) = i(2\pi)^{-3}\bar{u}_B(\bar{p}')[\gamma_\mu f_1^{\gamma B}(q^2)+\sigma_{\mu\nu}q_\nu f_2^{\gamma B}(q^2)]u_B(\bar{p}) \qquad (2.1)$$

In this manner it is seen that the electromagnetic current matrix element of a spin ½ baryon may be written as a sum of Dirac gamma matrices, γ_μ, $\sigma_{\mu\nu}=[\gamma_\mu,\gamma_\nu]/2i$; Dirac free-particle spinors, $\bar{u}_B(\bar{p}')$ and $u_B(\bar{p})$; and two form factors, $f_1^{\gamma B}(q^2)$ and $f_2^{\gamma B}(q^2)$, called the Dirac and Pauli form factors, respectively. The Hermiticity of $J_\mu^{\gamma H}(x)$ implies that these form factors are real for space-like values of q^2.

The Dirac form factor is related to the static charge (in units of e) and the Pauli form factor to the static anomalous magnetic moment (in Bohr magnetons) through the normalization conditions

$$\begin{aligned} f_1^{\gamma B}(0) &= Q_B, \\ f_2^{\gamma B}(0) &= \mu_B/2m_B. \end{aligned} \qquad (2.2)$$

These numbers determine the strength of the interaction between the baryon and a weak electromagnetic field. A linear combination of these, the electric (E) and magnetic (M) form factors, are defined as

$$\begin{aligned} G_E^B(q^2) &= f_1^{\gamma B}(q^2) - (q^2/2m_B)f_2^{\gamma B}(q^2), \\ G_M^B(q^2) &= f_1^{\gamma B}(q^2) + 2m_B f_2^{\gamma B}(q^2) \end{aligned} \qquad (2.3)$$

These form factors have a more transparent meaning than the Dirac and Pauli form factors. As discussed further in Appendix A, they are related to the Fourier transforms of the charge and magnetization density of the hadron. By Eq. (2.2), the electric and magnetic form factors are normalized according to

$$G_E^B(0) = Q_B,$$
$$G_M^B(0) = Q_B + \mu_B. \tag{2.4}$$

In SU(3) electrodynamics the electromagnetic current is written as the sum of an isoscalar current, $J_\mu^S(x)$, and the third component of an isovector current, $(J_\mu^V(x))_3$,

$$J_\mu^\gamma(x) = J_\mu^S(x) + (J_\mu^V(x))_3. \tag{2.5}$$

The matrix elements of the isospin current between $\frac{1}{2}^+$ baryon states may be written in terms of isospin form factors as

$$\langle B|J_\mu^{S,V}(0)|B\rangle = i(2\pi)^{-3}\bar{u}_B(\bar{p}')[\gamma_\mu f_1^{S,V}(q^2) + \sigma_{\mu\nu}q_\nu f_2^{S,V}(q^2)]u_B(\bar{p}),$$

where S, V denote the isoscalar and isovector form factors, respectively. These form factors are related to $f_{1,2}^{\gamma B}$ by Eq. (2.5) as the sum

$$f_{1,2}^{\gamma B}(q^2) = f_{1,2}^{SB}(q^2) + f_{1,2}^{VB}(q^2).$$

Since there are only four electromagnetic form factors, the eight isospin form factors are clearly redundant. This redundancy can be removed by using the group properties of the isospin generators. Then

the matrix elements of the isoscalar or isovector current taken between baryon states of the same hypercharge but opposite isospin are

$$\langle +|J^S_\mu(0)|+\rangle = \langle -|J^S_\mu(0)|-\rangle,$$
$$\langle +|(J^V_\mu(0))_3|+\rangle = -\langle -|(J^V_\mu(0))_3|-\rangle,$$

where + has been used to denote the state $B(Y,I_3)$ and - the state $B(Y,-I_3)$. As a result the form factors for these states may be written in terms of the isoscalar and isovector form factors according to the equations

$$f^+_{1,2}(q^2) = f^S_{1,2}(q^2) + f^V_{1,2}(q^2),$$
$$f^-_{1,2}(q^2) = f^S_{1,2}(q^2) - f^V_{1,2}(q^2). \qquad (2.6)$$

The inverse relations are

$$2f^V_{1,2}(q^2) = f^+_{1,2}(q^2) + f^-_{1,2}(q^2),$$
$$2f^S_{1,2}(q^2) = f^+_{1,2}(q^2) - f^-_{1,2}(q^2).$$

The isoscalar and isovector electric and magnetic form factors are defined similarly as

$$G^+_{E,M}(q^2) = G^S_{E,M}(q^2) + G^V_{E,M}(q^2),$$
$$G^-_{E,M}(q^2) = G^S_{E,M}(q^2) - G^V_{E,M}(q^2),$$
$$2G^V_{E,M}(q^2) = G^+_{E,M}(q^2) + G^-_{E,M}(q^2),$$
$$2G^S_{E,M}(q^2) = G^+_{E,M}(q^2) - G^-_{E,M}(q^2). \qquad (2.7)$$

The electromagnetic current matrix elements of a self-conjugate particle vanish by charge conjugation invariance (27). Thus the

form factors of Λ and Σ^0 vanish identically for all q^2:

$$f_{1,2}^{\gamma\Lambda}(q^2) = f_{1,2}^{\gamma\Sigma^0}(q^2) = 0.$$

2. Pseudoscalar meson form factors (S=0)

Unlike the baryons, which possess two form factors describing the momentum space distribution of their charge and magnetization density, the spinless pseudoscalar mesons possess only one form factor. This form factor describes their charge distribution. For any member, H=P, of the 0^- octet, P={K,π,η,η'}, Lorentz invariance and current conservation require that for P on the mass shell,

$$j_\mu^{\gamma P}(q) = (p + p')_\mu f^{\gamma P}(q^2),$$

where the pseudoscalar meson form factor, $f^{\gamma P}(q^2)$, is normalized to the total charge,

$$f^{\gamma P}(0) = Q_P,$$

and is real for space-like values of q^2. Again a decomposition into isoscalar and isovector form factors can be made. The charged pion has no isoscalar form factor by G-parity invariance. The charged and neutral kaons, however, possess both isoscalar and isovector form factors. Thus

$$\begin{aligned} f^{\gamma\pi}(q^2) &= f^{V\pi}(q^2), \\ f^{\gamma K^+}(q^2) &= f^{SK}(q^2) + f^{VK}(q^2), \\ f^{\gamma K^0}(q^2) &= f^{SK}(q^2) - f^{VK}(q^2). \end{aligned} \tag{2.8}$$

The π^0, η, and η' possess no form factors by charge conjugation invariance,

$$f^{\gamma\pi^0}(q^2) = f^{\gamma\eta}(q^2) = f^{\gamma\eta'}(q^2) = 0.$$

B. Experimental Data and Empirical Laws

There are several methods by which knowledge concerning the electromagnetic structure of hadrons is obtained. A discussion of these methods and an analysis of the validity of the experimental data is an important step prior to a theoretical analysis.

1. Proton Data

The electric and magnetic form factors of the proton are measured in electron-proton elastic scattering experiments. In the one-photon-exchange approximation this process is described by the Feynman graph of Fig. 2. In this graph p_1, s_1 are the initial and p_2, s_2 the final four-momentum and spin of the electron. The initial and final four-momenta of the proton are defined in a similar manner with subscripts 3 and 4, respectively. The momentum carried by the photon is $q=p_1-p_2=p_4-p_3$, by four-momentum conservation. The scattering amplitude for this graph, in terms of the matrix elements of the electromagnetic current operator, is written

$$i\langle ep|T|ep\rangle_f = j_\mu^{e\gamma}(q)D_F(q^2)_{\mu\nu}j_\nu^{\gamma p}(q), \qquad (2.9)$$

where $|ep\rangle_i$ represents the initial free-particle electron-proton state, $|\bar{p}_1,s_1;\bar{p}_3,s_3\rangle$, and $|ep\rangle_f=|\bar{p}_2,s_2;\bar{p}_4,s_4\rangle$ the final electron-proton two-particle state. As before, the current matrix elements are defined to be

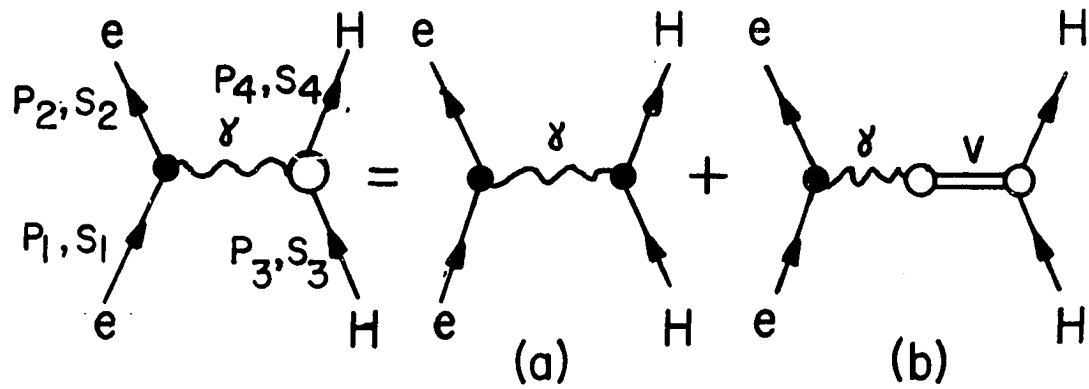

Figure 2. Feynman diagrams for the process e + H → e + H.

(a) The direct photon-hadron interaction term.

(b) The vector meson exchange term.

$$j_\mu^{e\gamma}(q) = \langle \bar{p}_1, s_1 | J_\mu^{e\gamma}(0) | \bar{p}_2, s_2 \rangle,$$
$$j_\nu^{\gamma p}(q) = \langle \bar{p}_3, s_3 | J_\nu^{\gamma p}(0) | \bar{p}_4, s_4 \rangle,$$

and $D_F(q^2)$ is the photon propagator,

$$D_F(q^2) = -i\delta_{\mu\nu}/q^2.$$

As discussed in Sec. I, experiment shows that the electron has no internal structure, so the electromagnetic current matrix element between one-electron states to lowest order in α can be written as

$$j_\mu^{e\gamma}(q) = i(2\pi)^{-3}\bar{u}_e(\bar{p}_1, s_1)\gamma_\mu u_e(\bar{p}_2, s_2).$$

The exact functional form of the proton part of the hadronic electromagnetic current operator is not known, but as indicated in the discussion in Sec. IIA, Eq. (2.1), the matrix element can in general be written in terms of the Dirac and Pauli form factors as

$$j_\mu^{\gamma p}(q) = i(2\pi)^{-3}\bar{u}_p(4)[\gamma_\mu f_1^{\gamma p}(q^2) + \sigma_{\mu\nu}q_\nu f_2^{\gamma p}(q^2)]u_p(2),$$

where

$$u_p(n) = u_p(\bar{p}_n, s_n);\ n=2,4.$$

Using the expression, Eq. (2.9), for the matrix element for electron-proton elastic scattering, it is straightforward to derive the Rosenbluth differential cross section formula (28):

$$\left(\frac{d\sigma}{d\Omega}\right)_R = \sigma_{NS}\left[\frac{(G_E^p)^2 + \tau(G_M^p)^2}{1+\tau} + 2\tau(G_M^p)^2\tan^2(\theta/2)\right], \qquad (2.10)$$

where q^2 is related to the electron scattering angle, θ, and the incident electron energy, E_0, in the lab system by the equation,

$$q^2 = \frac{4E_o^2 \sin^2(\theta/2)}{1 + (2E_o/m_p)\sin^2(\theta/2)},$$

$\tau = q^2/4m_p^2$, and σ_{NS} is the cross section for the scattering of a relativistic electron from a spinless point charge,

$$\sigma_{NS} = \frac{1}{4E_o^2 \sin^4(\theta/2)} \cos^2(\theta/2) \frac{1}{1+(2E_o/m_p)\sin^2(\theta/2)}.$$

Eq. (2.10) holds only in the extreme relativistic limit where errors on the order of α and m_e^2/q^2 can be ignored.

Typically, the form factors are extracted from the differential cross section measurements, after radiative corrections are applied, by making a Rosenbluth plot. The procedure is to measure $(d\sigma/d\Omega)_R$ for fixed q^2 and variable θ, plot $(d\sigma/d\Omega)_R/\sigma_{NS}$ against $\tan^2(\theta/2)$ and fit the data points with a straight line. The slope of the line is proportional to $(G_M^p)^2$ and the intercept is proportional to $(G_E^p)^2+\tau(G_M^p)^2$. In this way the squares of the form factors, but not their signs, can be determined. Deviations from this straight line behaviour can be taken as evidence for the breakdown of the one-photon-exchange mechanism due to the exchange of two or more virtual photons. No deviations from the Rosenbluth formula have been observed in elastic electron-proton scattering up to 25 $(GeV/c)^2$ (29). There is the possibility of con-

tamination from effects due to the exchange of weak neutral bosons. These have been calculated (30) and found to be an order of magnitude less than the present experimental accuracy of the cross section measurements.

The proton form factor data used in this analysis is taken from a compilation by E. Lohrmann (31). The measurements of G_E^p used extend from 0.47 to 3.77 $(GeV/c)^2$. For G_M^p the data ranges from 0.06 to 4.09 $(GeV/c)^2$. The electric and magnetic form factors are difficult to separate above 4 $(GeV/c)^2$ due to the existence of the momentum-dependent factor, 2τ, multiplying $(G_M^p)^2$. Data quoted for G_M^p above 4 $(GeV/c)^2$ is usually obtained from the cross section measurements by assuming that G_E^p and G_M^p scale according according to Eq. (1.1) and (1.2). Since this assumption may be in error, the cross section data is substituted for G_M^p data above 4 $(GeV/c)^2$. It extends from 3.11 to 25.03 $(GeV/c)^2$ to allow for a continuous overlap with the G_M^p measurements. The proton differential cross section and form factor data is recorded in Tables 2-4 and is seen graphically in Figs. 10 and 12. The errors quoted in these tables refer only to statistical errors. Systematic errors between data sets obtained from different experiments have been ignored.

According to the conventional interpretation placed upon the electromagnetic form factor data, the strong q^2 dependence of the data graphed in Figs. 10 and 12 means that the proton must be regarded as an extended particle. For a more rigorous clarification of this point, see the discussion in Appendix A.

Table 2. Proton Electric Form Factor Data

q^2 (GeV/c)^2	$G_E^p(q^2)[1+q^2/0.71]^2$	Error
0.06	1.00	±0.01
0.07	0.99	0.01
0.11	0.98	0.03
0.14	0.99	0.02
0.15	1.03	0.02
0.17	0.97	0.02
0.19	0.97	0.05
0.21	0.97	0.03
0.24	1.02	0.03
0.28	1.00	0.04
0.29	1.00	0.05
0.32	0.99	0.02
0.35	0.94	0.07
0.38	0.97	0.01
0.43	1.03	0.06
0.46	1.00	0.05
0.50	1.03	0.10
0.54	0.99	0.09
0.58	1.01	0.02
0.62	0.94	0.08
0.65	0.94	0.09
0.70	1.08	0.09
0.74	1.06	0.15
0.78	0.97	0.04
0.98	0.99	0.04
1.18	0.97	0.06
1.59	0.89	0.07
1.79	1.23	0.13
1.98	0.96	0.17
2.91	1.07	0.26
4.09	1.53	0.49

Table 3. Proton Magnetic Form Factor Data

q^2(GeV/c)^2	$G_M^p(q^2)[1+q^2/0.71]\ /[1+\mu_p]$	Error
0.47	0.97	±0.03
0.50	0.96	0.02
0.54	0.99	0.01
0.58	0.98	0.05
0.62	0.99	0.03
0.66	1.02	0.02
0.70	0.99	0.02
0.76	1.02	0.03
0.79	1.03	0.01
0.88	1.08	0.02
1.05	1.04	0.02
1.10	1.05	0.03
1.20	1.07	0.01
1.56	1.04	0.02
1.76	1.00	0.04
1.96	1.03	0.04
2.33	0.99	0.04
2.44	1.06	0.03
2.46	1.06	0.03
2.51	1.07	0.03
2.53	1.06	0.03
2.61	1.09	0.04
2.92	1.07	0.02
3.11	0.984	0.02
3.27	1.021	0.05
3.77	1.051	0.09

Table 4. Electron-Proton Differential Cross Section Data

q^2(GeV/c)^2	Energy	Angle	$(d\sigma/d\Omega)_p$	Error
3.11	4.12	0.562	0.199	±0.0169
3.11	3.47	0.719	0.089	0.0072
3.11	2.67	1.138	0.0282	0.0032
3.27	4.002	0.611	0.123	0.01
3.77	10.0	0.218	0.97	0.017
3.88	2.777	1.571	0.0081	0.0014
3.881	4.874	0.541	0.1	0.087
4.08	3.82	0.829	0.0178	0.00178
4.09	5.886	0.436	0.113	0.0057
4.16	3.87	0.826	0.0185	0.00185
4.2	3.11	1.335	0.00457	0.000457
4.28	8.46	1.073	0.00887	0.0011
4.88	4.34	0.831	0.00769	0.000769
5.0	10.001	0.262	0.1772	0.0077
5.082	10.702	0.244	0.1913	0.0048
5.89	4.96	0.829	0.00334	0.000334
6.276	11.349	0.263	0.0571	0.0023
6.81	5.988	0.731	0.0058	0.0011
6.85	5.54	0.829	0.00138	0.000138
7.512	12.00	0.281	0.0195	0.001
7.58	6.13	0.831	0.00074	0.000074
8.766	12.7	0.294	0.00707	0.00053
8.78	5.71	1.311	0.00011	0.000033
9.528	6.13	1.323	0.0000604	0.0000085
9.59	6.13	1.321	0.000077	0.0000308
9.992	13.32	0.307	0.00392	0.00023
12.49	14.657	0.328	0.00084	0.000087
15.02	16.008	0.344	0.000328	0.000038
20.0	17.314	0.419	0.0000284	0.0000066
20.03	17.806	0.34	0.000045	0.000013
25.03	17.314	0.612	0.0000042	0.000002

2. Neutron data

Since no pure neutron targets exist, the neutron form factors have to be determined indirectly by either elastic or inelastic electron-deuteron scattering. In elastic electron-deuteron scattering the electromagnetic field may interact with either the proton or the neutron, so proton effects have to be separated out in order to determine the neutron form factors (see Fig. 3). This separation is usually done in the impulse approximation, which states that the electron-deuteron scattering amplitude is the sum of the amplitudes for the scattering of electrons by a free proton and a free neutron. In addition some ansatz for the deuteron wave function must also be made. From these two assumptions the theory of electron-deuteron elastic scattering (32) predicts that the electric and magnetic form factors of the deuteron (33) are related to those of the neutron and proton by the equations

$$G_E^d(q^2) = G_E^S(q^2) f_E^d(q^2),$$
$$G_M^d(q^2) = G_M^S(q^2) f_M^d(q^2),$$

where $f_{E,M}^d(q^2)$ are deuteron structure functions defined by integrals over the ground-state dueteron wave functions. Only the isoscalar form factors enter because the deuteron has isospin=0. Thus a measurement of the differential cross section for electron-deuteron scattering can be used to deduce the nucleon isoscalar form factors. If the proton and deuteron form factors are measured at the same value of q^2, by Eq. (2.7) it may be seen that the relative sign and magnitude of the neutron form factors can be determined. More often, a four-pole phenomenological fit to the proton form factor data is used to represent the proton contribution.

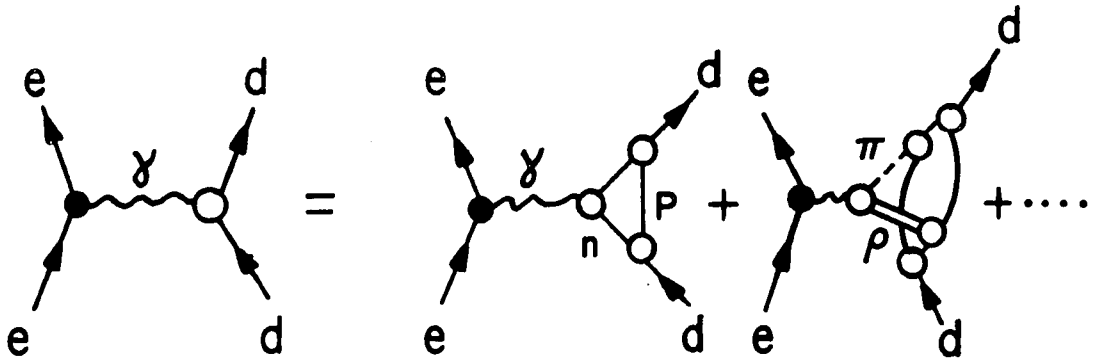

Figure 3. Feynman diagrams for elastic electron-deuteron scattering.

As a practical matter, only G_E^n is actually measured in electron-deuteron elastic scattering because scattering by the deuteron's magnetic dipole moment is only a 5% contribution at small q^2. Even then, G_E^n is a very small quantity, and thus very sensitive to errors in experiment and theory.

There are at least five factors limiting the accuracy of the $G_E^n(q^2)$ measurements:

(1.) The value of G_E^n is uncertain due to the model-dependent extrapolation of G_E^p and G_M^p.

(2.) The model dependence of the ground state deuteron wave functions also adds uncertainty because the exact functional form of the two-nucleon potential is unknown. Galster et al. (34) have shown that $(d\sigma/d\Omega)_{ed}$ varies as much as 75% when different deuteron wave functions are used. Some of the popular choices are given in reference (35).

(3.) The assumption that the free and bound-state neutron form factors are identical cannot be exactly valid because the nucleons in the deuteron are off the mass shell.

(4.) The use of a non-relativistic theory in the calculation of the deuteron wave function is not exactly valid because the scattering takes place at relativistic velocities. However, relativistic corrections have been made by Gross (36).

(5.) Meson exchange current contributions to the deuteron electromagnetic current are usually ignored, which means that important corrections to the Born approximation involving the interaction of the virtual photon with virtual mesons binding the neutron and proton to form the deuteron are being excluded (37).

The neutron form factors can also be measured in inelastic electron-deuteron scattering; i.e., deuteron electrodisintegration experiments. The relevant amplitudes in the one-photon-exchange approximation are given in Fig. 4, and represent the dominant contributions at the quasi-elastic peak. The theoretical analysis is complicated and will not be discussed (38).

In these experiments, usually it is the ratio, R, of the neutron to proton differential cross sections that is actually measured. This has the advantage that errors due to final state interactions cancel out. If the scattered electron is detected at the quasielastic peak in coincidence with the recoiling neutron, R is nearly equal to the ratio of the free particle Rosenbluth cross sections. Thus, a measurement of R and of the proton form factors at the same value of q^2 may be used to deduce the neutron form factors according to Eq. (2.10). This experiment is subject to the same errors that occur in elastic electron-deuteron scattering. In addition, a correction for final state interactions between the outgoing proton and neutron has to be made, though it is usually ignored in the analysis.

In view of these limitations on the validity of the neutron form factor data, only data for low values of the momentum transfer have been kept. The G_M^n data used in this analysis is obtained from a compilation by E. Lohrmann (31), and extends from 0.03 to 1.16 $(GeV/c)^2$. This data is determined experimentally from both elastic and inelastic electron deuteron scattering. The data for G_E^n, also obtained by such experiments, is taken from a compilation by R. Wilson (39). It ranges from 0.0117

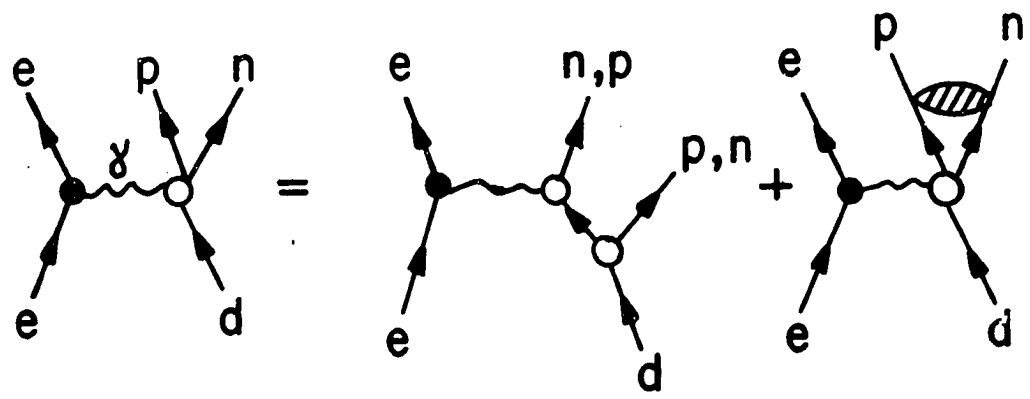

Figure 4. Feynman diagrams for inelastic electron-deuteron scattering.

to 0.989 $(GeV/c)^2$. Recent measurements (40) have resulted in knowledge of G_E^n up to 2.7 $(GeV/c)^2$ and of G_M^n up to 3.75 $(GeV/c)^2$, but this data has not yet been incorporated in the analysis due to the inconsistencies mentioned above. Some experiments report negative values for $(G_E^n)^2$, but these are ignored in the analysis.

Finally, the initial slope of G_E^n has been measured in experiments in which very low energy neutrons scatter off electrons bound in atoms. Since reliable theories of low energy scattering from atoms exist, the initial slope measurements are usually regarded as being highly precise.

The electric and magnetic form factor data for the neutron is plotted in Figs. 11 and 13. The form factor data and the initial slope measurements are tabulated in Tables 5-7.

3. Pion data

The pion form factor data for space-like values of q^2 is taken from references (41) to (44). In all cases the pion form factor has been deduced from the pion electroproduction reaction, $ep \rightarrow e\pi^+ n$. In Fig. 5 the first few diagrams which describe this inelastic process are given.

Because of the large number of diagrams contributing to pion electroproduction, kinematic conditions have to be carefully chosen to isolate the pion-pole term, which corresponds to electron scattering off the virtual pion. From an analysis of the three-body kinematics Akerlof (42) has shown that the pion pole term is dominant at small electron scattering angles and at zero angle between the photon and outgoing pion momentum. Mistretta et al. (43) take their measurements close to the $\Delta(1236)$; i.e., in the region where the pion-proton center-of-mass energy is close to the mass of the $\Delta(1236)$ resonance. In this case contributions from the first

Table 5. Neutron Electric Form Factor Data

q^2(GeV/c)^2	$G_E^n(q^2)$	Error
0.0117	0.024	±0.013
0.0234	0.015	0.013
0.0389	0.019	0.014
0.0545	0.025	0.012
0.0662	0.046	0.014
0.0857	0.027	0.015
0.1170	0.083	0.023
0.1560	0.052	0.019
0.1950	0.051	0.02
0.2410	0.055	0.017
0.2610	0.042	0.017
0.273	0.054	0.018
0.296	0.071	0.02
0.381	0.053	0.017
0.424	0.073	0.019
0.428	0.050	0.014
0.46	0.058	0.014
0.467	0.037	0.027
0.483	0.073	0.016
0.506	0.07	0.018
0.576	0.038	0.015
0.6	0.08	0.017
0.623	0.058	0.018
0.654	0.036	0.016
0.673	0.054	0.016
0.701	0.038	0.015
0.732	0.009	0.016
0.763	0.057	0.016
0.783	0.05	0.036
0.794	0.046	0.017
0.818	0.034	0.014
0.849	0.029	0.016
0.884	0.019	0.019
0.915	0.05	0.022
0.942	0.012	0.027
0.989	0.025	0.023

Table 6. Neutron Magnetic Form Factor Data.

q^2(GeV/c)^2	$G_M^n(q^2)[1+q^2/0.71]^2/\mu_n$	Error
0.03	1.38	±0.34
0.05	1.05	0.07
0.09	1.10	0.04
0.12	1.00	0.10
0.16	0.97	0.07
0.18	1.10	0.11
0.20	1.01	0.08
0.29	0.93	0.03
0.38	0.98	0.03
0.43	0.99	0.16
0.48	1.03	0.05
0.56	1.08	0.06
0.77	1.03	0.14
0.97	1.18	0.15
1.16	1.00	0.22

Table 7. Experimental Values of the Initial Slope of $G_E^n(q^2)$.

Slope (GeV/c)$^{-2}$	Error	Ref.
0.459	±0.02	149
0.575	0.019	150
0.512	0.019	151

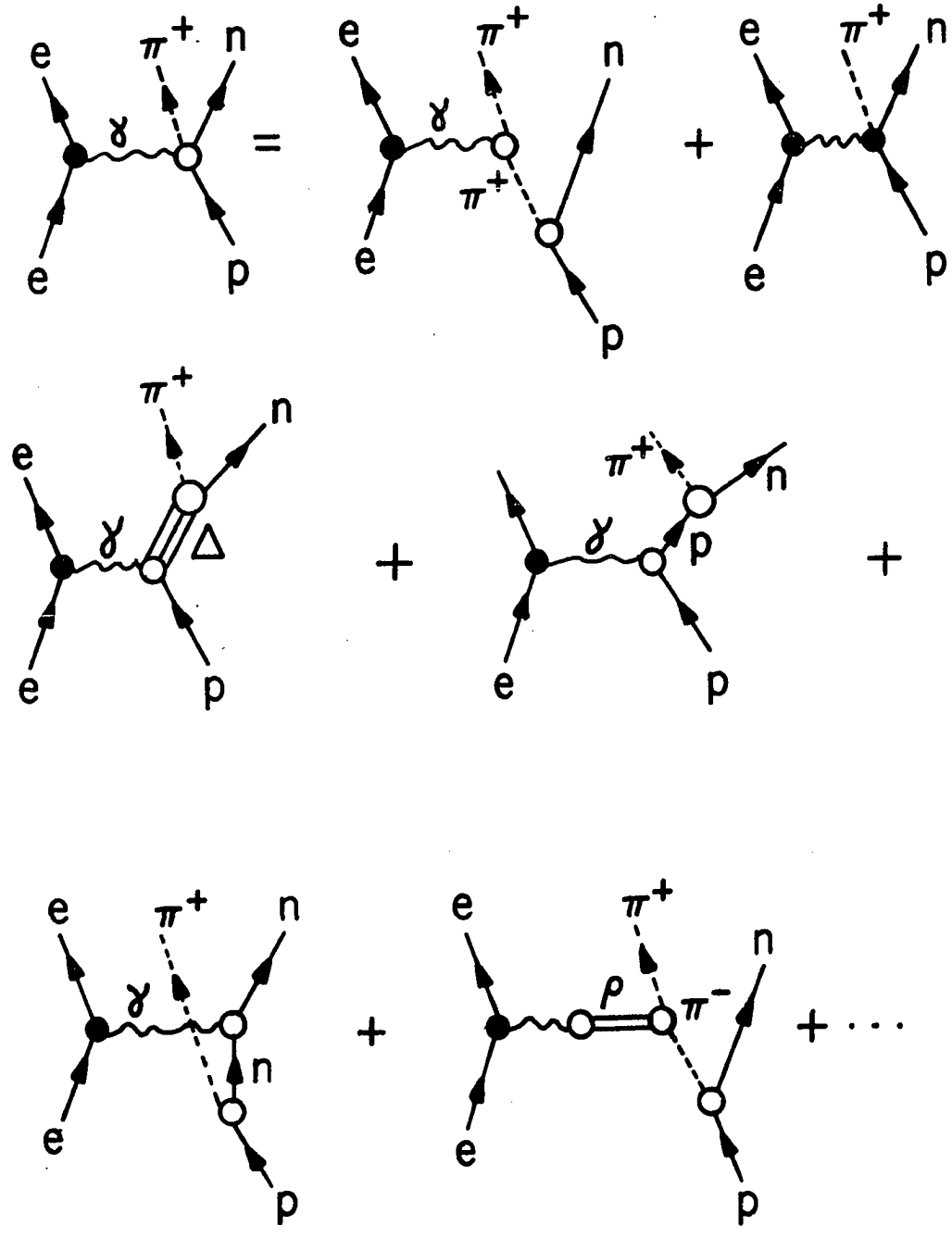

Figure 5. Feynman diagrams for pion electroproduction.

two graphs must be separated from the others using one of the many theories of electroproduction (45).

Extraction of the space-like pion form factor from the differential cross section for $ep \rightarrow e\pi^+ n$ is thus a very theory-laden process. The pion form factor, $f^{\gamma\pi}(q^2)$, is treated as a free parameter determined by fitting the theory cross section to the cross section data for each value of q^2. The electromagnetic form factors of the proton also enter the calculation due to the nucleon-pole terms (see Fig. 5). The standard procedure is to use the dipole and scaling laws to account for these effects.

Kellet and Verzegnassi (46) have re-analyzed the electroproduction models and concluded that single pion electroproduction cannot give an unambiguous determination of the pion form factor due to the existence of an unknown subtraction constant, usually ignored, entering the dispersion relation formalism. This purely theoretical uncertainty means that the pion form factor deduced from electroproduction experiments can vary at least between the values predicted by simple ρ-dominance, $f_\rho = m_\rho^2/(q^2+m_\rho^2)$, and by G_E^p.

Dombey and Read (47) have argued that because a pseudoscalar, rather than a pseudovector, pion-nucleon coupling is chosen for the Born approximation terms in pion electroproduction, a contribution from the weak axial-vector form factor of the nucleon, $g_A(q^2)$, is ignored in all analyses to date. Since $g_A(q^2)$ is not a well-measured quantity, the pion electroproduction data allows a wide variation in the value of the pion form factor even beyond that of the other errors mentioned.

The data, recorded in Table 8, includes values for the pion form factor from 0.039 to 3.991 $(GeV/c)^2$. Most experimentalists include only statistical errors in their measurements, whereas Akerlof and Mistretta include theoretical uncertainties as well. These are estimated to be about 5%, ignoring the uncertainties mentioned above. The high q^2 measurements are least reliable as they depend on a theory which fails to fit the angular distribution of the pions for $q^2 >> m_\pi^2$.

There are two other sources of error in experiments which deduce the pion form factor from electroproduction measurements in addition to the theoretical uncertainties:

(1.) The values of $f^{\gamma\pi}$ determined are heavily dependent on the electroproduction theory used to deduce them. Different theories give results for $f^{\gamma\pi}$ varying as much as 25%.

(2.) Final state interactions between the outgoing pion and nucleon are often ignored. This leads to a value of the pion form factor larger than its real value.

As a consequence of the heavy theory-dependence required in extracting the space-like pion form factor data, agreement with experimental results is not to be taken as a high priority. It is preferable to try to predict the space-like pion form factor data by relating it to more reliable experimental results.

4. Kaon data

No direct electron-kaon scattering experiments have ever been performed. Only recently have kaon electroproduction experiments, $ep \rightarrow eK^+\Lambda$, $eK^+\Sigma^0$, been conducted (48). The theoretical interpretation

Table 8. Space-like Pion Form Factor Data

q^2(GeV/c)^2	$f^{\gamma\pi}(q^2)$	Error
0.039	0.624	±0.190
0.046	0.922	0.283
0.047	1.061	0.247
0.048	0.922	0.134
0.117	0.672	0.262
0.176	0.656	0.071
0.234	0.325	0.08
0.294	0.411	0.036
0.396	0.333	0.018
0.62	0.208	0.014
0.795	0.16	0.01
1.069	0.11	0.011
1.712	0.257	0.018
1.19	0.076	0.008
1.198	0.321	0.018
1.2	0.083	0.007
1.204	0.085	0.006
1.216	0.324	0.028
1.314	0.071	0.007
1.988	0.221	0.016
2.015	0.034	0.004
3.301	0.136	0.017
3.991	0.124	0.022

Table 9. Space-like Kaon Form Factor Data

q^2(GeV/c)^2	$f^{\gamma K}(q^2)$	Error
0.1	0.948	±0.006
0.2	0.892	0.011
0.3	0.833	0.014
0.4	0.773	0.018
0.5	0.712	0.020
0.6	0.651	0.021

has not yet led to a determination of the space-like kaon form factor, however. The kaon form factor has been determined indirectly by Mickens and Rush (49) from a study of K^+K^+ scattering data using the method of Wu and Yang (50). Their idea is that the asymptotic differential cross section for hadron-hadron scattering is related to the electromagnetic form factor of the hadron (51), leading them to predict a decaying exponential formula for the asymptotic electromagnetic form factor of the hadron. From the known pp and $\pi\pi$ scattering data Chou and Yang were able to predict the asymptotic proton and pion electromagnetic form factors, which were found to be in qualitative agreement with the data even for small q^2, outside the expected region of validity. By using the known K^+K^+ scattering data, Mickens used their technique to determine the space-like kaon electromagnetic form factor. The results are given in Table 9 and plotted in Fig. 16.

A plot of the kaon form factor data against q^2 shows that it is suspiciously well-represented by straight-line behaviour. For this reason it is subject to doubt. Furthermore, the Chou-Yang model for the form factors, despite its "success" for the proton and pion data, has the wrong analytic properties when analytically continued into the time-like region. It predicts an infinitely oscillating behaviour for the time-like form factors, corresponding to an infinite number of equally-spaced higher vector meson resonances. Thus it can only be regarded as providing a limited phenomenological understanding of the data.

5. Empirical laws

From a careful analysis of the nucleon electromagnetic form factor data three empirical generalizations, the dipole, scaling and asymptotic laws, have been deduced. These results will be discussed separately.

a. The dipole law The dipole law, Eq. (1.1), gives a simple first approximation to the data. It experiences deviations of 5% for $q^2<5$ $(GeV/c)^2$ and -15% for $q^2>10$ $(GeV/c)^2$, so it is not a perfect fit. In fact, the dipole law has no accepted theoretical foundation (52-53) and is probably only of fitting origin. The dipole law gives a non-resonant behaviour when analytically continued into the time-like region. This contradicts the existence of known vector meson resonances in the time-like form factors, so the dipole law has only limited validity over a limited range of q^2.

b. The scaling law The form factor scaling law,

$$G_E^p(q^2) = \frac{G_M^p(q^2)}{1+\mu_p} = \frac{G_M^n(q^2)}{\mu_n} = \frac{4m_n^2}{\mu_n q^2} G_E^n(q^2), \qquad (2.11)$$

gives a simple relation between the proton and neutron form factors in which the magnetic moments act as scaling parameters. In the scaling law for the neutron electric form factor, the μ_n is introduced in order to obtain close agreement to the initial slope measurement, which is nearly given by the "Foldy term", $\mu_n/4m_n^2=0.542$. The scaling law is not an exact result. Fluctuations of 10% in the quantity $f_s=(1+\mu_p)G_E^p/G_M^p$ between 1 and 3 $(GeV/c)^2$ are known (54), however. Recent very accurate measurements (55)

between 0.05 and 0.30 $(GeV/c)^2$ show evidence for an oscillatory behaviour in f_s, but this may be an instrumental effect.

The scaling law used to be written with $G_E^n(q^2)=0$, as predicted by SU(6) and the relativistic quark model (56) and supported by the data of Drickey and Hand (57). Their experiment, which gave a zero value for the neutron electric form factor within experimental errors, contradicts the initial slope measurements. Discrepancies between low q^2 electron-deuteron scattering and the thermal neutron data have been traced to the model-dependence of the deuteron wave function used in the analysis (58). Present data definitely rules out the possibility that $G_E^n(q^2)=0$ for all q^2 (59).

The scaling law for the neutron electric form factor as written in Eq. (2.11) is due to Hand et al. (10). It is usually favored because it reproduces the initial slope of $G_E^n(q^2)$, though it fails to fit the higher q^2 data well. The generalization

$$G_E^n(q^2) = (\mu_n\tau/(1+4\tau))G_E^p(q^2),$$

has been predicted on ad hoc grounds (60) and yields a better fit to the data for large q^2.

For time-like q^2 the scaling law violates the annhilation threshold constraint,

$$G_E^N(-4m_N^2) = G_M^N(-4m_N^2), \qquad (2.12)$$

which requires that in $e^+e^-\to N\bar{N}$ the nucleon-antinucleon pair be produced

isotropically at threshold. As a result, like the dipole formula, the scaling law has only a phenomenological significance (61).

c. The asymptotic law or superconvergence condition The asymptotic law,

$$\lim_{q^2\to\infty}[q^4 G^p_{E,M}(q^2)] = 0, \qquad (2.13)$$

holds trivially if the dipole law is valid for large q^2. New data suggests (62) that the electromagnetic form factors of the proton may drop even more rapidly than q^{-4}. The existence of an elementary bare proton would be manifest by the appearance of a hard core term in the electromagnetic form factor. The asymptotic law implies, then, that there exists no hard core to the proton; i.e., the proton is a composite particle. The form factor data for the neutron does not extend to high enough values of q^2 to allow a valid speculation as to its asymptotic behaviour. If the scaling law does apply for high q^2, then it also follows that the neutron is a composite particle.

In terms of a physical picture, the dipole and scaling laws are usually taken to imply that the proton and neutron possess a continuous, exponential distribution of charge and magnetization density, and that only one form factor is needed to describe them. This cannot be exactly correct for the neutron, as implied by the scaling law for G^n_E, because the net charge of the neutron is zero, requiring the charge density to change sign someplace. In any case, this interpretation is flawed by its lack of rigor. For a further discussion see Appendix A.

C. The Theory of Space-like Form Factors

Consider the elastic scattering of an electron, e, and a spin ½ or spin 0 hadron, H. If the possibility of a direct point-like interaction is allowed for, then in the framework of the one-photon-exchange approximation and the vector dominance model this process is described by the Feynman graphs shown in Fig. 2. Graph 2(a) represents the pure electromagnetic interaction of the electron with the hadron. Graph 2(b) represents the possibility that the photon may also interact with the hadron by materializing into a vector meson, V, which in turn interacts with the hadron.

In terms of the current matrix elements defined previously, the T-matrix element representing this process is

$$\langle eH|T|eH\rangle = \langle eH|T_{em}|eH\rangle + \langle eH|T_{strong}|eH\rangle,$$

where

$$\begin{aligned}\langle eH|T_{em}|eH\rangle &= j_{\mu}^{e\gamma}(q)[-i\delta_{\mu\nu}/q^2]j_{\nu}^{\gamma H}(q^2=0),\\ \langle eH|T_{strong}|eH\rangle &= j_{\mu}^{e\gamma}(q)[-i\delta_{\mu\nu}/q^2]D_{\nu\alpha}^{V}(q^2)j_{\alpha}^{VH}(q).\end{aligned} \qquad (2.14)$$

The direct photon-hadron interaction term is described by the current $j_{\nu}^{\gamma H}(q^2=0)$, where the functional dependence $q^2=0$ means that the form factors appearing in $j_{\nu}^{\gamma H}(q)$ are to be evaluated at $q^2=0$. The strong interaction contribution is represented by the term $D_{\nu\alpha}^{V}j_{\alpha}^{VH}$. The quantity $j_{\alpha}^{VH}(q)$ is the matrix element of the vector meson source current taken between hadronic states. Since the vector mesons are spin one, this matrix element has the same Lorentz structure as the matrix element of the

electromagnetic current operator. The quantity $D^V_{\nu\alpha}$ represents the Lorentz product of the unstable vector meson propagator, $[\Delta^V_F(q2)]_{\nu\beta}$, and the photon-vector meson vertex operator, $\Gamma_{\beta\alpha}(q^2)$. The leptonic current and the photon propagator may be factored out so that the total hadronic current matrix element can be written as

$$j^{\gamma H}_\mu(q) = j^{\gamma H}_\mu(q^2=0) + \sum_V D^V_{\mu\nu}(q^2) j^{\gamma H}_\nu(q), \qquad (2.15)$$

where the sum goes over all the vector mesons contributing to the form factor. Due to their complexity, the vector meson propagator and the photon-vector meson vertex operator will be discussed separately.

1. The photon-vector meson vertex operator

Since $\Gamma_{\beta\alpha}(q^2)$ is a second rank Lorentz tensor that depends only on q^2, its most general form is given by the expression

$$\Gamma_{\beta\alpha}(q^2) = f_1(q^2)\delta_{\beta\alpha} + f_2(q^2)[q_\mu q_\nu/q^2] + f_3(q^2)[q_\mu q_\nu/q^2]\varepsilon_{\mu\nu\beta\alpha}.$$

The last term vanishes identically due to the properties of the four-index symbol, $\varepsilon_{\mu\nu\beta\alpha}$. By gauge invariance $\Gamma_{\beta\alpha}$ satisfies

$$q_\beta \Gamma_{\beta\alpha}(q^2) = 0,$$

which implies

$$\Gamma_{\beta\alpha}(q\ ) = f_1(q2)[\delta_{\beta\alpha} - (q_\mu q_\nu/q^2)].$$

It is usual to assume that the photon-vector meson form factor, $f_1(q^2)$, is a slowly-varying function of q^2 so that for all practical purposes

it can be regarded as a constant. Usually this coupling is redefined as

$$f_1(-m_V^2) = m_V^2/2\gamma_V.$$

The coupling constant, f_1, is best measured in experiments involving the decay of neutral vector mesons into lepton pairs. The matrix element for such a process is represented by the Feynman diagram in Fig. 6 and described by the expression

$$\langle V|T|e^+e^-\rangle = -if_1\varepsilon_\mu^\lambda j_\mu^{e\gamma}(-m_V^2),$$

where $q^2=-m_V^2$ since the vector meson is on the mass shell, and ε_μ^λ is the polarization operator of the vector meson. The half-width for the process is given by

$$\Gamma(V\rightarrow e^+e^-) = (4\pi\alpha^2/3)(f_1/m_V^2)^2 m_V.$$

where terms of order m_e/m_V have been ignored. Thus a measurement of the decay rate for a vector meson to go into leptons gives the magnitude, but not the sign, of the photon-vector meson coupling.

The photon-vector meson couplings have also been measured in experiments involving the photoproduction of vector mesons on nuclei. The experimental values deduced from the photoproduction data are given in Table 1 and were taken from a compilation of coupling constants by Pilkuhn *et al*. (63). The photon-vector meson couplings deduced from the leptonic decay rates of vector mesons are much lower than the values

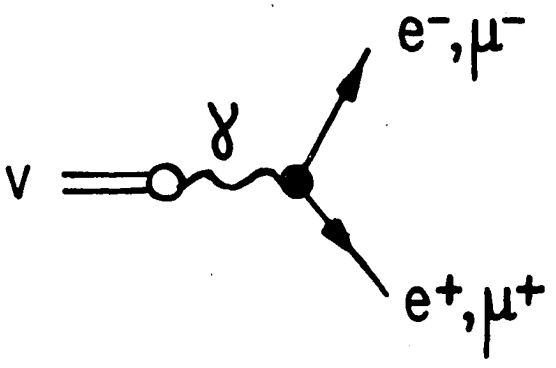

Figure 6. Feynman diagrams for the leptonic decay of a neutral vector meson, V.

reported in Table 1. It is not yet clear whether this discrepancy is due to a possible q^2 dependence of γ_V or to other experimental errors, for example, a contribution to γ_ρ from electromagnetic ρ-ω mixing, or from the two-pion decay mode of heavy vector mesons like the ρ'.

2. The vector meson propagator

The vector meson dominance hypothesis is usually introduced using stable particle propagators for the vector mesons. Although it is an experimental fact that the vector mesons are highly unstable particles with half-lives on the order of 10^{-21} seconds, it is usually expected that the effects of this instability are small, being of order Γ_V/m_V. However, for vector mesons like the ρ, this ratio is on the order of 20%, so their instability cannot be ignored in any process in which they are produced as intermediate states. Even the importance of finite-width effects for the ω and ϕ should not be prejudged on the basis of their small Γ_V/m_V ratio, but should only be tested against fits to the data.

The ρ meson has long been an annoying meson in the sense that the determination of its width have varied from experiment to experiment and process to process. Colliding beam experiments give the pion form factor directly which, when fitted with a Breit-Wigner formula with constant width yields a Γ_ρ on the order of 0.145 GeV, which is much different from Γ_ρ=0.130 GeV obtained from 2π production in purely hadronic interactions. This may be due to the fact that the instability of the ρ has never been consistently taken into account. The problem is aggravated by the fact that at least three different empirical defintions of the ρ mass and half-width are in use:

(1.) The value of energy at which the ρ-production cross section maximizes and the width of the ρ peak at half-maximum.

(2.) The value of m_ρ and Γ_ρ such that $\cot[\delta_{\pi\pi}(-m_\rho^2)]=0$ and $d/dq\ [\cot[\delta_{\pi\pi}(-m_\rho^2)]]=1/m_\rho\Gamma_\rho$, where $\delta_{\pi\pi}(q^2)$ is the I=J=1 ππ phase shift.

(3.) The position of the associated pole, $m_\rho - i(\Gamma_\rho/2)$, in the scattering amplitude.

The real mass and width of the ρ correspond to its pole position in the complex energy plane. The other definitions are approximations which are valid only in the small-width limit. A determination of this pole position using a propagator capable of including the effects of the ρ instability can thus lead to valuable information about the parameters chacterizing the ρ.

The model to be considered is an improvement over the standard vector dominance model in that propagators possessing analytic properties capable of representing unstable particles are used in the analysis. These propagators are derived from a relativistic quantum field theory of unstable particles, and not from ad hoc parametrizations of dispersion relations. Using standard methods for the evaluation of the propagator in the Heisenberg representation, and the formalism of Hammer and Weber (64), it is possible to show that the exact spin-one propagator for a stable or unstable vector meson of mass m_V is

$$[\tfrac{1}{2}\Delta_V(q^2)]_{\mu\nu} = \frac{1}{2\pi m_V^2}\int_C \frac{dm'\ (m_V/m')^4}{m'-m_V-R_V(m')}\ \frac{q_\mu q_\nu - q^2\delta_{\mu\nu}}{q^2+m'^2-i\varepsilon}\ . \qquad (2.16)$$

The quantity, $R_V(m')$, is the level shift in the center-of-mass system of the vector meson, and satisfies the dispersion relation

$$R_V(m') = \langle m_V|U|m_V\rangle + \frac{1}{\pi}\int_{C'} dm'' \frac{\mathrm{Im}[R_V(m'')]}{m''-m'},$$

where $R_V(m')$ is connected to the dynamics through the relation

$$\mathrm{Im}[R_V(m')] = \pi\langle V|R_V(m')\Lambda(m'-H_0)\Lambda R_V(m')|V\rangle. \qquad (2.17)$$

In these equations Λ is a projection operator chosen to eliminate the single-particle states, U is the interaction Hamiltonian responsible for the vector meson decay, H_0 is the free-particle Hamiltonian, and $|V\rangle$ is the single-particle vector meson state. The contour, C', starts at threshold and goes to infinity below the pole at m', as shown in Fig. 7(a).

The path of integration, C, used in the definition of the propagator, is along a contour which encircles only the singularities of the function

$$D_V(m') = m'-m_V-R_V(m') \qquad (2.18)$$

in the physical sheet of the complex m'-plane.

In the stable particle case the interaction, U, is of such a nature as to result in a bound state pole on the real m' axis below threshold, corresponding to the physical rest mass of the particle, and a branch cut from threshold to infinity corresponding to the multiparticle states which involve the particle. The pole and cut singularities may be

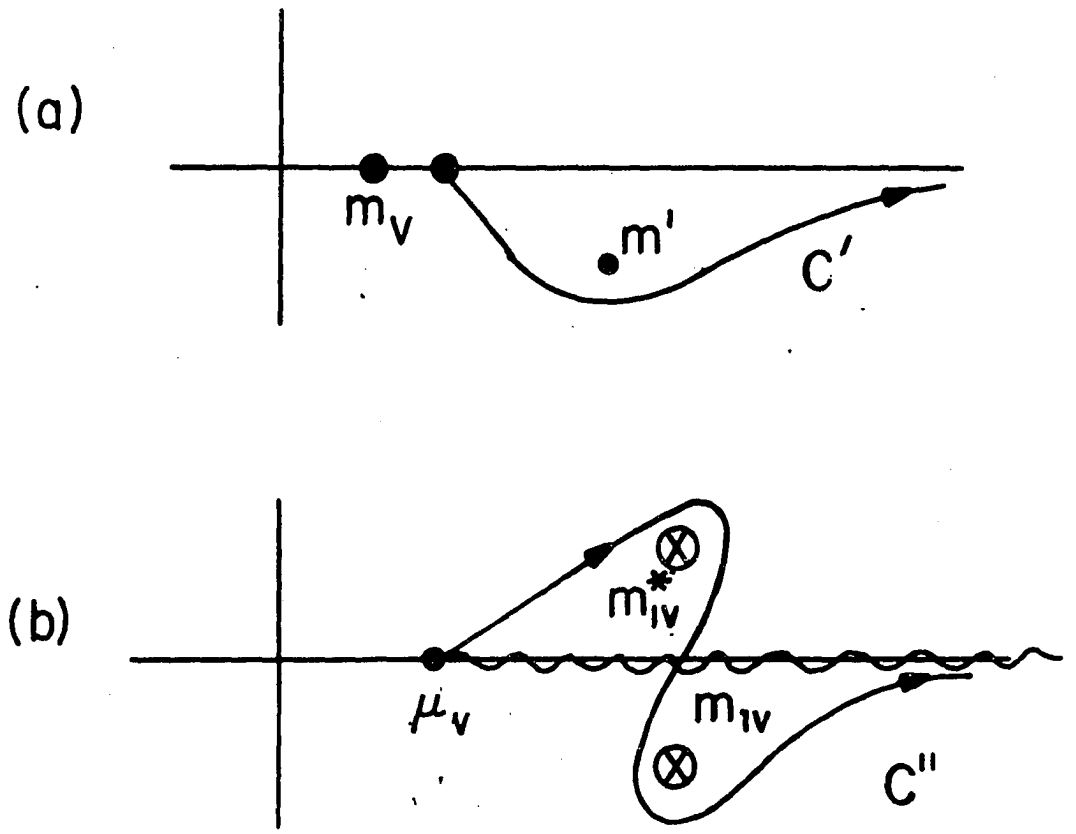

Figure 7. Integration contours in the definition of (a) $Z^{-1}(m',m_v)$ and (b) $Z_1^{-1}(m',m_{1v},m^*_{1v})$.

explicitly shown by writing

$$D_V(m') = (m'-m_V)Z^{-1}(m',m_V),$$

where the function, $Z^{-1}(m',m_V)$ is defined by

$$Z^{-1}(m',m_V) = 1 + \frac{1}{\pi}\int_{C'} dm'' \frac{\mathrm{Im}[R_V(m'')]}{(m''-m_V)(m''-m')},$$

and the contour, C', extends from μ_V to ∞ below both poles of the integrand, as shown in Fig. 7(a). The contour C then encircles the pole at m_V as well as the cut. This contour may be deformed as in Fig. 8(a). In general the cut contribution is higher order in the interaction strength and as a first approximation is usually ignored relative to the simple pole. In this approximation the propagator may be written

$$[\tfrac{1}{2}\Delta_V(q^2)]_{\mu\nu} = -iZ(m_V,m_V)\frac{q_\mu q_\nu - q^2\delta_{\mu\nu}}{q^2+m_V^2}, \qquad (2.19)$$

which is the renormalized form of Eq. (2.16) and leads to the stable particle (Clementel-Villi) form for the electromagnetic form factors.

For an unstable particle the singularities of $D_V^{-1}(m')$ consist of a conjugate pair of poles, m_{1V}, m_{1V}^*, and a branch cut corresponding to the decay products of the vector meson. The poles lie on the unphysical sheet and are defined by

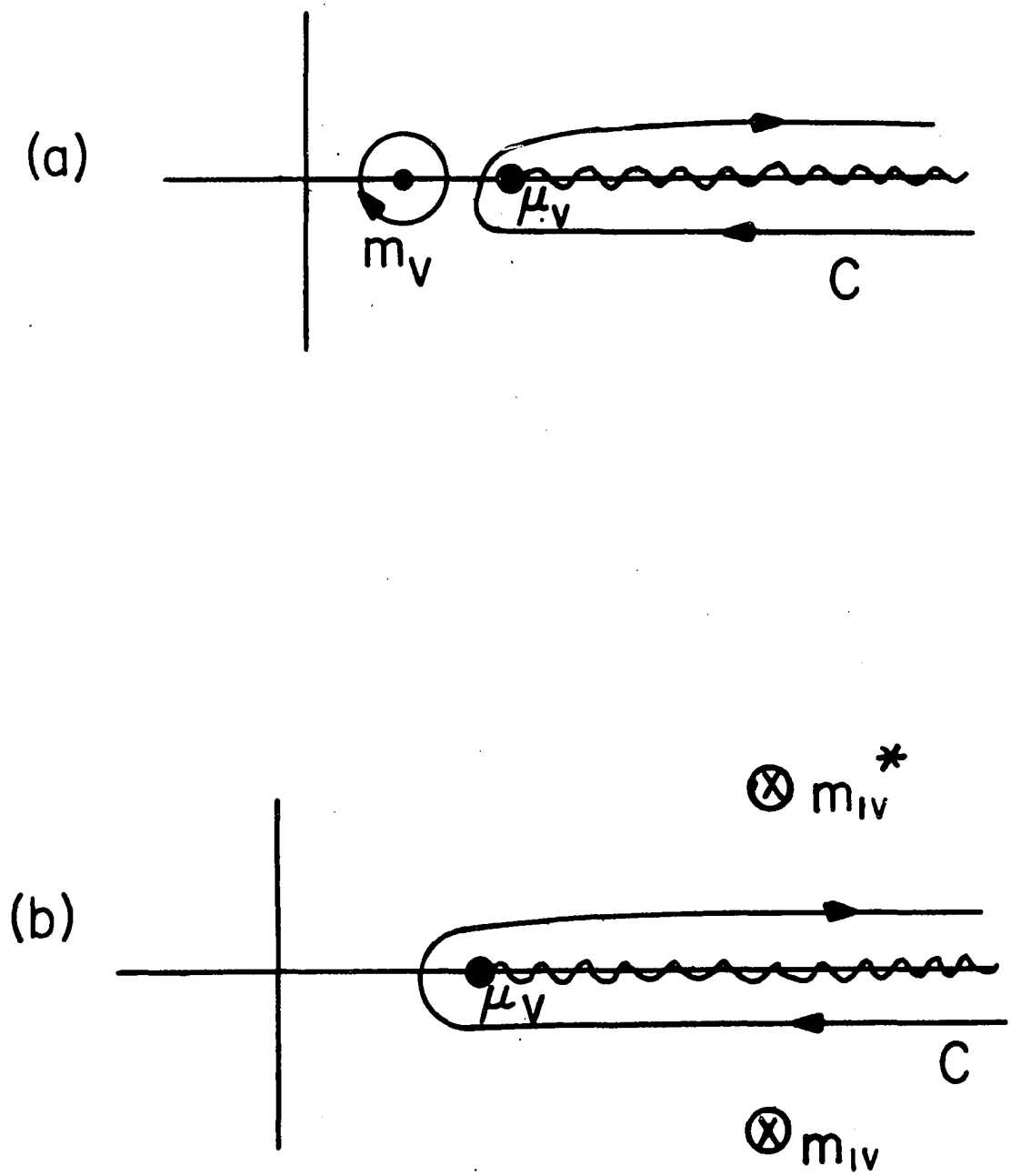

Figure 8. Integration contours in the definition of (a) the stable and (b) the unstable vector meson propagators.

$$m_{1V} = m_V - i(\Gamma_V/2),$$
$$m^*_{1V} = m_V + i(\Gamma_V/2), \qquad (2.20)$$

where m_V is the mass and Γ_V the total decay rate of the vector meson. The parameters m_V and $\Gamma_V/2$ correspond roughly to the center and width at half-maximum of a Breit-Wigner resonance shape.

The vector meson poles may be factored out of $D_V^{-1}(m')$ and a new function, $Z_1(m',m_{1V},m^*_{1V})$, defined so that

$$D_V(m') = (m'-m_{1V})(m'-m^*_{1V})Z^{-1}(m',m_{1V},m^*_{1V}),$$

where Z_1^{-1} contains the cut contribution and is defined by

$$Z_1^{-1}(m',m_{1V},m^*_{1V}) = \frac{1}{\pi}\int_{C''} dm'' \frac{\mathrm{Im}[R_V(m'')]}{(m''-m')(m''-m_{1V})(m''-m^*_{1V})}, \qquad (2.21)$$

where C'' is the contour shown in Fig. 7(b). Except for the cut, the function $Z_1(m',m_{1V},m^*_{1V})$ is analytic everywhere on the unphysical sheet and everywhere on the physical sheet except at the vector meson poles.

3. The electromagnetic form factors

Using the expressions for the vector meson propagator and the photon-vector meson vertex operator, the function $D^V_{\mu\nu}(q^2)$ can now be constructed. In order to facilitate analysis it is convenient to define a function, $G_V(q^2)$, by the equation

$$G_V(q^2) = I'_V(0) + q^{-2}[\, I_V(0) - I_V(q^2)\,], \qquad (2.22)$$

where

$$I_V(q^2) = \frac{m_V^2}{2\pi i}\int_C dm' \frac{Z_1(m',m_{1V},m_{1V}^*)}{(m'-m_{1V})(m'-m_{1V}^*)} \frac{1}{q^2+m'^2-i\varepsilon}, \qquad (2.23)$$

and

$$I_V'(0) = (dI_V(q^2)/dq^2)_{q^2=0}.$$

Then the propagator may be written

$$[\tfrac{1}{2}\Delta_F^V(q^2)]_{\mu\nu} = -i[\delta_{\mu\nu} - (q_\mu q_\nu/q^2)]G_V(q^2),$$

since

$$[\delta_{\mu\beta}-(q_\mu q_\beta/q^2)][\delta_{\beta\nu}-(q_\beta q_\nu/q^2)] = \delta_{\mu\nu}-(q_\mu q_\nu/q^2).$$

The $D_{\mu\nu}^V$ function becomes

$$D_{\mu\nu}^V(q^2) = -i(m_V^2/2\gamma_V)[\delta_{\mu\nu}-(q_\mu q_\nu/q^2)]G_V(q^2).$$

The electromagnetic and vector meson source currents, $J_\mu^{\gamma H}(x)$ and $J_\mu^{VH}(x)$, respectively, are conserved; i.e.,

$$\partial_\mu J_\mu^{\gamma H}(x) = \partial_\mu J_\mu^{VH}(x) = 0.$$

Space-translation invariance then requires that the single-particle momentum state matrix elements of these currents vanish,

$$q_\mu j_\mu^{\gamma H}(q) = q_\mu j_\mu^{VH}(q) = 0.$$

Consequently, the $q_\mu q_\nu$ terms drop out, leaving

$$D^V_{\mu\nu}(q^2)j^{VH}_\nu(q) = -i(m_V/2\gamma_V)G_V(q^2)j^{VH}_\mu(q). \tag{2.24}$$

Finally, using Eq. (2.2), the electromagnetic form factors of a spin ½ baryon are

$$\begin{aligned} f_1^{\gamma B}(q^2) &= Q_B - \sum_V g_1^{VB}(m_V^2/2\gamma_V)G_V(q^2), \\ f_2^{\gamma B}(q^2) &= (\mu_B/2m_B) - \sum_V g_2^{VB}(m_V^2/2\gamma_V)G_V(q^2), \end{aligned} \tag{2.25}$$

where the strong vector meson-baryon form factors, $g^{VB}_{1,2}$, are taken to be constants independent of q^2 and are defined by the matrix element

$$j^{VB}_\alpha(q) = i(2\pi)^{-3}\bar{u}_B(\bar{p}')[\gamma_\alpha g_1^{VB} + \sigma_{\alpha\beta}q_\beta(\mu_B/2m_B)g_2^{VB}]u_B(\bar{p}). \tag{2.26}$$

By a similar analysis, the form factor of a pseudoscalar meson is written

$$f^{\gamma P}(q^2) = Q_P - \sum_V g_{VP}(m_V^2/2\gamma_V)G_V(q^2). \tag{2.27}$$

The monopole approximation to the unstable particle propagator is obtained as outlined in Section IIC, Eq.(2.19). In this approximation the nucleon form factors take the form

$$\begin{aligned} f_1^{\gamma N}(q^2) &= Q_N - \sum_V g_1^{NV}\frac{m_V^2}{2\gamma_V}\frac{(q^2/m_V^2)}{q^2 + m_V^2}, \\ f_2^{\gamma N}(q^2) &= \frac{\mu_N}{2m_N} - \sum_V \frac{\mu_N}{2m_N} g_2^{NV}\frac{m_V^2}{2\gamma_V}\frac{(q^2/m_V^2)}{q^2 + m_V^2}. \end{aligned} \tag{2.28}$$

Using the identity

$$\frac{q^2}{q^2 + m_V^2} = 1 - \frac{1}{1 + (q^2/m_V^2)},$$

the baryon form factors may be re-written in a form originally due to Clementel-Villi (65),

$$f_1^{\gamma N}(q^2) = (Q_N - \sum_V \frac{g_1^{NV}}{2\gamma_V}) + \sum_V \frac{g_1^{NV}}{2\gamma_V} \frac{1}{1+(q^2/m_V^2)},$$
$$f_2^{\gamma N}(q^2) = (\frac{\mu_N}{2m_N} - \sum_V \frac{\mu_N}{2m_N} \frac{g_2^{NV}}{2\gamma_V}) + \sum_V \frac{\mu_N}{2m_N} \frac{g_2^{NV}}{2\gamma_V} \frac{1}{1+(q^2/m_V^2)}. \qquad (2.29)$$

It is possible that there exists no point-interaction between the photon and hadron. In that case the form factors vanish asymptotically, so Eqs. (2.29) become

$$f_1^{\gamma N}(q^2) = \sum_V g_1^{NV} \frac{(m_V^2/2\gamma_V)}{q^2 + m_V^2},$$
$$f_2^{\gamma N}(q^2) = \sum_V g_2^{NV} (\mu_N/2m_N) \frac{(m_V^2/2\gamma_V)}{q^2 + m_V^2}, \qquad (2.30)$$

which are known as the pole formulas.

4. A model for the electromagnetic form factors

As can be seen from Eq. (2.17), since $\mathrm{Im}[R_V(m')]$ receives contributions from all the elastic and inelastic decay channels of the

vector meson to all orders of the decay couplings, it cannot be calculated exactly. Thus some assumption for $\mathrm{Im}[R_V(m')]$ must be made which leads to a simplification of the mathematics. To construct such an ansatz, use can be made of the experimental fact that the vector mesons have preferred decay modes. Experimentally it is known, for example, that the ρ decays into a pair of charged pions and the ϕ into a pair of charged kaons with branching ratios of 1.0 and 0.86, respectively. Similarly, the ω decays into three pions with a branching ratio of 0.9. From dimensional analysis it is expected that the finite-width effects of an unstable vector meson depend on terms proportional to Γ_V/m_V, μ_V/m_V, and $\Gamma_V\mu_V/m_V^2$. For the ω these ratios are small quantities, so the treatment of the ω as an unstable particle is optional except for energies near the ω mass. For the ρ and ϕ on the other hand, these ratios are large, so the effects of their instability cannot be ignored.

The large two-particle decay modes of the ρ and ϕ, and the small width of the ω suggests that a reasonable ansatz is to assume that $\mathrm{Im}[R_V(m')]$ is completely determined by the two-particle decay modes. For purposes of calculation, the ω-propagator might just as well be replaced by the Breit-Wigner form. This cannot be done for the ϕ-propagator, however, due to threshold effects coming from the close proximity of the two-kaon branch point and the ϕ mass.

In order to calculate the contribution to $\mathrm{Im}[R_V(m')]$ arising from the two-particle decay, $V \to P^+P^-$, minimal vector meson coupling,

$$\partial_\mu \to \partial_\mu - ig_{VP}V_\mu, \tag{2.31}$$

is used in the free-field Lagrangian density to generate the PPV current,

$$J_\mu^{VP} = \tfrac{1}{2}i[P^+ \overleftrightarrow{\partial}_\mu P^- - P^- \overleftrightarrow{\partial}_\mu P^+] + g_{VP}P^+P^-V_\mu .$$

The interaction Lagrangian is then

$$L_{PPV} = g_{VP}V_\mu J_\mu^{VP},$$

which (except for normal-dependent terms) is physically equivalent to first order in the coupling constant to coupling the ρ to the conserved isospin current of the pion,

$$L_{\rho\pi\pi} = g_{\rho\pi}\bar{\rho}_\mu \cdot \bar{\pi} \times \partial_\mu \bar{\pi}, \tag{2.32}$$

and coupling the ϕ to the conserved strangeness current,

$$L_{\phi KK} = g_{\phi K}K^+ \overleftrightarrow{\partial}_\mu K^-\phi_\mu .$$

Using these Lagrangian densities it is straightforward to calculate the imaginary part of the level shift. The result is

$$\mathrm{Im}[R_V(m')] = (m'/24)(g_{VP}^2/4\pi)[1 - (\mu_V^2/m'^2)\ ]^{3/2}. \tag{2.33}$$

Note that for $m_V >> \mu_V$ this simplifies to

$$\mathrm{Im}[R_V(m')] = \alpha_V m', \tag{2.34}$$

where

$$\alpha_V = (1/24)(g_{VP}^2/4\pi). \tag{2.35}$$

The simplest ansatz for a model for the electromagnetic form factors is therefore to assume that the significant contributions to $R_V(m')$ occur for values of $Im[R_V(m')]$ well above threshold so that

$$Im[R_V(m')] = \alpha_V m' \; ; \; m' \geq \mu_V,$$
$$Im[R_V(m')] = 0 \quad ; \; m' \leq \mu_V, \tag{2.36}$$

where the decay thresholds are given in Table 1. This is expected to be a reasonable approximation for the space-like form factors because the q^2 values are well above threshold. Using this ansatz in Eq. (2.21), Z_1^{-1} becomes

$$Z_1^{-1}(m', m_{1V}, m_{1V}^*) = \frac{1}{\pi}\int_{C''} dm'' \frac{\alpha_V m''}{(m''-m')(m''-m_{1V})(m''-m_{1V}^*)}.$$

The pole terms are evaluated using Cauchy's residue theorem and the integral along the cut from μ_V to ∞ is evaluated using the method of partial fractions. This gives the algebraically complicated result

$$D_V(m', m_{1V}, m_{1V}^*) = -2m_V\{\frac{\Gamma_V m'}{8\pi m_V^2} \log_e[\frac{(m'-\mu_V)^2}{(m_{1V}-\mu_V)(m_{1V}^*-\mu_V)}] +$$
$$[1-\frac{m'}{m_V}+(\frac{\Gamma_V}{2m_V})^2][1 - \frac{i}{4\pi}\log_e(\frac{m_{1V}^*-\mu_V}{m_{1V}-\mu_V})] \}. \tag{2.37}$$

The phase of $m'-\mu_V$ is zero on the physical sheet above the cut and 2π below the cut. The points m_{1V} and m_{1V}^* in the logarithmic terms are

evaluated on the physical sheet. The function $D_V(m',m_{1V},m_{1V}^*)$ has a logarithmic branch point at $m'=\mu_V$ and conjugate zeros at $m'=m_{1V}$ and $m'=m_{1V}^*$ on the unphysical sheet. With this choice of phases, if m' is real and $m'<\mu_V$, then $R_V(m')$ is real, and if $m'>\mu_V$ on the real axis, then $R_V(m')$ is complex, as required.

With the choice of phase angles indicated in Fig. 9 it follows that

$$m_{1V}-\mu_V = |m_{1V}-\mu_V|\exp[-i(2\pi-\phi)],$$
$$m_{1V}^*-\mu_V = |m_{1V}^*-\mu_V|\exp(i\phi),$$
$$\phi = \tan^{-1}[\Gamma_V/2(m_V-\mu_V)],$$

for the relevant poles on the unphysical sheet, and

$$\pm iq-\mu_V = |\pm iq-\mu_V|\exp[-i(-\pi\pm\Theta)],$$
$$\Theta = \tan^{-1}(q/\mu_V),$$

for the poles on the physical sheet. Thus one has

$$1-\frac{i}{4\pi}\log_e\left(\frac{m_{1V}^*-\mu_V}{m_{1V}-\mu_V}\right) = \tfrac{1}{2}\left(1+\frac{1}{\pi}\tan^{-1}[\Gamma_V/2(m_V-\mu_V)]\right),$$

$$\log_e\frac{(\pm iq-\mu_V)^2}{(m_{1V}-\mu_V)(m_{1V}^*-\mu_V)} = \log_e\frac{\mu_V^2+q^2}{(m_V-\mu_V)^2+(\Gamma_V^2/4)} \mp 2i\tan^{-1}(q/\mu_V).$$

This phase choice is made to give $D_V(m_{1V})=D_V(m_{1V}^*)=0$ only on the unphysical sheet.

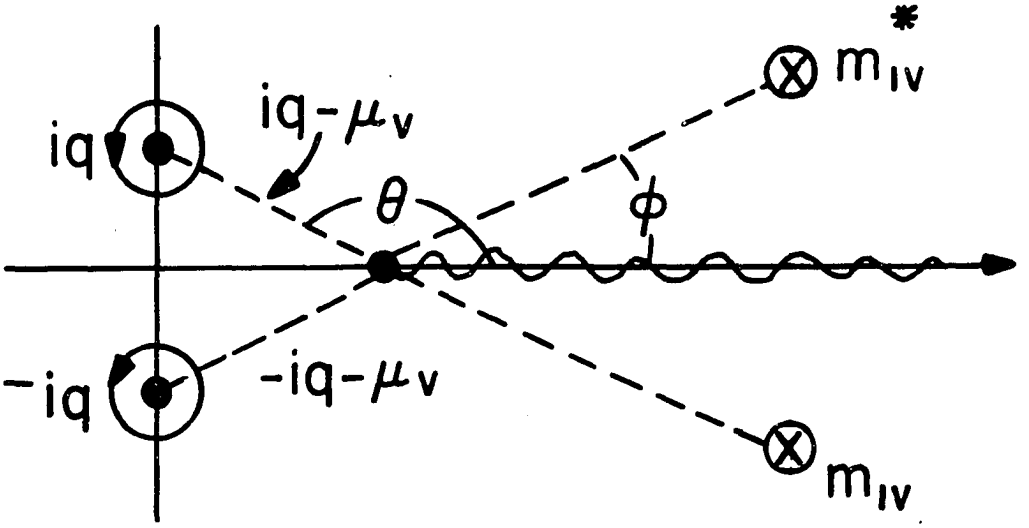

Figure 9. Phase angle definitions of the simple poles of $D_V(m')$ for space-like values of m'.

The function $I_V(q^2)$, defined by Eq. (2.23), has poles at m_{1V} and m^*_{1V} in the unphysical sheet, and at $\pm iq$ for $q^2>0$. The contour, C, in Fig. 8(b) may be closed at infinity to obtain the result depicted in Fig. 9. The pole contributions then give

$$I_V(q^2) = (m_V^2/2iq)[\ (1/D_V(iq)) - (1/D_V(-iq))\ ]. \qquad (2.38)$$

The function, I_V, is thus determined by Eq. (2.37) with $m'=\pm iq$.

In order to complete the calculation of the electromagnetic form factors the constant terms $I_V(0)$ and $I_V'(0)$ must also be calculated. This can be achieved by noting that a power series expansion of both $I_V(q^2)$ and $D_V(iq,m_{1V},m^*_{1V})$ for small values of q^2 gives, by virtue of Eq. (2.38),

$$I_V(0) = m_V^2[D_V^{-1}(0)]',$$
$$I_V'(0) = (1/6)m_V^2[D_V^{-1}(0)]'''.$$

The derivatives of $D_V^{-1}(m')$ may be written in terms of the derivatives of $D_V(m')$, which are determined by a power series expansion of $D_V(m')$ for small m'. The details are given in Appendix C.

With these results, the explicit form of the vector meson propagator, $G_V(q^2)$, can be calculated using Eq. (2.22), and thus the form factors, by Eq. (2.25)

D. Nucleon Form Factors

Since the nucleon is a member of the baryon octet, its Pauli and Dirac electromagnetic form factors are given by Eq. (2.25) with the substitution H=N, where N=p,n represents the nucleon. The corresponding electric and magnetic form factors are defined by Eqs. (2.3) as

$$G_E^N(q^2) = (Q_N-(\mu_N/4m_N^2)q^2)+\sum[q^2 g_2^{NV}(\mu_N/4m_N^2)-g_1^{NV}](m_V^2/2\gamma_V)G_V(q^2),$$
$$G_M^N(q^2) = Q_N-\mu_N-\sum_V(g_1^{NV}+\mu_N g_2^{NV})(m_V^2/2\gamma_V)G_V(q^2). \qquad (2.39)$$

As usual, the vector meson-nucleon couplings, $g_{1,2}^{NV}$, are assumed to be q^2-independent parameters. The data is fit using these expressions by minimizing the total χ^2, defined by

$$\chi^2 = \sum_{q^2}\sum_{G}\left(\frac{G_{exp}(q^2) - G(q^2)}{\sigma(q^2)}\right)^2,$$

with respect to the parameters $g_{1,2}^{NV}$. The sums are over the number of data points for each form factor, over all four form factors and the electron-proton differential cross section. The quantity $G_{exp}(q^2)$ is the experimental value of the form factor and the function $\sigma(q^2)$ is the mean standard deviation of each data point. The computer program used to locate the minima of this function is described in Appendix D.

The most abundant and accurate data on the hadronic form factors in the space-like region has been obtained for the proton and neutron. For low q^2, these measurements are precise enough to place strong constraints on theories of hadronic structure. In view of this, the nucleon form factor analysis based on the theory described in Sec. IIC is carried out in two parts. Since the space-like form factors are influenced only by the tails of the vector meson resonance peaks, the data is first fit for low q^2 with contributions from just the ρ, ω, and ϕ. The experimental evidence indicates that the higher vector mesons are so massive that

their contribution to the low q^2 behaviour cannot be very great. This part of the analysis has been reported elsewhere (66).

In the second part of the analysis, the data is fit over the whole q^2 range up to 25 $(GeV/c)^2$ with form factors containing a contribution from a heavy isovector-vector meson. This is necessary because it appears that just three vector meson propagators do not result in a rich-enough momentum structure to explain the low and high q^2 data. The extra degrees of freedom obtained by treating the mass, width and couplings of this heavy ρ as adjustable parameters is important in obtaining a satisfactory fit.

Throughout the discussion to follow this heavy ρ meson will be denoted ρ' for brevity. It is important to distinguish this particle from the experimental ρ' with a mass of 1.6 GeV and a width of 0.4 GeV. The resonance interpretation of this particle has not yet been established with certainty, so it is judicious to treat the heavy ρ resulting from a fit to the high energy nucleon form factor data as a prediction of the theory.

1. Nucleon form factors with ρ, ω, and ϕ dominance.

Considering contributions from just the three least massive vector mesons, there are a total of twelve nucleon-vector meson coupling constants to be determined by minimizing the total χ^2. Isotopic spin invariance is used to obtain six relations between these twelve couplings. From Eq. (2.26), these relations read

$$g_1^{p\rho} + g_1^{n\rho} = 0,$$
$$g_1^{p\omega} - g_1^{n\omega} = g_1^{p\phi} - g_1^{n\phi} = 0,$$
$$(\mu_p/2m_p)g_2^{p\rho} + (\mu_n/2m_n)g_2^{n\rho} = 0,$$
$$(\mu_p/2m_p)g_2^{p\omega} - (\mu_n/2m_n)g_2^{n\omega} = (\mu_p/2m_p)g_2^{p\phi} - (\mu_n/2m_n)g_2^{n\phi} = 0.$$

The six independent coupling constants are chosen as

$$g_{1,2}^{pV} \; ; \; V=\rho, \; \omega, \; \phi.$$

The minimum χ^2 determined by fitting the data with various theory functions is shown in Table 10 and was obtained with the masses and widths of the ρ, ω, and ϕ fixed at their best experimental values. The values of the coupling constants obtained are given in Table 12 under the heading, Fit 1. Table 10 includes results obtained using the unstable vector meson propagators, the monopole propagators, and the dipole and scaling laws as theory functions. As can be seen, the minimum χ^2 values correspond to a fit using the exact vector meson propagator for either the momentum range 0 to 1 GeV/c or 0 to 2 GeV/c. The chi-square per degree of freedom, χ_F^2, for the exact propagator over the range 0 to 2 GeV/c is 1.3 as compared to 2.8 for the monopole propagators and 4.2 for the dipole and scaling law model. In the latter case, the large minimum χ^2 is due to the breakdown of the scaling law and the assumption that $G_E^n=0$. These results suggest that vector meson exchange with ρ, ω, and ϕ dominance provides an adequate description of the nucleon form factors up to $q^2= 4$ $(GeV/c)^2$.

To further investigate the goodness of the fit the masses and widths of the vector mesons are included as adjustable parameters and

Table 10. Comparison of Minimum Chi-square for n Data Points

Form Factor	n	Monopole	Dipole	Exact Propagator
		Momentum Transfer 0-1 GeV/c		
G_E^p	26	16	21	22
G_M^p	13	26	40	10
G_E^n	36	37	274	24
G_M^n	15	171	19	28
Total	90	250	354	84
		Momentum Transfer 0-2 GeV/c		
G_E^p	31	22	28	31
G_M^p	27	74	131	52
G_E^n	36	36	274	24
G_M^n	15	151	19	30
Total	109	283	452	137

Table 11. Vector Meson Masses and Widths Obtained from Nucleon Form Factor Fits (in GeV).

	Fit 1[a]	Fit 2[b]	Fit 3[c]
m_ρ	0.765	0.767±0.004	0.772
Γ_ρ	0.135	$0.115^{+0.023}_{-0.002}$	0.113
m_ω	0.789	$0.797^{+0.004}_{-0.015}$	0.797
Γ_ω	0.010	0.010±0.001	0.0102
m_ϕ	1.019	1.066±0.05	1.077
Γ_ϕ	0.004	0.005±0.001	0.0048
$m_{\rho'}$			3.000
$\Gamma_{\rho'}$			0.048

[a] Fit 1: Fit to nucleon form factor data with only couplings as adjustable parameters. For a fuller discussion of this fit see Hammer, Weber, and Zidell, reference 66.

[b] Fit 2: Best fit to nucleon data for $q^2 \leq 4$ $(GeV/c)^2$ with all masses, widths and coupling constants allowed to float.

[c] Fit 3: Best fit to low and high q^2 nucleon form factor data with a contribution from a heavy ρ meson.

Table 12. Vector Meson-Nucleon Coupling Constants Obtained from Nucleon Form Factor Fits[a]

	Fit 1	Fit 2	Fit 3
$g_1^{p\rho}$	2.15	$2.6^{+0.1}_{-0.3}$	2.8
$g_2^{p\rho}$	5.50	6.67 ± 0.13	6.9
$g_1^{p\omega}$	16.17	$16.0^{+0.04}_{-1.2}$	16.2
$g_2^{p\omega}$	10.4	10.1 ± 0.2	9.3
$g_1^{p\phi}$	-6.72	-6.43 ± 0.26	-6.87
$g_2^{p\phi}$	-12.23	-12.2 ± 0.1	-11.23
$g_1^{p\rho'}$			-0.01[b]
$g_2^{p\rho'}$			-0.005[b]

[a]For a definition of the fits, see Table 11.

[b]The values of these couplings are calculated assuming $\gamma_{\rho'} = 2\gamma_{\rho}$.

the data is re-fit. The best fit corresponds to χ^2_F=1.3 and to the set of masses, widths and coupling constants labeled Fit 2 and given in Tables 11 and 12. As can be seen from these tables, the best values for the masses and widths compare favorably to the experimental masses and widths determined from an analysis and compilation of many different experiments. The results are shown graphically in Fig. 10-13. The vector dominance model utilizing the exact vector meson propagators seems to give a realistic picture of the electromagnetic form factors of the nucleon.

The variances in the masses, widths and couplings are determined by fixing the relevant parameter at some value, floating all the others, and re-minimizing the χ^2. The results obtained for the ρ mass, width and coupling constants are plotted in Fig. 14. These variances correspond to a chi-square change of 12 units, equal to the number of adjustable parameters when the masses and widths are included. They measure the sensitivity of the theory function to the parameters used to fit the data. This sensitivity is due to the strong constraints placed upon the fit by the different functional forms of the four form factors, the accuracy of the data, and the unequal amounts of data for each form factor. The values of the parameters in general change quite dramatically if, for example, only one form factor is fit.

The ratios of the vector meson-nucleon coupling constants obtained in this analysis have been measured in πN and NN scattering experiments. Only the ρ couplings deduced from such experiments are well-enough determined to permit a comparison with theory. For the ratio of the

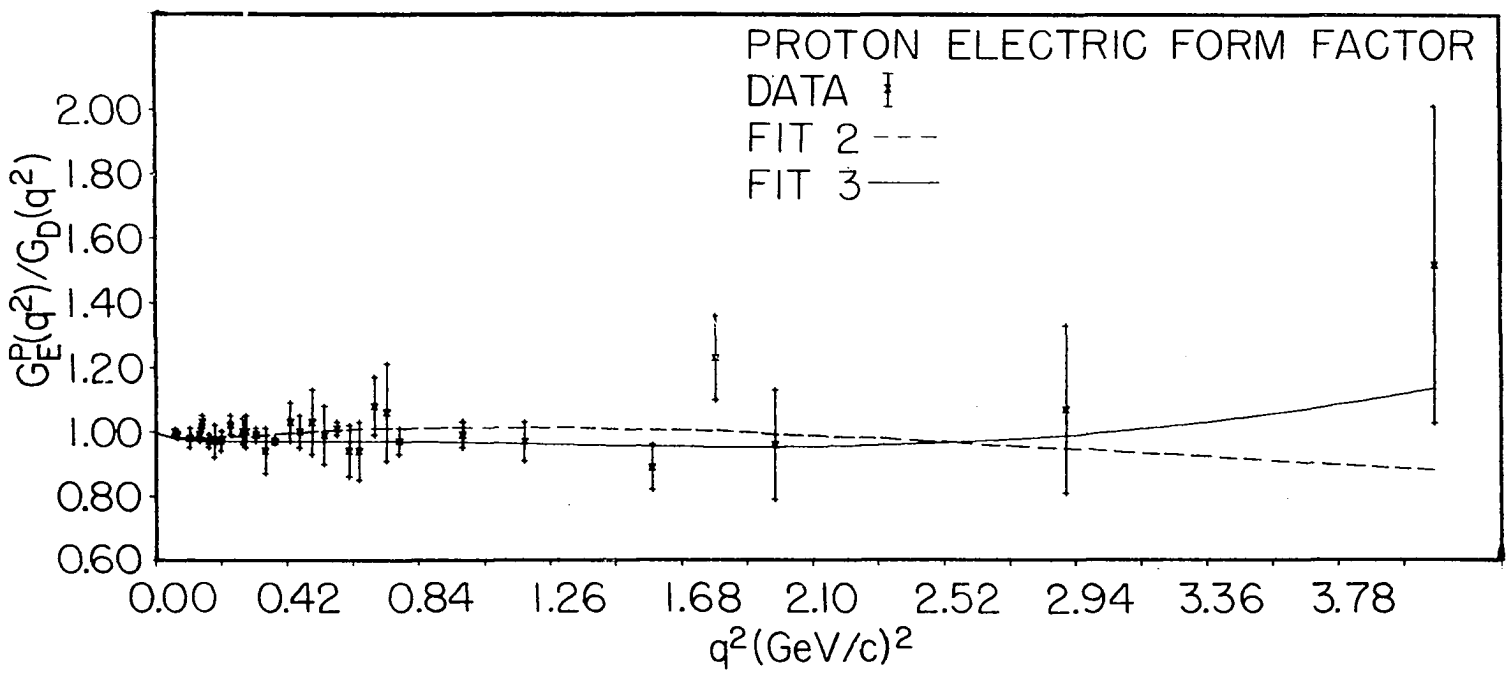

Figure 10. Dipole-normalized proton electric form factor vs q^2.

$G_D^P\ (q^2) = [\ 1 + (q^2/0.71)\ ]^2$.

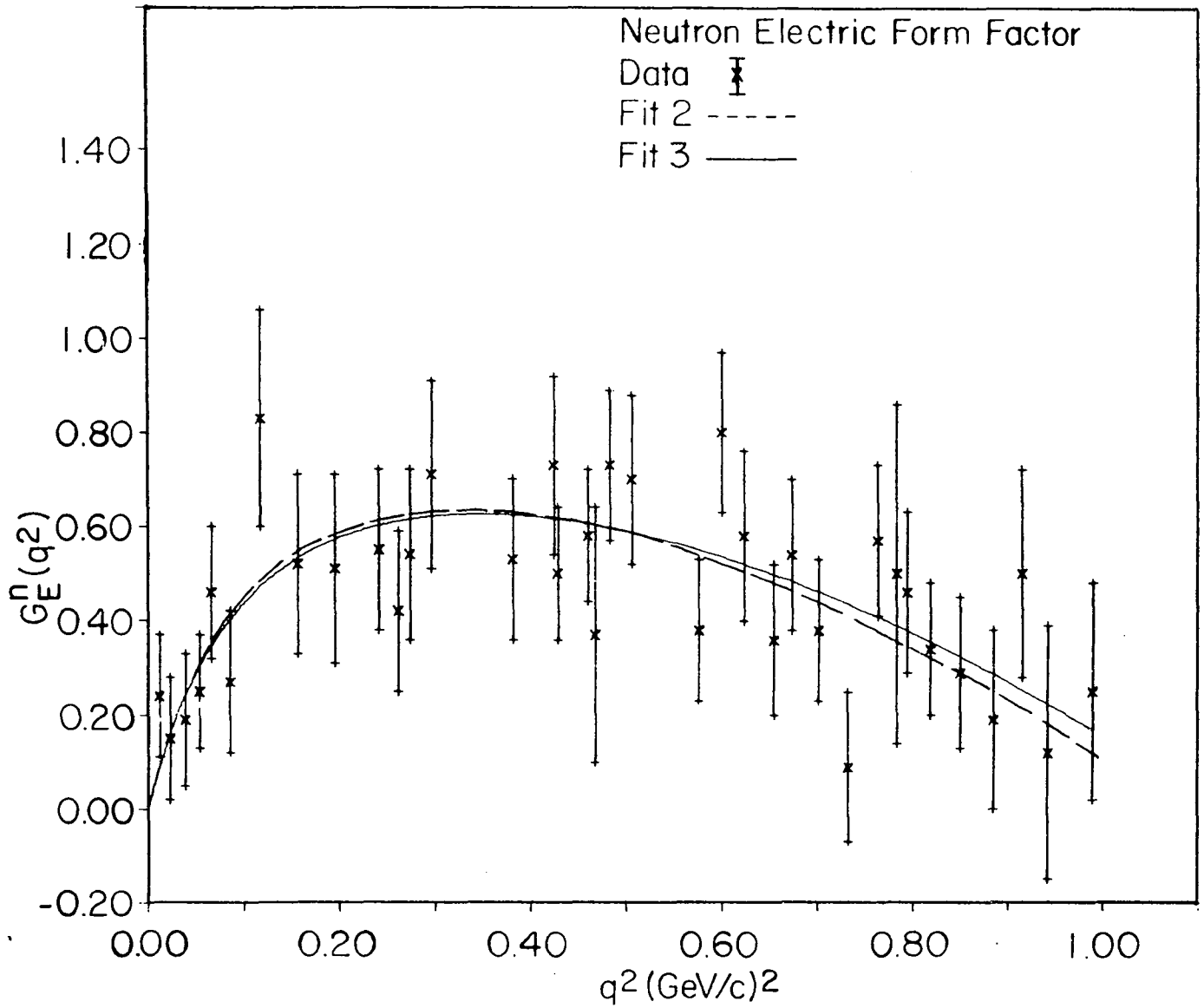

Figure 11. Neutron electric form factor vs q^2.

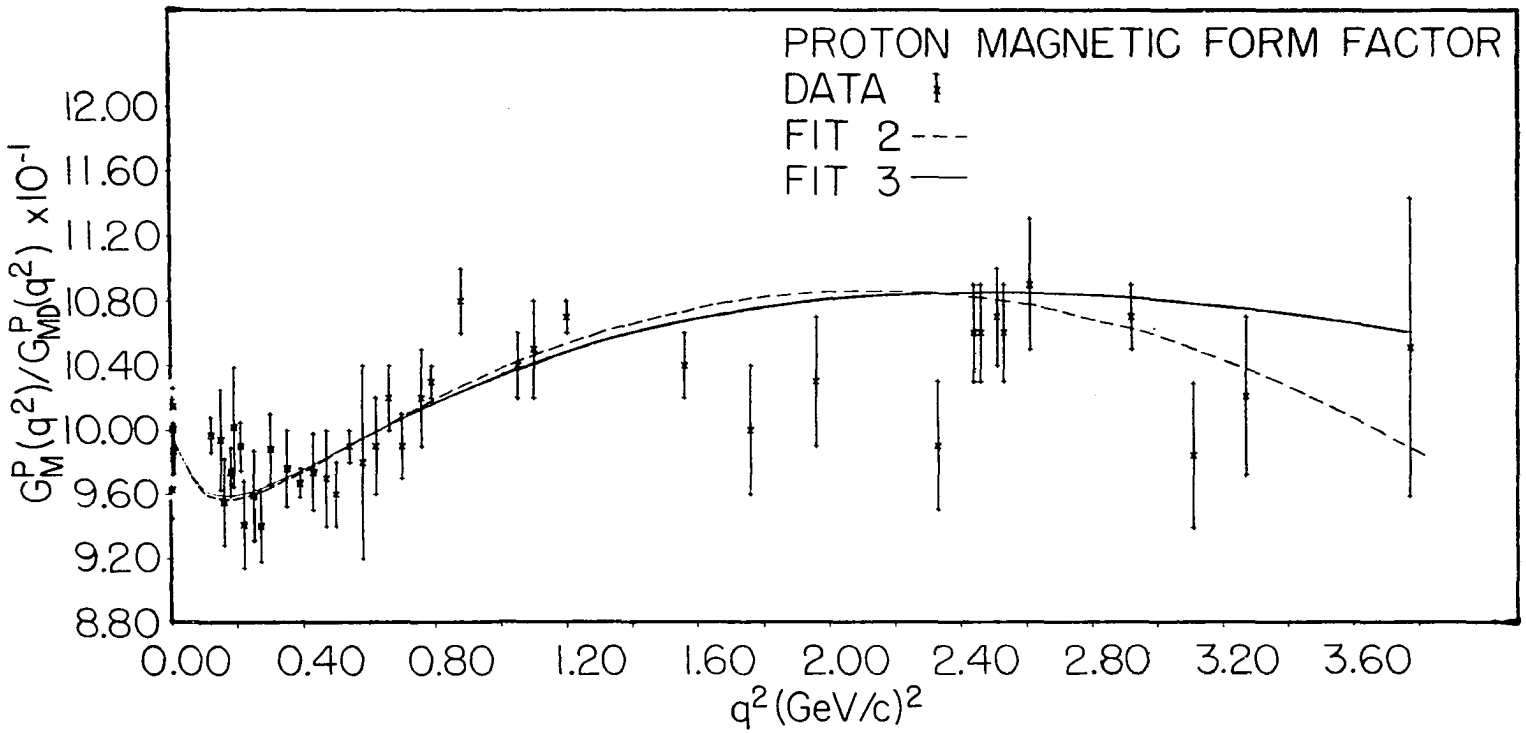

Figure 12. Dipole-normalized proton magnetic form factor vs q^2.

$$G_{MD}^{p}(q^2) = [\ 1 + (q^2/0.71)\ ]^2/\ (\ 1 + \mu_p).$$

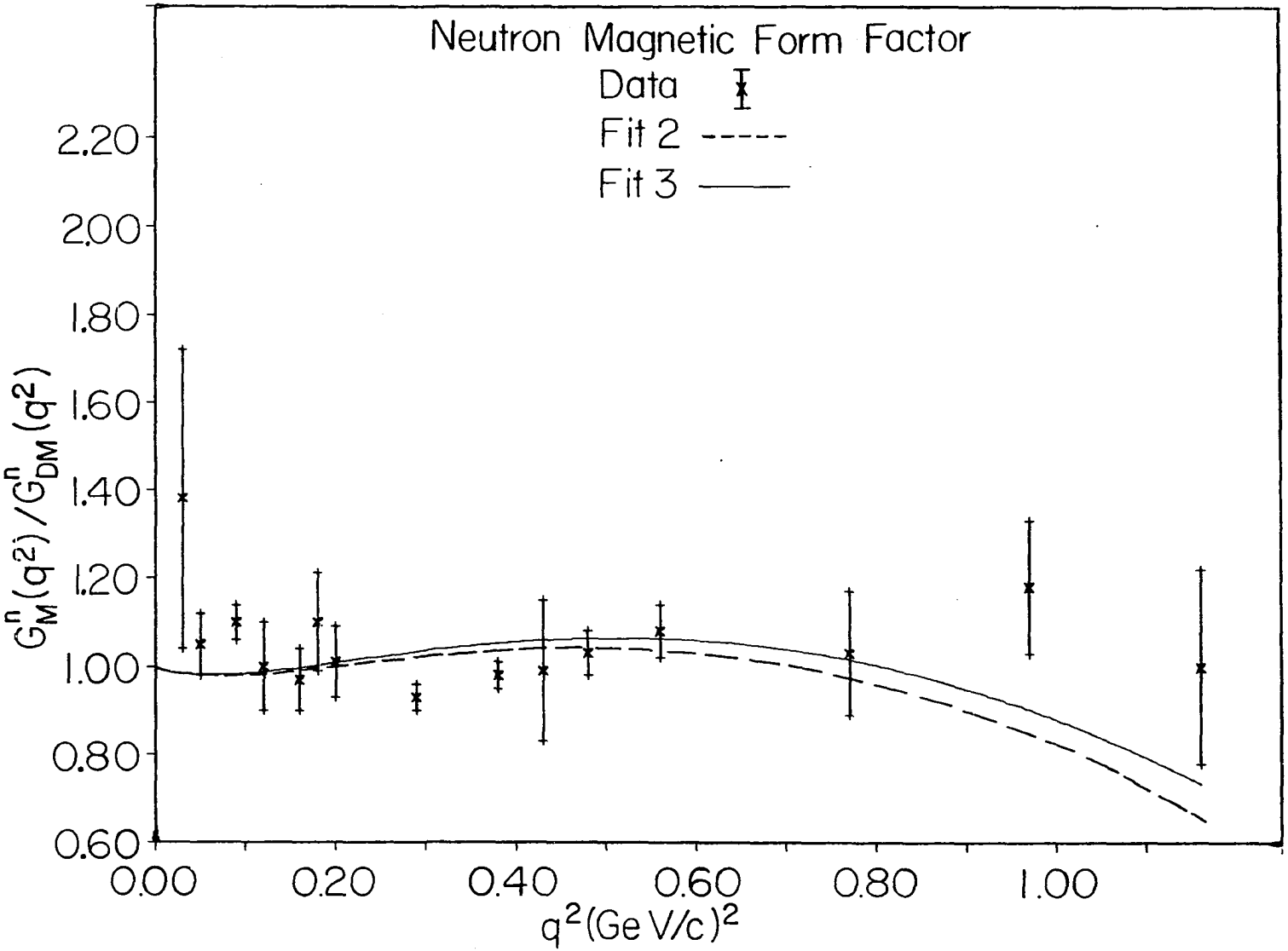

Figure 13. Dipole-normalized neutron magnetic form factor vs q^2.
$G^n_{DM}(q^2) = [\ 1 + (q^2/0.71)\ ]^2/\mu_n$.

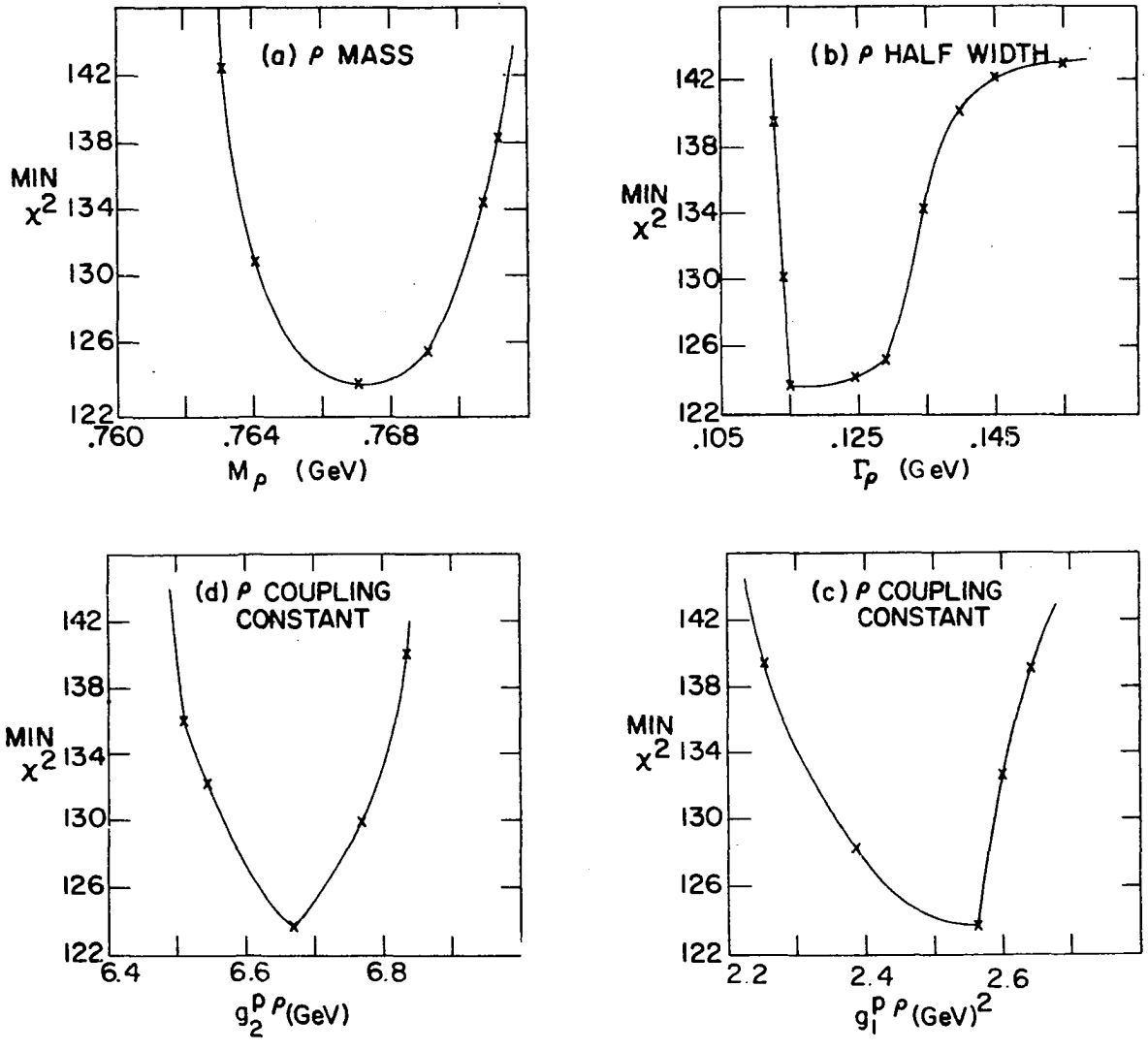

Figure 14. Correlated error plots for the ρ-parameters. (a) m_ρ vs χ^2; (b) Γ_ρ vs χ^2; (c) $g_1^{p\rho}$ vs χ^2; (d) $g_2^{p\rho}$ vs χ^2.

tensor and vector couplings of the ρ to the nucleon, experiment gives

$$\mu_p g_2^{p\rho}/g_1^{p\rho} = 1.85 - 5.2$$

depending on which model is used for the interaction. The result obtained in this analysis,

$$\mu_p g_2^{p\rho}/g_1^{p\rho} = 4.6\pm0.5,$$

falls within the generous bounds placed by experiment.

2. Nucleon sum rules

In the model constructed in Sec. IIC the possibility of a direct coupling of the photon to the nucleon is explicitly assumed. If hadronic interactions are mediated solely by vector mesons then the electromagnetic form factors must vanish as $q^2\to\infty$. By Eq. (2.25) this means that the following sum rules must be obeyed:

$$\begin{aligned} Q_N &= \sum g_1^{NV}(m_V^2/2\gamma_V)I_V'(0), \\ \mu_N/2m_N &= \sum_V g_2^{NV}(m_V^2/2\gamma_V)(\mu_N/2m_N)I_V'(0), \end{aligned} \tag{2.40}$$

since

$$\lim_{q^2\to\infty} G_V(q^2) = I_V'(0).$$

If the width of the vector meson is negligible, then the derivatives of I_V are given by the approximate forms

$$\begin{aligned} I_V(0) &= -1, \\ I_V'(0) &= 1/m_V^2, \end{aligned} \tag{2.41}$$

as discussed in Appendix C. A measure of the finite-width effects of the vector meson is the degree to which the exact values of the initial derivatives of I_V differ from Eq. (2.41).

In the small-width approximation the sum rules become

$$\begin{aligned} Q_N &= \sum (g_1^{NV}/2\gamma_V), \\ 1 &= \sum_V (g_2^{NV}/2\gamma_V). \end{aligned} \tag{2.42}$$

Thus the sum rules for the unstable particle case reduce to those for the stable particle case, Eq. (1.8). These equations may also be written in terms of their isoscalar and isovector parts. The exact charge sum rules then become

$$\begin{aligned} \tfrac{1}{2} &= (m_\rho^2/2\gamma_\rho) g_1^{p\rho} I_\rho'(0), \\ \tfrac{1}{2} &= (m_\omega^2/2\gamma_\omega) g_1^{p\omega} I_\omega'(0) + (m_\phi^2/2\gamma_\phi) g_1^{p\phi} I_\phi'(0), \end{aligned} \tag{2.43}$$

and in the small-width approximation, from Eq. (2.42),

$$\begin{aligned} g_1^{p\rho} &= \gamma_\rho, \\ g_1^{p\omega}/\gamma_\omega + g_1^{p\phi}/\gamma_\phi &= 1. \end{aligned} \tag{2.44}$$

The experimental evidence supports the conclusion that the nucleon electric and magnetic form factors drop at least as fast as q^{-4}, and perhaps faster, as q^2 goes to infinity. The representation of G_V in terms of I_V and its derivatives, Eq. (2.22), may then be used to show that, if the Pauli and Dirac form factors obey

$$\lim_{q^2 \to \infty} q^2 f_{1,2}^{\gamma N}(q^2) = 0, \tag{2.45}$$

then in addition to the charge and magnetic moment sum rules there exist the relations

$$Z_1^N = \sum_V g_1^{NV}(m_V^2/2\gamma_V)I_V(0) = 0,$$
$$Z_2^N = \sum_V g_2^{NV}(m_V^2/2\gamma_V)I_V(0) = 0. \qquad (2.46)$$

No new relations are implied if $f_{1,2}^{\gamma N}(q^2)$ goes as fast as q^{-4} as $q^2 \to \infty$.

It is clear that Eq. (2.40) may be used to define the theoretical values of the charge and anomalous magnetic moment of the nucleon which may be calculated from a knowledge of the initial derivatives of $I_V(q^2)$. Similarly, Eq. (2.46) may be used to define the asymptotic parameters Z_1^N and Z_2^N. An asymptotic bound of the form given by Eq. (2.45) thus implies $Z_1^N = Z_2^N = 0$.

The exact sum rules have been tested for 48 different data sets giving χ^2 values within 12 units of χ^2_{min}. In this way theoretical uncertainties are placed on the values of the nucleon charges, magnetic moments and asymptotic parameters determined in the analysis. The results are given in Table 13. As can be seen, they suggest that the sum rules for the proton and neutron charge and the proton magnetic moment are satisfied to within 5%, whereas the sum rule for the neutron anomalous moment is off by 50%. Physically, this means that there exists no elementary point proton; that is, in electromagnetic interactions the proton behaves as if it were a composite particle. There also exists no point charge in the neutron, though the presence of the hard core term in its magnetic structure could indicate the presence of a bare neutron. It is to be expected, however, that form factor measurements at higher

Table 13. Theoretical Values of the Proton and Neutron Charge, Magnetic Moment and Asymptotic Parameters Determined by Nucleon Form Factor Fits[a]

	Experiment[b]	Fit 1	Fit 2	Fit 3
Q_p	1.0	1.04	$1.04^{+0.01}_{-0.01}$	1.00
Q_n	0.0	0.046	$0.026^{+0.027}_{-0.011}$	0.047
μ_p	1.79	1.83	$1.80^{+0.03}_{-0.02}$	1.78
μ_n	-1.91	-2.76	$-2.87^{+0.12}_{-0.03}$	-2.81
z_1^p	0.0	-0.35	$-0.32^{+0.12}_{-0.12}$	0.11
z_1^n	0.0	1.16	$1.68^{+0.20}_{-0.50}$	-1.72
z_2^p	0.0	0.026	$0.049^{+0.017}_{-0.018}$	0.21
z_2^n	0.0	1.24	$1.24^{+0.02}_{-0.14}$	1.05

[a]For a definition of the fits see Table 11.

[b]The values in this column for the asymptotic parameters are not true experimental measurements; they are only weakly implied by the data.

q^2 will also show that the neutron is a composite particle. The quark structure of the proton and neutron, for example, is very similar, suggesting that the form factors have the same degree of compositeness and therefore possess electromagnetic form factors with the same asymptotic behaviour.

The values of Z_1^N and Z_2^N obtained from this analysis are displayed in Table 13. The experimental values quoted in this table are supported by the dipole behaviour of the form factor. Only Z_2^p is in reasonable agreement with this behaviour. This is presumably due to the lack of high q^2 data for the other form factors, making it difficult to determine the asymptotic fall-off of the form factor by extrapolation from low q^2 measurements alone. As discussed in Appendix A, the functional form of this fall-off is related to the degree of compositeness of the particle. Obviously, nothing can be said about the number of constituents in the nucleon from this analysis.

3. Nucleon electromagnetic radii

Experimentalists customarily quote values for the initial slopes of the nucleon form factors as well as the form factors themselves. The initial slopes have a special significance because they are used to define the electromagnetic radii according to the equation

$$\langle r^2 \rangle = (-6/G(0))[dG(q^2)/dq^2]_0. \qquad (2.47)$$

In this equation, $G(q^2)$ is any nucleon form factor and $G(0)$ is its value $q^2=0$. The derivative of $G(q^2)$ at $q^2=0$ is denoted by the subscript, $_0$.

The quantity $\langle r^2 \rangle$ represents the mean-square radius of the nucleon. The theoretical motivations underlying this definition are discussed at length in Appendix A. The experimental values of the nucleon radii, compiled in Table 14, are determined by fitting the small q^2 form factor data with the function

$$G(q^2) = 1 + aq^2 + bq^4 \tag{2.48}$$

and defining the charge radius by (67)

$$\langle r^2 \rangle = -6a/G(0).$$

Theoretical expressions for the nucleon radii result by taking the derivatives of both sides of Eq. (2.39). For the electric form factors,

$$[dG_E^N(q^2)/dq^2]_0 = -(\mu_N/4m_N^2) + \sum_V (m_V^2/2\gamma_V) g_1^{NV} \tfrac{1}{2} I_V''(0),$$

since $G_V(0)=0$ and

$$[dG_V(q^2)/dq^2]_0 = -\tfrac{1}{2} I_V''(0).$$

Mathematical forms for the second derivative of $I_V(q^2)$ are given in Appendix C. The definition of the charge radius then gives

$$\begin{aligned} \langle r^2 \rangle_E^p &= -6[\ (-\mu_p/4m_p^2) + \sum_V (m_V^2/2\gamma_V) g_1^{pV} \tfrac{1}{2} I_V''(0)\ ], \\ \langle r^2 \rangle_E^n &= -6[\ (-\mu_n/4m_n^2) + \sum_V (m_V^2/2\gamma_V) g_1^{nV} \tfrac{1}{2} I_V''(0)\ ]. \end{aligned} \tag{2.49}$$

Similar expressions follow for the radius of the magnetic moment distribution,

$$\langle r^2 \rangle_M^p = [-6/(1+\mu_p)] \sum_V (g_1^{pV} + \mu_p g_2^{pV}) (m_V^2/2\gamma_V) \tfrac{1}{2} I_V''(0),$$

Table 14. Nucleon Charge and Magnetic Moment Radii in Fermi

$\langle r^2 \rangle_E^{p\frac{1}{2}}$	$\langle r^2 \rangle_M^{p\frac{1}{2}}$	$\langle r^2 \rangle_E^{n\frac{1}{2}}$	$\langle r^2 \rangle_M^{n\frac{1}{2}}$	Notes
0.82±0.06	0.84±0.03	0.35±0.02	0.78±0.36	Experimental values (31)
0.81±0.03				Experimental value (152)
0.88±0.03				Experimental value (69), dipole parametrization
0.92±0.03	0.83±0.07			Experimental value (69), monopole parametrization
0.80	0.77	0.07	0.36	Three-pole theory fit (75)
0.84	0.73	0.29	0.71	Four-pole theory fit (75)
0.79	0.79	0.32	0.77	Seven-pole theory fit (75)
0.81	0.81	0.36	0.81	Dipole and scaling law fit
0.89	0.95	0.46	0.95	Fit 1
0.88±0.01	0.93±0.02	0.45±0.02	0.93±0.02	Fit 2
0.88	0.93	0.44	0.92	Fit 3

$$\langle r^2\rangle_M^n = [-6/\mu_n] \sum_V (g_1^{nV}+\mu_n g_2^{nV})(m_V^2/2\gamma_V)\tfrac{1}{2}I_V''(0), \qquad (2.50)$$

since

$$[dG_M^N(q^2)/dq^2]_0 = \sum_V (g_1^{NV}+\mu_N g_2^{NV})(m_V^2/2\gamma_V)\tfrac{1}{2}I_V''(0).$$

In Table 14 predictions for the nucleon radii using this model and using the monopole and dipole models are given. The radii calculated using the monopole propagators are based on the expressions

$$[dG_E^N(q^2)/dq^2]_0 = -\sum_V (1/2\gamma_V)[\,(g_1^{NV}/m_V^2) + (g_2^{NV}/2m_N)\,],$$
$$[dG_M^N(q^2)/dq^2]_0 = -\sum_V (1/2\gamma_V)[g_1^{NV} + 2m_N g_2^{NV}](1/m_V^2),$$

with parameters determined by a phenomenological fit to the data (68). The dipole and scaling laws imply

$$\langle r^2\rangle_E^p = \langle r^2\rangle_M^p = \langle r^2\rangle_M^n = (0.81\ \text{f.})^2,$$
$$\langle r^2\rangle_E^n = (0.36\ \text{f.})^2.$$

As can be seen, the equality between the electric and magnetic radii of the proton calculated using the theory functions in this analysis is well satisfied. However, the predicted radii obtained by fitting the form factor data using unstable particle propagators are larger than the radii determined by fitting the same data using Eq. (2.48) for small q^2. A more recent electron-proton scattering experiment (69) performed over the momentum range $0.0051 \leq q^2 \leq 0.0837$ $(\text{GeV/c})^2$ indicates that the proton radii are larger than their accepted values. This new measurement agrees with the results of this analysis. By contrast, the monopole model containing only the known vector meson pole terms

predicts radii much too small compared to even the accepted experimental values. Even formulations utilizing as many as seven monopole terms result in small nucleon radii. For details see Table 14.

The prediction for the initial slope of the neutron electric form factor given by Fit 2 is

$$[dG_E^n(q^2)/dq^2]_0 = 0.85\pm0.08 \ (\mathrm{GeV/c})^{-2},$$

which, by comparison with the experimental values reported in Table 7, is seen to be too large by about a factor of 3/2. The prediction for the neutron charge radius is therefore too large by the same factor. This slope is well measured experimentally, and constitutes an important discrepancy between theory and experiment. It may be traced to the anomalous threshold behaviour of the propagator to be discussed in Sec. IV.

4. Higher vector meson contributions to nucleon form factors

The need for high-mass particles to account for the rapid fall-off of the nucleon form factor data has been expressed by many authors. Massam and Zichichi (15) have suggested including the heavy photon of Lee and Wick (70), and Chanowitz and Drell (71) have suggested the inclusion of a 10 GeV gluon presumably responsible for binding partons in the nucleon. It has also been suggested (72-73) that a ρ' is needed in the isovector form factors in order to saturate the charge and asymptotic sum rules.

There have been a few attempts to fit the nucleon data using higher vector mesons. At least six vector mesons are needed to obtain a good fit. Zovko (74) has made six-pole fits with four free parameters,

His best fit required isovector mesons at 1.14 and 1.45 GeV, and an isoscalar meson at 1.18 GeV, in addition to the known ρ, ω, and ϕ. There is no experimental evidence for the existence of such low-mass vector mesons.

Filho and Meyer (68) have made a detailed analysis of higher vector meson contributions to the nucleon form factor data using a vector dominance model with stable particle propagators. A fit to all available data using only ρ, ω, and ϕ contributions gave $\chi_F^2=3600$. This chi-square was reduced by a factor of 300 when a ρ' at 1.6 GeV was added, and by another factor of 10 when its SU(6) partners, ω' and ϕ', were included with their couplings as free parameters. It is noteworthy that their best fit occurred for a ρ at 0.98 GeV, where none has ever been found. This points up the problem that the stable particle propagators have in fitting the low q^2 data. A similar analysis with similar results has been made by R. Felst (75), whereas Bilenkaya et al. have expressed the need for a contribution from a ρ'' at 5 GeV in addition to a ρ' at 1.28 GeV (76).

There are several theoretical grounds for believing in the existence of at least one $J^{PC}=1^{--}$ resonance above the ρ:

(1.) The quark model allows for the existence of massive quark-antiquark pairs bound in $^3D_1$ states in addition to the known $^3S_1$ octet, as well as for radial excitations of the L=0 $q\bar{q}$ ground states which act like vector mesons (77).

(2.) The Veneziano model (78) allows for the existence of an unlimited number of vector meson resonances above the known ρ, ω, and ϕ.

In this model the cuts in the scattering amplitude are approximated by an infinite set of equally-spaced poles associated with recurrences on a linearly rising Regge trajectory in the momentum-spin plane. For every parent trajectory there exists an infinite set of parallel daughter trajectories with q^2 intercepts given by the so-called "duality mass formula",

$$m_{Vn}^2 = m_V^2(1+2n); \; n=0,1,\ldots$$

For example, for the ρ it is expected from this theory that the higher vector mesons occur at the mass values

$$m_{\rho n}^2 = \{0.765,\ 1.33,\ 1.71,\ 2.03,\ldots\}.$$

There also exists ω and ϕ trajectories and their daughters (79).

(3.) Higher vector mesons have also been predicted in gauge models of the weak, strong and electromagnetic interactions (53), in an optical model description of pp scattering (80), in an analysis of πN charge exchange scattering (81), from a theoretical treatment utilizing SU(3)⊗ SU(3) (82), and in a dual resonance model of $\pi\pi$ scattering (83).

On experimental grounds many $J^{PC}=1^{--}$ enhancements are known (84, 85-86), but there is still some question as to whether they are genuine resonances or not, and if so, what their masses and widths are. A compilation of these experimental results is given in Table 15. This table may be summarized by the observation that e^+e^- annhilation into multi-meson states indicates the presence of a vector meson resonance at

$$m_{\rho'} = 1.6 \text{ GeV}; \quad \Gamma_{\rho'} = 0.35\pm0.05 \text{ GeV},$$

Table 15. Experimental Data on the Higher Vector Mesons.

	Mass (GeV)	Width (GeV)	Ref.
ρ'	1.24 ±0.02		153[a]
	1.25	0.13	154[b]
	1.25	0.150	155[c]
	1.256±0.01	0.130±0.02	156[d]
	1.3 1.8		157[a]
	1.43 ±0.05	0.65 ±0.1	157[b]
ρ'' (or ρ')	1.5	0.4	158[b]
	1.55	0.26 ±0.11	159[b]
	1.55 ±0.06	0.36 ±0.10	155[c]
	1.6		153[a]
	1.6	0.35	160[c]
	1.6 ±0.1	0.5 ±0.1	161[b]
ρ'''	1.968	0.35	162[e]
	1.6 2.0		154[a]
	1.8 2.1		153[a]

[a] Produced in $\gamma p \to p\pi^+\pi^-$ + neutrals.
[b] Produced in $\gamma p \to \omega\pi p$.
[c] Produced in $e^+e^- \to 4\pi$.
[d] Produced in $p\bar{p} \to (\omega\pi)\omega$.
[e] Produced in $p\bar{p} \to K^0\bar{K}^0$.

that couples to the photon with a strength, $\gamma_{\rho'}$, that obeys

$$(\gamma_{\rho'}/\gamma_{\rho})^2 = 4.$$

Pion-photoproduction data, on the other hand, indicates the presence of a ρ' with the parameters

$$m_{\rho'} = 1.43\pm0.05 \text{ GeV}; \; \Gamma_{\rho'} = 0.65\pm0.1 \text{ GeV};$$
$$(\gamma_{\rho'}/\gamma_{\rho})^2 = 6\pm2.$$

The discrepancies in these results is a reflection of the difficulty in identifying these enhancements as bona fide resonances due to background contamination from other processes or particles, or to the lack of a clear signature. In neither experiment is it possible to decide whether the purported enhancement is a resonance or a kinematic effect. There is some evidence, for example, for a $J^{PC}=1^{--}$ vector meson at about 1.2 GeV, though the evidence is also consistent with the assumption that it is actually a pure kinematic enhancement (87). These results tend to cast suspicion on fits incorporating higher vector mesons in monopole models. In all of the models incorporating higher vector mesons previously mentioned, vector mesons not yet observed have been introduced.

In addition to contributions from the ρ, ω, and ϕ, a contribution from a heavy ρ meson, called the ρ', is allowed for in this analysis. It is important not to confuse this ρ' with the experimental candidate for that label at 1.6 GeV. The mass, width and coupling constants of this ρ' are determined by fitting the high-energy nucleon form factor data.

For the full-range up to 25.03 $(GeV/c)^2$, the results for a minimum χ^2_F=2.5 are

$$m_{\rho'} = 3.0 \text{ GeV}; \quad \Gamma_{\rho'} = 0.048 \text{ GeV}.$$

This result should be compared to the fit over the low momentum transfer region which gave a chi-square per degree of freedom of 1.3. It is clear that the high momentum transfer region causes a significant deterioration in the quality of the fit.

The ρ' determined by this fit does not find an easy slot in the spectrum of vector meson candidates. However, recently two high mass mesons, $\psi(3105)$ and $\psi'(3695)$, have been discovered in experiments involving the production of hadronic states from electron-positron annhilation (88) and in proton scattering from light nuclei (89). Their masses and total decay rates are given in Table 1. No definite evidence for other narrow resonances with a mass less than 5.9 GeV has been found (90), though there is the hint of a broad resonance at 4.1 GeV (91).

The spin, isospin, parity, G-parity and charge conjugation properties of these particles has still to be established with certainity. Theoretical interpretations suggest they are isoscalar vector meson states: either bound states of charmed quarks (92), $\Omega\bar{\Omega}$ bound states (93), or gauge vector bosons (94). Presumably they couple to the photon and should show up in the nucleon and meson electromagnetic form factor data. It is curious that the heavy vector meson identified in this analysis should possess a mass so close to that of the $\psi(3105)$. The identification of the

two would stand on firmer ground if it turned out that $\psi(3105)$ were an isovector meson rather than an isoscalar meson as predicted by SU(4). The ρ'-nucleon couplings determined by the data analysis, for example,

$$g_1^{p\rho'}/2\gamma_{\rho'} = -0.0017,$$
$$g_2^{p\rho'}/2\gamma_{\rho'} = -0.00083,$$

are qualitatively in agreement with the experimental observation that the two-body decay modes of the ψ and ψ' into hadrons are strongly suppressed. From Tables 13 and 14 it is apparent that the addition of the ρ' does not improve the predictions for the sum rules or the electromagnetic radii significantly. This is a consequence of the large mass and small width of the ρ'. Since it is located at a smaller value of time-like q^2 than the other mesons, its effect at the origin is diminished.

E. Pion and Kaon Form Factors

From Eq. (2.27) the electromagnetic form factor of the charged pion is written

$$f^{\gamma\pi}(q^2) = 1 - \sum_V g_{V\pi}(m_V^2/2\gamma_V)G_V(q^2), \qquad (2.51)$$

where the sum includes only contributions from the isovector mesons because $g_{\omega\pi}=g_{\phi\pi}=0$ by G-parity conservation of the strong interactions. The neutral pion has no charge form factor because it is its own antiparticle; that is, the π^0 field transforms into itself under charge conjugation (27).

For the charged kaon no symmetry considerations exist which prevent the existence of isoscalar or isovector contributions to its electromagnetic form factors. Furthermore, $K^0 \neq \bar{K}^0$ under charge conjugation, so the neutral kaon may possess a form factor. By analogy to the pion, then,

$$2f^{VK}(q^2) = 1 - \sum 2g_{VK}(m_V^2/2\gamma_V)G_V(q^2),$$
$$2f^{SK}(q^2) = 1 - \sum_V 2g_{VK}(m_V^2/2\gamma_V)G_V(q^2). \qquad (2.52)$$

The form factors of the charged and neutral kaons are defined by Eq. (2.8). The sums in Eq. (2.52) are over the isovector and isoscalar mesons, respectively.

Since neither the space-like pion or kaon data represents direct measurements of the electromagnetic form factors, an attempt to fit the data would lead to misleading values of the vector meson-pion and kaon coupling constants. However, the pion form factor may be related to the isovector nucleon form factor under the assumption of vector meson universality. Analogous to charge universality, vector meson universality is the statement that the vector mesons couple to all hadrons with a universal strength. The exact form of the universality relations between coupling constants depends on utilizing some internal symmetry group to describe the hadrons collectively. The minimum symmetry obeyed by the hadrons appears to be broken SU(4). If g_ρ, g_ω, and g_ϕ represent the universal couplings constants of the known vector mesons, then SU(4) predicts that

$$g_\rho = g_{\rho\pi} = 2g_1^{p\rho} = 2g_{\rho K},$$
$$g_\omega = 2g_{\omega K} = (2/3)g_1^{p\omega};\ g_{\omega\pi} = 0,$$
$$g_\phi = \sqrt{2}g_{\phi K};\ g_1^{p\phi} = g_{\phi\pi} = 0. \qquad (2.53)$$

The assumptions going into these predictions and a deeper discussion of vector meson universality is given in Appendix B.

The value for the ρ-π coupling constant obtained from this analysis is

$$g_{\rho\pi} = 2g_1^{p\rho} = 5.2\pm0.4,$$

or

$$g^2_{\rho\pi}/4\pi = 2.2\pm0.4,$$

which is in excellent agreement with the experimental value (63) set by the 2π decay mode of the ρ,

$$g^2_{\rho\pi}/4\pi = 2.56\pm0.25.$$

Banerjee and Levinson (95) have made an analysis of the data bearing on the question of ω-universality. Their result for the universal ω-coupling gives

$$g_{\omega K} = 4.0\pm0.5,$$

which is in fair agreement with the coupling predicted on the basis of this analysis,

$$g_{\omega K} = g_1^{p\omega}/3 = 5.3\pm0.3.$$

The universality relations given in Eq. (2.53) may be used to obtain expression for the form factors of the pseudoscalar mesons according to Eqs. (2.51) and (2.52),

$$f^{\gamma\pi}(q^2) = 1 - 2g_1^{p\rho}(m_\rho^2/2\gamma_\rho)G_\rho(q^2) + \text{HVMT} = 2f_1^V(q^2),$$

$$f^{\gamma K^+}(q^2) = 1 - g_1^{p\rho}(m_\rho^2/2\gamma_\rho)G_\rho(q^2) - (g_1^{p\omega}/3)(m_\omega^2/2\gamma_\omega)G_\omega(q^2)$$
$$- g_{\phi K}(m_\phi^2/2\gamma_\phi)G_\phi(q^2) + \text{HVMT},$$
$$f^{\gamma K^0}(q^2) = g_1^{p\rho}(m_\rho^2/2\gamma_\rho)G_\rho(q^2) - (g_1^{p\omega}/3)(m_\omega^2/2\gamma_\omega)G_\omega(q^2)$$
$$- g_{\phi K}(m_\phi^2/2\gamma_\phi)G_\phi(q^2) + \text{HVMT}, \qquad (2.54)$$

where HVMT means Higher Vector Meson Terms. These equations permit a prediction of the pion and kaon charge form factors in the space-like region from a knowledge of the nucleon charge couplings and an experimental value for $g_{\phi K}$.

Here, as in the nucleon case, the analysis is divided into two parts: pion and kaon form factors with ρ, ω, and ϕ dominance, and higher vector meson contributions to pion and kaon form factors.

1. Pion and kaon form factors with ρ, ω, and ϕ dominance

In Fig. 15 a comparison of the fit to twice the isovector part of the nucleon charge form factor, $2f_1^V(q^2)=f^{\gamma\pi}(q^2)$, and to the space-like pion data is made. The upper and lower solid curves labeled "bounds" correspond to the upper and lower bounds on f_1^V within the parameter tolerances listed in Tables 11 and 12. Both nucleon fits 2 and 3 are seen to fall between the bounds. The curves give good agreement with the high q^2 data considering the heavy theory dependence going into the determination of the pion data. The data is seen to lie higher than the theory predictions for q^2 values less than 2 $(\text{GeV/c})^2$. Note that the addition of the 3 GeV ρ' does not alter the prediction for the pion form factor significantly.

In Fig. 16 the predictions for the space-like kaon form factor using SU(4)-universality and an experimental value, $g_{\phi K}=4.6\pm0.2$, for the

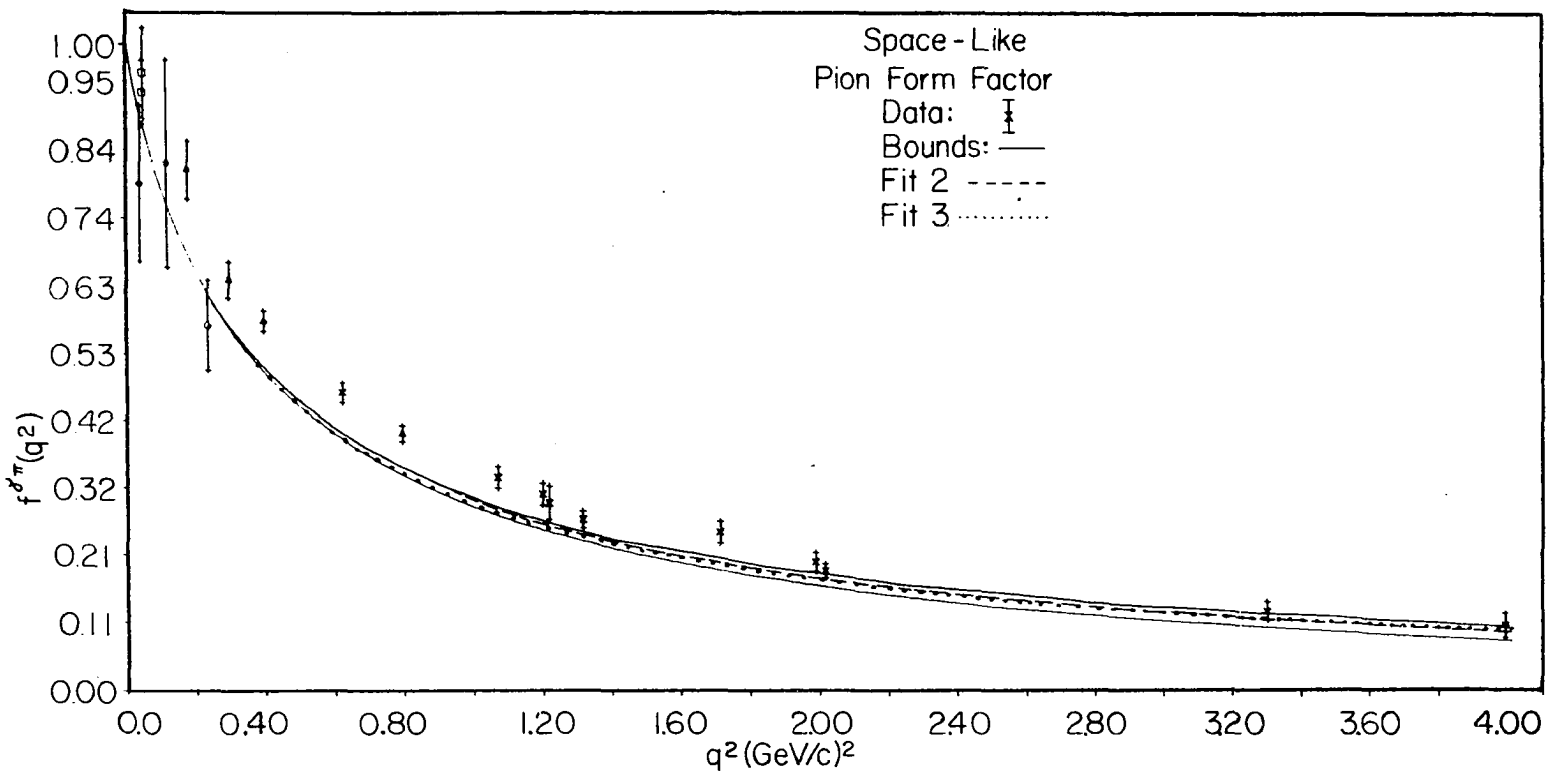

Figure 15. Space-like pion form factor vs q^2. The curves represent ρ-universality predictions based on fits to the nucleon form factor data.

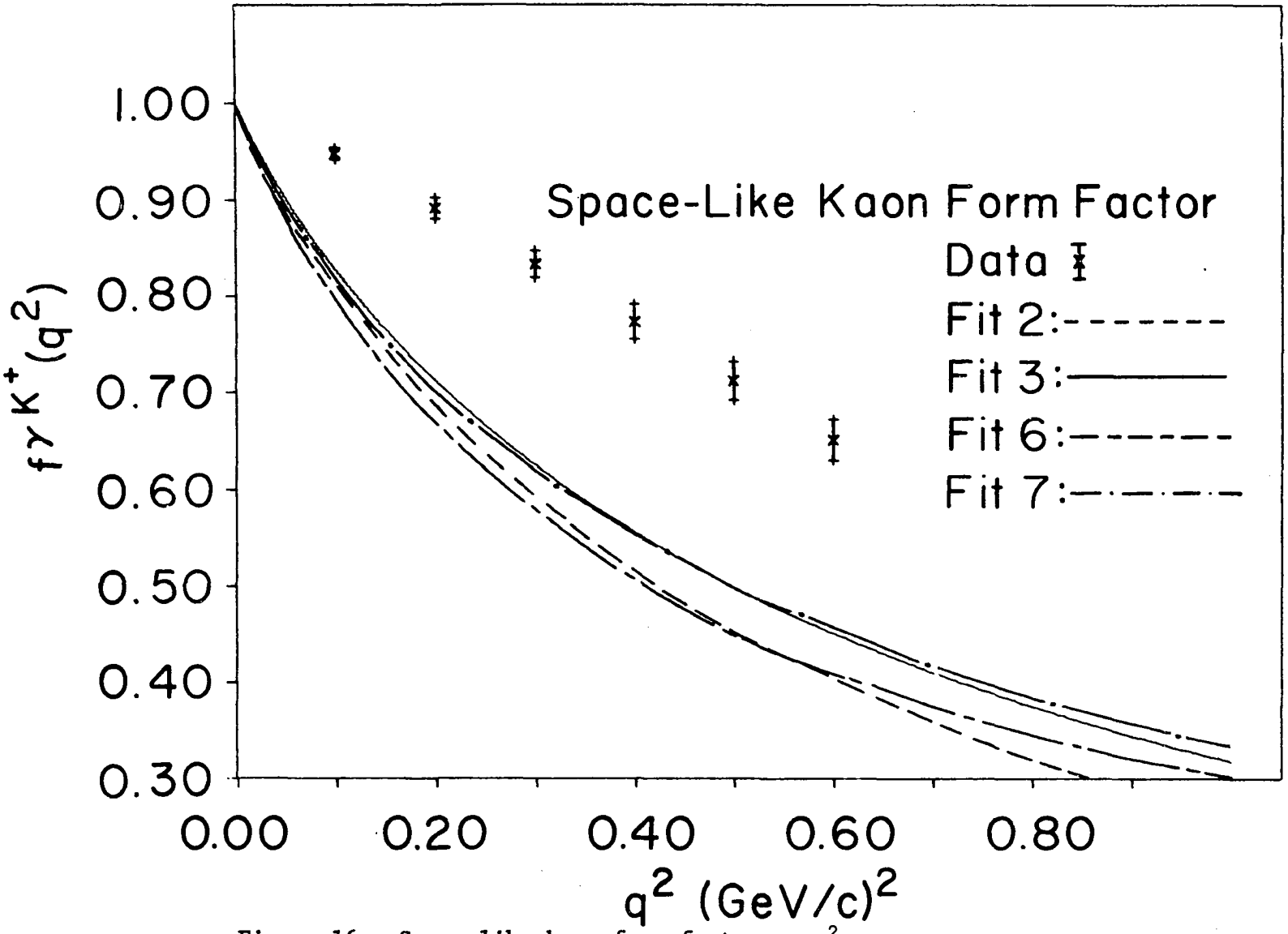

Figure 16. Space-like kaon form factor vs q^2.

ϕ-kaon coupling are given. The theory predictions for both Fits 2 and 3 are clearly inconsistent with the data, but this data is unreliable for the reasons outlined in Sec. IIB. The validity of the universality relations used to derive this form for the kaon form factor are also open to question.

2. Pion and kaon sum rules

If the pseudoscalar meson form factors vanish at least as fast as q^{-2}, then the two conditions,

$$\lim_{q^2\to\infty} f^{\gamma P}(q^2) = 0,$$
$$\lim_{q^2\to\infty} q^2 f^{\gamma P}(q^2) = 0, \tag{2.55}$$

imply the two sum rules,

$$Q_P = \sum_V g_{VP}(m_V^2/2\gamma_V) I_V'(0),$$
$$Z_P = \sum_V g_{VP}(m_V^2/2\gamma_V) I_V(0) = 0. \tag{2.56}$$

For the pion, the sums in Eq. (2.56) cover only the isovector mesons. Complete ρ-dominance of the pion form factor then implies

$$1 = g_{\rho\pi}(m_\rho^2/2\gamma_\rho) I_\rho'(0),$$
$$0 = g_{\rho\pi}(m_\rho^2/2\gamma_\rho) I_\rho(0) = Z_\pi.$$

Since the initial derivatives of I_ρ are non-zero, these equations are inconsistent. This suggests that either complete ρ-dominance of the pion form factor is faulty and higher isovector resonances are required to saturate Eq. (2.56), or that the momentum dependence of the ρ-

propagator is more complicated. The parameters of Fit 2, for example, yield

$$Q_\pi = 1.02;\ Z_\pi = -0.49,$$

where Z_π is the asymptotic parameter for the pion defined by analogy to Z_1^N. The charge sum rule is in good agreement with $Q_\pi=1$, whereas Z_π is seen to be very different from zero, suggesting that the pion form factor predicted by universality decreases at a rate no faster than the monopole. Note that the addition of a ρ' in the sum of Eq. (2.56) changes the situation significantly. For Fit 3,

$$Q_\pi = 0.95;\ Z_\pi = 0.3.$$

The change of sign of Z_π suggests that a set of ρ' parameters exists for which $Z_\pi=0$ exactly.

These predictions as well as those for the charged and neutral kaons are compiled in Table 16. The experimental values quoted for Z_P are only weakly supported by the data; they do not represent real measurements. As can be seen from this table, the kaon charge sum rules differ from the experimental values of the charge by more than 20%. This is probably an indication that SU(4) universality is not an adequate basis for predicting the behaviour of the kaon charge form factors.

3. Pion and kaon electromagnetic radii

The electromagnetic charge radii of the pion and kaon are defined according to Eq. (2.47) by the equations

$$\langle r^2\rangle_\pi = -6[g_{\rho\pi}(m_\rho^2/2\gamma_\rho)\tfrac{1}{2}I_\rho''(0)] + \text{HVMT},$$

Table 16. Predictions of Pseudoscalar Meson Charges and Asymptotic Parameters based on Nucleon Fits

	Experiment	Fit 1	Fit 2	Fit 3
Q_π	1.0	1.00	1.02	0.95
Q_{K^+}	1.0	1.23	1.24	1.20
Q_{K^0}	0.0	0.23	0.22	0.24
Z_π	0.0	-0.46	-0.49	0.30
Z_{K^+}	0.0	-0.84	-0.90	-0.50
Z_{K^0}	0.0	-0.38	-0.41	-0.77

$$\langle r^2\rangle_K = -6\left[\sum_V (g_{VK}/2)(m_V^2/2\gamma_V)^{1/2} I_V'(0)\right] + \text{HVMT.} \qquad (2.57)$$

Complete ρ-dominance of the pion form factor in the zero-width limit suggests that

$$\langle r^2\rangle_\pi = -6/m_\rho^2 = 0.36\ f^2,$$

since $I_\rho''(0)=1/m_\rho^4$ in this approximation.

In Tables 17 and 19 experimental values for the charge radii of the charged pion and charged and neutral kaons are quoted. The experimental measurements obtained from different experiments are seen to be in poor agreement with one another. The general trend is that pion electroproduction experiments predict smaller values for the pion charge radius than direct measurements in eπ scattering experiments.

Kellet and Verzegnassi (96) have argued that values of the pion form factor extracted from pion electroproduction experiments have a latent theoretical error of unknown magnitude due to the existence of subtraction constants usually ignored in the analysis. The data is consistent with a pion form factor varying at least between $f^{\gamma\pi}$ and G_E^p, or, with a pion radius varying at least from 0.63 to 0.88 f. The values of the pion charge radius derived from the electroproduction data are thus too indefinite for a comparison with theory. In an attempt to improve this situation, the same authors have employed an optimal extrapolation technique to determine the charge radius using the electroproduction experiments (97). They conclude that the pion charge radius is very large relative to the simple vector meson dominance result: $\langle r^2\rangle_\pi^{1/2}=0.96\pm0.2$ f.

Table 17. Experimental Values of the Pion Charge Radius in Fermi

$\langle r^2 \rangle_\pi^{\frac{1}{2}}$		Notes	Ref.
0.86 ±0.14	(m)[a]	$e^- p \to e^- \pi^+ n$ (pion electroproduction)	43
0.80 ±0.10	(m)		42
0.60 ±0.02	(m)	Data region: $q^2 \leq 1$ (GeV/c)^2	41
0.67 ±0.02	(d)[b]		41
0.61	(p)[c]	Data region: $q^2 \leq 2$ (GeV/c)^2	44
0.704±0.007	(d)	Data region: $q^2 \leq 4$ (GeV/c)^2	44
0.73 ±0.13	(m)	$\pi^- p \to e^+ e^- n$ (inverse pion electroproduction)	105
0.78 ±0.10	(m)	$e^- \pi^- \to e^- \pi^-$ (electron-pion scattering)	98
0.71 ±0.05	(c)[d]		99
0.98 ±0.24	(m)	$e^- p \to e^- \pi^+ n$ (pion electroproduction)	163

[a](m) indicates a fit using the monopole formula.

[b](d) indicates a fit using the dipole formula.

[c](p) indicates a fit using a polynomial formula.

[d](c) indicates a fit using Chebykov polynomials.

The most precise and model-independent determination of the charge radius of the pion was made in a recent electron-pion elastic scattering experiment (98) over the momentum transfer range 0.0353 to 0.0138 $(GeV/c)^2$. This experiment gives

$$\langle r^2 \rangle_\pi^{\frac{1}{2}} = 0.78 \pm 0.10 \text{ f} \qquad (2.59)$$

for the charge radius of the pion and

$$[\langle r^2 \rangle_\pi / \langle r^2 \rangle_E^p]^{\frac{1}{2}} = 0.96 \pm 0.12$$

for the ratio of the pion and proton charge radii (99).

Models of the pion form factor based on complete ρ-dominance are therefore seen to be in poor agreement with recent experimental results. In Table 18 values for the pion charge radius based on a variety of vector meson dominance theories are given. It is apparent that the introduction of finite-width effects, correct threshold behaviour, or additional vector mesons in the conventional manner do not seem to improve the situation markedly. The pion charge radius predicted on the basis of the model presented in this work is

$$\langle r^2 \rangle_\pi^{\frac{1}{2}} = 0.85 \pm 0.02 \text{ f},$$

for fit 2. The other fits fall within the narrow limits allowed by the correlated errors of the ρ parameters. This prediction is in good agreement with the latest experimental result. This underscores the importance of incorporating instability into the vector meson dominance model in a consistent manner.

Table 18. Theoretical Values of the Pion Charge Radius in Fermi

$\langle r^2 \rangle_\pi^{1/2}$	Notes	Ref.
0.63	Simple pole model (m_ρ=0.770)	
0.59 0.69	Dipole model	
0.81	Assume $f^{\gamma\pi}(q^2)=G_E^p(q^2)$	
0.65	Three-pole fit (ρ,ρ',ρ'')	120
0.58 0.69	Gounaris-Sakurai propagator	164
0.709±0.011	Generalized Gounaris-Sakurai	112
0.63	Frazer-Fulco	165
0.67	Veneziano model	119
0.87	Fit 1	
0.85 ±0.02	Fit 2	
0.86	Fit 3	
0.98	Fit 4	
0.94	Fit 5	
0.94 ±0.13	Fit 7	
0.94	Fit 9	
0.75 ±0.05	Fit 10	

The predictions for the charged and neutral kaon radii are in agreement with the data only for the K^0. The K^+ radius is based on form factors indirectly determined by Mickens and Rush (49) on the basis of K^+K^+ scattering. This data has been ignored in the analysis due to the dubious status of the theory used to deduce it.

4. Higher vector meson contributions to pion and kaon form factors

In Fit 3 a contribution from a 3 GeV ρ' is needed to obtain a fit to the four nucleon form factors. Thus a contribution from this particle automatically accrues to the pion and kaon form factors through the universality relations, Eq. (2.53). These relations are easily extended to include the ρ' through the requirement of isovector dominance of the pion form factor; that is, $2g_1^{p\rho}=g_{\rho\pi}$, $2g_1^{p\rho'}=g_{\rho'\pi}$.

The predictions for Q_p, Z_p and $\langle r^2\rangle_p$ based on these universality relations and on the parameters determined by Fit 3 are given in Tables 16, 18 and 19. The charge sum rules are essentially unchanged by the introduction of this particle, but a large change is to be noted in the predictions for the asymptotic parameters. It is difficult to connect this change solely to the introduction of the ρ' because the ρ, ω, and ϕ masses, widths and couplings also take on new values. Due to the small $\Gamma_{\rho'}/m_{\rho'}$ ratio of the ρ', its effect on the charge sum rules is only to change them by an amount $g_1^{p\rho'}/2\gamma_{\rho'}\simeq 2\times 10^{-3}$. Its effect on the asymptotic sum rule is about ten times larger due to the factor m_ρ^2, multiplying $g_1^{p\rho'}/2\gamma_{\rho'}$.

Note that there is no appreciable effect on the radii of either the pion or the charged and neutral kaons due to the introduction of the ρ'. This is consistent with the observation that the contribution to the radius

Table 19. Experimental and Theoretical Values of the Charged and Neutral Kaon Radii in Fermi

$\langle r^2 \rangle^{1/2}_{K^0}$	$\langle r^2 \rangle^{1/2}_{K^+}$	Notes	Ref.
	0.39±0.03	K^+K^+ scattering	49
	0.58	SU(3)-monopole	
0.25-0.28		Kroll-Lee-Zumino	16
0.22±0.22		eK^0 scattering	166
0.17	0.63	Six-pole fit	120
0.40	0.78	Fit 1	
0.39	0.76	Fit 2	
0.40	0.76	Fit 3	
0.42	0.80	Fit 6	
0.56	0.76	Fit 7	
0.54	0.76	Fit 9	

from a given vector meson is $6g_{VP}(m_V^2/2\gamma_V)\frac{1}{2}I_V''(0)$. For the ρ' this amounts to only $6g_1^{p\rho'}/2\gamma_{\rho'}m_{\rho'}^2 \simeq 6\times10^{-4}$ $(GeV/c)^{-2}$ since $I_V''(0)\simeq -1/m_V^4$ in the small-width approximation.

III. TIME-LIKE ELECTROMAGNETIC FORM FACTORS

This chapter consists of a discussion of the time-like electromagnetic form factors of hadrons. These form factors are measured in colliding beam experiments involving the annhilation of leptons with the subsequent creation of hadronic states. The form factors involved in such a process are defined in Section A and the character of the experiments used to measure them are discussed in Section B. The theory of time-like form factors, presented in Section C, closely follows that of the space-like form factors because they are related simply by analytic continuation. Finally, the time-like electromagnetic form factors of the proton, pion and kaon are discussed in Section D.

A. Definition

Consider the annhilation of an electron-positron pair into a hadron-antihadron pair. The Feynman diagram describing this process is given in Fig. 17. In this diagram $p_-=(\bar{p}_-,E_-)$ and $p_+=(\bar{p}_+,E_+)$ are the four-momenta of the electron and positron, respectively. To denote the hadron momenta primed quantities are used in a similar way. The four-momentum of the virtual photon is given as usual by four-momentum conservation as

$$q = p_- + p_+ = p'_- + p'_+,$$

and is a time-like quantity; i.e., $q^2<0$. The blob at the photon-hadron vertex in Fig. 17 represents the set of all strongly-interacting states which mediate the conversion of a time-like virtual photon into hadronic matter. This vertex is described by the matrix element

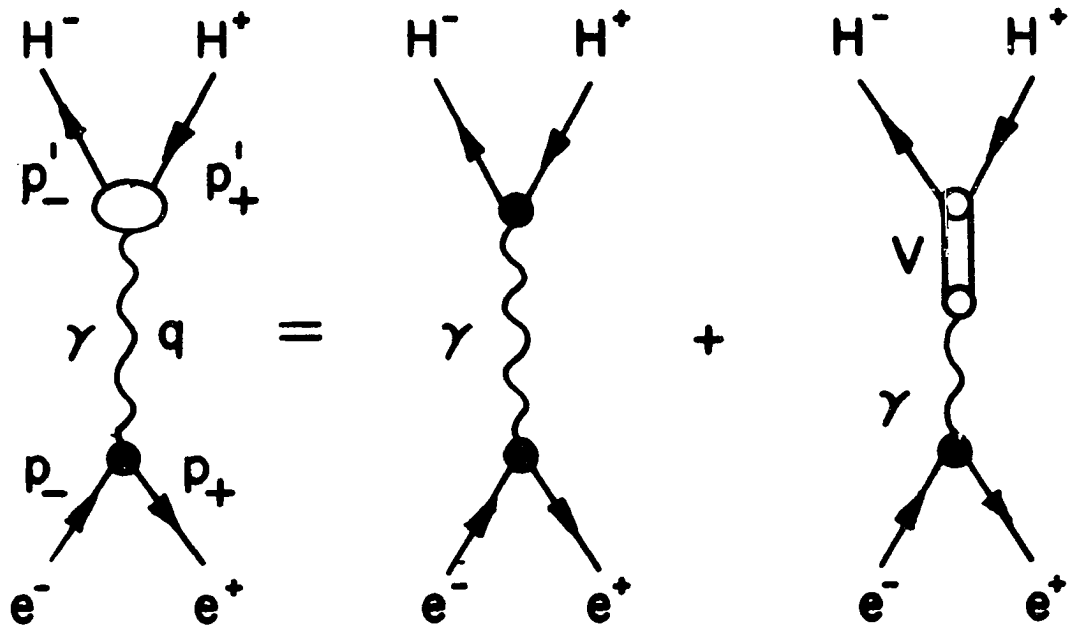

Figure 17. Feynman diagrams for the annhilation of an electron-positron pair into a hadron-antihadron pair in the context of vector meson dominance.

$$j_\mu^{\gamma H}(q) = \langle 0|J_\mu^{\gamma H}(0)|H^+H^-\rangle$$

which may be expanded in terms of Lorentz spin covariants and form factors, $\bar{f}(q^2)$. The time-like form factors, $\bar{f}(q^2)$, are complex-valued functions of q^2 and take on physical values only on the branch cut; i.e., for $q^2<-\mu^2$, where μ is the threshold for the production of the least-massive hadronic state. The form factors may be defined off the cut by analytic continuation, and are related to the space-like form factors describing the crossed process (eH→eH) by dispersion relations. Only time-like form factors for particles of spin 0 and spin ½ will be considered here.

1. Baryon form factors (S=½)

For any member, H=B, of the $1/2^+$ baryon octet, Lorentz invariance and current conservation require that for B on the mass shell,

$$j_\mu^{\gamma B}(q) = i(2\pi)^{-3}\bar{v}_B(\bar{p}_+)[\gamma_\mu \bar{f}_1^B(q^2)+\sigma_{\mu\nu}q_\nu \bar{f}_2^B(q^2)]u_B(\bar{p}_-), \quad (3.1)$$

where $u_B(\bar{p}_-)$ and $\bar{v}_B(\bar{p}_+)$ are free-particle spinors for the baryon and anti-baryon, respectively. The time-like form factors have the same normalization as their space-like counterparts, only now they must be analytically continued across the unphysical region, $-\mu^2\leq q^2\leq 0$.

2. Pseudoscalar meson form factors (S=0)

For H=P, a 0^- pseudoscalar meson, it follows by an analogous argument that

$$j_\mu^{\gamma P}(q) = (p_+ - p_-)_\mu \bar{f}^{\gamma P}(q^2), \quad (3.2)$$

where $\bar{f}^{\gamma P}(q^2)$ is the time-like form factor of the pseudoscalar meson, P.

B. Experimental Data

1. Proton data

The natural frame in which to discuss the colliding beam experiments and thus the time-like form factors and propagators is the center-of mass frame of the incident electrons. In this frame the total three-momentum vanishes, so

$$q = i2E,$$

$$q = -4E^2,$$

where E is the total energy of the electron in the center-of-mass system. Let θ be the angle between the proton and electron, then the differential cross section for $e^+e^- \to p\bar{p}$ is easily shown to be

$$(d\sigma/d\Omega)_p = (\alpha^2/]6E^2)[1-(m_p/E)^2]^{\frac{1}{2}}[|\bar{G}_M^p(q^2)|^2(1+\cos^2\theta) + (m_p/E)^2|\bar{G}_E^p(q^2)|^2\sin^2\theta].$$

This equation is easily integrated to give the total cross section,

$$\sigma(e^+e^- \to p\bar{p}) = (\alpha^2/6E^2)[1-(m_p/E)^2]^{\frac{1}{2}}[2|\bar{G}_M^p(q^2)|^2+(m_p/E)^2|\bar{G}_E^p(q^2)|^2].$$

Measurements of the total cross section, therefore, yield knowledge of the modulus of the proton form factor, not its real or imaginary parts.

The known time-like proton electromagnetic form factor data is summarized by three upper limits and two cross section measurements obtained from experiments involving the reaction, $e^+e^- \to p\bar{p}$. The form factors obtained from these measurements are given in Table 20 (100) and are obtained assuming $G_E^p = G_M^p$ for values of q^2 near the two-nucleon threshold.

Table 20. Time-like Proton Form Factor Data

q^2(GeV/c)^2	$\|G_E^p(q^2)\|^2$	Error
-4.41	0.19	±0.03
-4.41	0.27	0.04
-5.1	<0.20	
-6.6	<0.16	
-6.8	0.25	

Inverse electroproduction, $\pi^- p \to e^+ e^- n$, has been studied (101) as a source for information on the time-like electromagnetic form factors of the nucleon for $q^2 \leq -4m_N^2$. The major difficulty lies in the separation of the Born terms from nucleon resonances and background, so data is not presently available.

2. Pion data

The time-like pion electromagnetic form factor has been measured in colliding beam experiments involving the reaction $e^+ e^- \to \pi^+ \pi^-$. In the one-photon-exchange approximation this process is described by the Feynman graph in Fig. 17. The differential cross section is

$$(d\sigma/d\Omega)_\pi = (\alpha^2 \beta^3/32E^2) |\bar{f}^{\gamma\pi}(q^2)|^2 \sin^2\theta,$$

where $\beta = p/E$. The total cross section for $e^+ e^- \to \pi^+ \pi^-$ is then found by integrating out the angular dependence. The result is

$$\sigma(e^+ e^- \to \pi^+ \pi^-) = (\pi\alpha/12)(\beta^3/E^2) |\bar{f}^{\gamma\pi}(q^2)|^2.$$

The major problem associated with the determination of the time-like pion form factor in colliding beam experiments is to distinguish between pion and kaon particle-antiparticle pairs produced in the final state. At high q^2 only the total number of such pairs can be measured. Such measurements therefore establish only upper limits on the pion form factor. The technique used to separate these events, invented by Bernadini *et al.* (102), is to make use of the SU(3) prediction for the ratio of the pion and kaon total cross sections to separate the pion and kaon form factors at high q^2. This technique depends on assuming that the vector meson pole terms are represented by the zero-width approximation,

$$P_V(q^2) = \frac{m_V^2}{q^2 + m_V^2},$$

so that the form factors are written (the ratios of the vector meson couplings to the photon couplings are determined by SU(3); see Appendix B) in the following form

$$f^{\gamma\pi}(q^2) = P_\rho(q^2),$$
$$f^{\gamma K}(q^2) = (1/2)P_\rho(q^2) + (1/6)P_\omega(q^2) + (1/3)P_\phi(q^2).$$

This assumption is expected to describe the tail of the pion and kaon form factors reasonably well because the q^2 values are far from the resonance peaks. The consistency of the procedure is checked by testing the SU(3) ratio at low q^2, where the pions can be counted and the kaons lack the energy necessary to cause a trigger in the detector.

Again there is the possibility of two-photon-exchange contributions to e^+e^- annhilation into pseudoscalar mesons. They have been calculated (103) and found to be limited to a few percent.

The pion form factor data used in this analysis is taken from the experiments reported in Ref. (102) and (104-107). All of these are colliding beam experiments with the exception of Berezhnev (105) which involves a determination of the pion form factor near the 2π threshold using the inverse electroproduction reaction $e^-p \to e^+e^-n$. The analysis used in this kind of experiment is subject to the same errors that occur in the derivation of the space-like pion form factor from electroproduction experiments. Only two of the data points taken in this experi-

ment are used in the data analysis. The others lay too close to threshold, where the propagator has a small local maximum due to the logarithmic branch cut.

Of the six data sets used, only that obtained by Bernadini et al. (102) resulted from an attempt to separate the pion and kaon pairs. Consequently, only this data is used for $q^2 \leq -2$ $(GeV/c)^2$. The data of Augustin et al. (108) has been excluded from the analysis because his results give consistently larger values for $|\bar{f}^{\gamma\pi}(q^2)|^2$ than other experiments.

In the data of Bernadini et al. the q^2 values range from -1.44 to -9.0 $(GeV/c)^2$. The interesting feature of this experiment is that the values for the pion form factor lie above the tail of the ρ meson at high q^2, an effect which cannot be accounted for either by statistical fluctuations or the mathematical form of the propagator used to represent the ρ (109-111).

3. Kaon data

The time-like electromagnetic form factor of the charged kaon is measured in colliding beam experiments involving the reaction $e^+e^- \rightarrow K^+K^-$ (the form factor of the neutral kaon has not been measured). This experiment is analogous in every detail to those involving the pion form factor in colliding beam experiments. The data used in this study is taken from Ref. (102) and (107) and is compiled in Table 22.

C. Theory of Time-Like Form Factors

The annhilation of an electron-positron pair into a hadron-antihadron pair is described in the one-photon-exchange approximation and in

Table 21. Time-like Pion Form Factor Data

q^2(GeV/c)^2	$\|f^{\gamma\pi}(q^2)\|^2$	Error
-0.067	1.32	±0.20
-0.087	1.3	0.32
-0.112	1.69	0.42
-0.497	22.3	2.5
-0.575	39.0	3.5
-0.593	40.5	3.5
-0.604	44.7	3.6
-0.613	35.6	2.5
-0.624	24.8	1.7
-0.637	23.9	3.0
-0.656	22.3	2.5
-0.697	15.0	2.0
-0.98	2.9	0.5
-1.04	2.03	0.07
-1.3924	1.5	0.8
-1.44	1.28	0.34
-1.69	0.72	0.24
-1.96	0.67	0.19
-2.56	0.13	0.07
-3.61	0.135	0.06
-3.76	0.068	0.07
-4.41	0.034	0.023
-9.0	0.026	0.027

Table 22. Time-Like Kaon Form Factor Data

q^2(GeV/c)^2	$\|f^{\gamma K}(q^2)\|^2$	Error
-1.39	1.2	±2.8
-1.59	1.1	2.5
-2.4	0.25	0.08
-2.56	0.28	0.15
-3.2	0.32	0.18
-3.61	0.22	0.09
-3.76	0.11	0.11
-4.41	0.05	0.03
-5.76	0.02	0.02
-9.0	0.04	0.04

the context of the vector meson dominance model by Fig. 17., where the possibility of a direct photon-hadron interaction has again been allowed for. The transition matrix element describing this process is given by

$$<e^+e^-|T|H^+H^-> = j_\mu^{e\gamma}(q)(-i\delta_{\mu\nu}/q^2)j_\mu^{\gamma H}(q),$$

where, for time-like q^2,

$$j_\mu^{e\gamma}(q) = i(2\pi)^{-3}\bar{u}_e(\bar{p}_-)\gamma_\mu v_e(\bar{p}_+).$$

As before, there is a separation of the current, $j_\mu^{\gamma H}(q)$, into two parts: one corresponding to the direct photon-hadron interaction and the other representing the vector meson piece, which is described by the vector meson propagator and strong form factors.

1. The time-like propagator

Since $G_V(q^2)$ is an analytic function of q^2, the time-like vector meson propagator is obtained by analytic continuation from the space-like region. The poles in $I_V(q^2)$ are now at $q=\pm 2E \pm i\varepsilon$, as shown in Fig. 18. Again the contour C may be closed at infinity with the result that

$$I_V(q^2) = (m_V^2/2q)[\ (1/D_V(q)) - (1/D_V(-q))\ ], \qquad (3.4)$$

where $D_V(q)$ has the same functional form as Eq. (2.37), with iq replaced by q. With the phase definitions given in Fig. 18 it follows that

$$q - \mu_V = |q - \mu_V|,$$
$$-q - \mu_V = |q + \mu_V|\exp(i\pi).$$

The $D_V(m')$ function may then be written

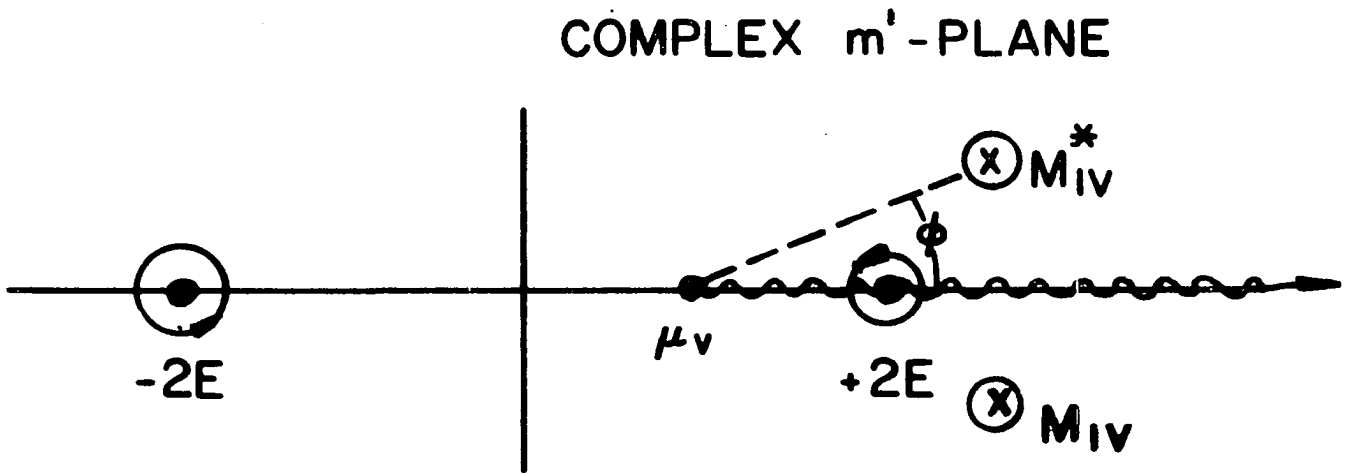

Figure 18. Phase angle definitions of the simple poles of $D_V(m')$ for time-like values of m'.

$$D_V(\pm iq) = (\pm q\Gamma_V/4\pi\mu_V)\log_e \frac{(\pm q-\mu_V)^2}{(m_{1V}-\mu_V)(m^*_{1V}-\mu_V)}$$

$$-m_V[1\mp(q/m_V)+(\Gamma_V/2m_V)^2][1\mp\frac{1}{\pi}\tan^{-1}(\frac{\Gamma_V}{2(m_V-\mu_V)}) \qquad (3.5)$$

where

$$\log_e \frac{(\pm\ q-\mu_V)^2}{(m_{1V}-\mu_V)(m^*_{1V}-\mu_V)} = \log_e \frac{(\pm q-\mu_V)^2}{|m_{1V}-\mu_V|^2} + (1\pm1)\pi i. \qquad (3.6)$$

The functions $I_V(0)$, $I'_V(0)$ and $I''_V(0)$ are all independent of q^2, so Eq. (3.4), (3.5) and (3.6) are enough to determine the exact time-like propagator for the vector mesons. The expression for the form factors have the same form as Eqs. (2.25) and (2.27).

In the small $\Gamma_V/(m_V-\mu_V)$ approximation, for q near the resonance, the $D_V(q)$ functions may be approximated by the equations

$$D_V(q) = q-m_V+i(\Gamma_V/2m_V)q,$$
$$D_V(-q) = -(q+m_V).$$

This leads to the Breit-Wigner form,

$$G_V(q^2) = m_V^2[q^2-m_V^2-im_V\Gamma_V]^{-1}.$$

The nature of the approximations used to derive the Breit-Wigner propagator washes out many of the interesting details of the vector meson peak, for example, the sharpness of the ρ peak on the high energy side.

D. Time-Like Proton Form Factors

The time-like nucleon form factors are identical in structure to the space-like form factors when the space-like propagators are replaced by the time-like propagators. The strong vector meson-hadron form factors are assumed to be the same constant for both space-like and time-like values of q^2. This assumption is made for simplicity, and to allow a direct comparison with the decay constant involved in the hadronic decay modes of vector mesons. In principal they could be quite different since the decay couplings are defined for vector mesons on the mass shell and can in general be complex functions of q^2.

It is important that the time-like form factors of the proton obey the so-called annhilation threshold constraint, Eq. (2.12), which requires that the electric and magnetic form factors of the proton be equal at the two-nucleon threshold. As can be seen from Eq. (2.3), this condition is obeyed trivially if the electric and magnetic form factors are first formulated in terms of the Pauli and Dirac form factors, as is done in this analysis. In theories beginning with dispersion relations for the electric and magnetic form factors the threshold constraint need not be satisfied and must be imposed as an auxiliary condition. Failure to do so results in contradicting the assumed analytic properties of the form factors. This may be seen by writing the Pauli and Dirac form factors in terms of the electric and magnetic form factors according to the equations

$$f_1^{\gamma N}(q^2) = [G_E^N(q^2) + \tau G_M^N(q^2)]/[1 + \tau],$$

$$f_2^{\gamma N}(q^2) = [G_M^N(q^2) - G_E^N(q^2)\ ]/2m_N[1 + \tau],$$

where $\tau=q^2/4m_N^2$. Unless the annhilation threshold constraint is obeyed, the Pauli and Diracs form factors possess a singularity at $q^2=-4m_N^2$.

Due to the scarcity of data not too much can be said about the time-like structure of the proton. The predictions, based on the parameters of Fits 2 and 3, are plotted along with the data in Figs. 19 and 20. As may be seen by examining these figures, the prediction based on Fit 2, in which no higher vector mesons are included, falls-off much too rapidly to give a good fit to the data. The inclusion of the ρ' at 3 GeV results in a rapidly rising curve which peaks at -9 $(GeV/c)^2$. The width of this peak is too large to be consistent with the upper limits shown in the figure. Several computer runs have shown, however, that ρ' widths as small as 0.015 GeV give equally good fits to the space-like nucleon data because the unstable particle propagator is insensitive to small width/mass ratios. Such a small width would easily bring the curve for Fit 3 into line with the data. The disagreement between the prediction based on the unstable particle propagator and the measurements at -4.41 $(GeV/c)^2$ is probably not significant. Note that the data is inconsistent at this point.

E. Pion and Kaon Form Factors

The analysis of the time-like pion form factor has been a popular topic for many years. Gounaris and Sakurai (109) have used the N/D method to construct a ρ-propagator incorporating finite-width effects.

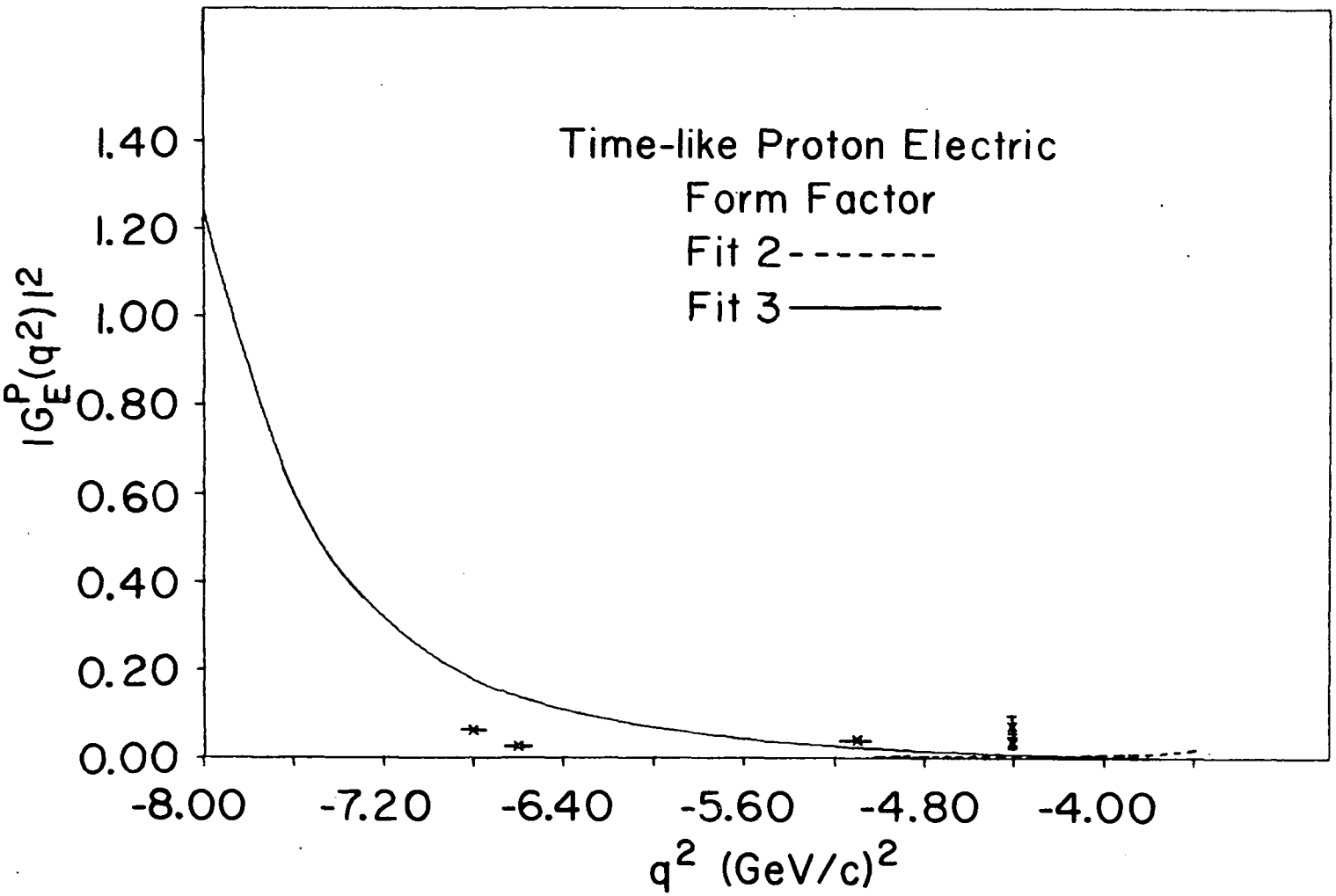

Figure 19. Time-like proton electric form factor vs q^2.

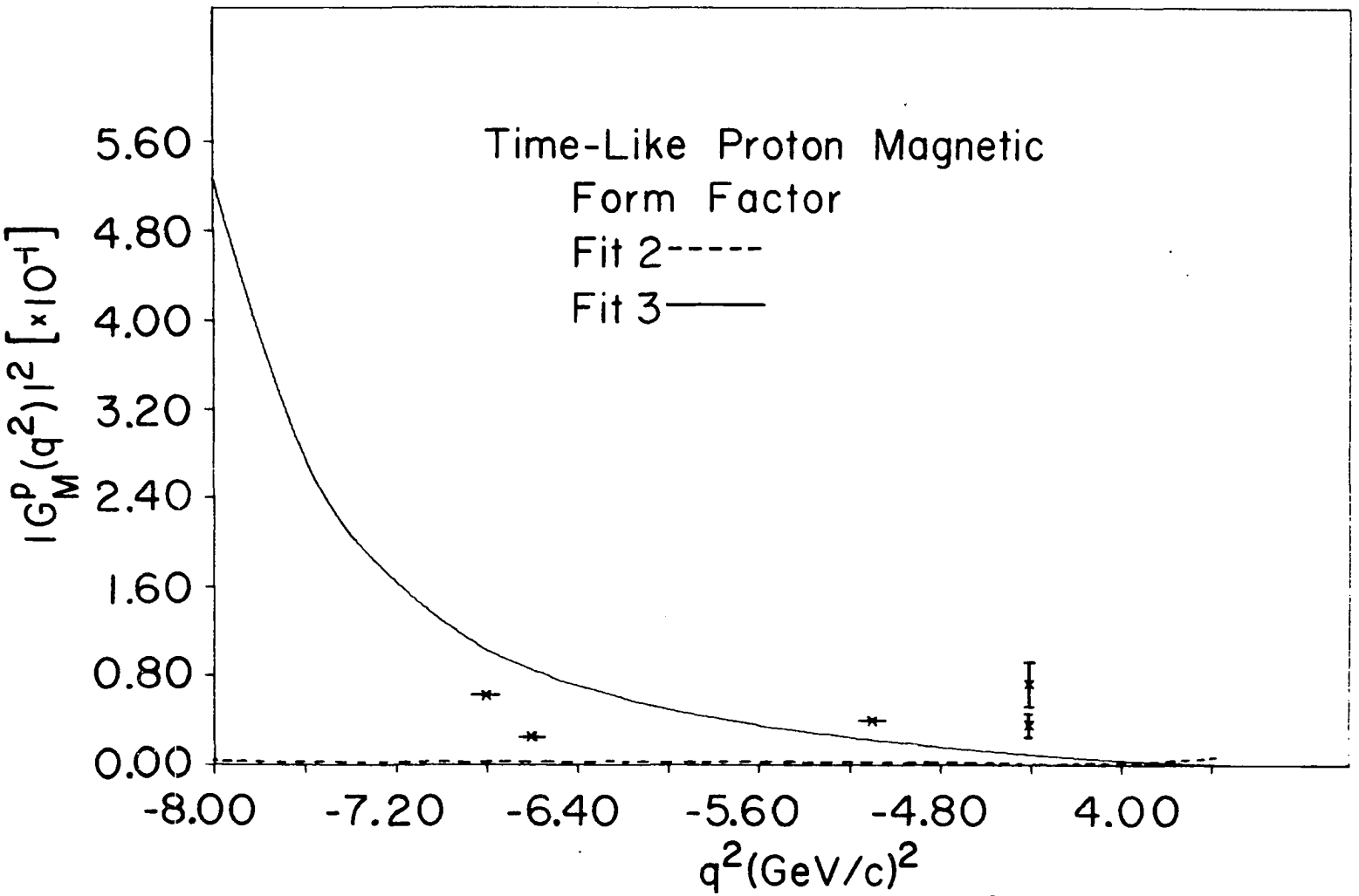

Figure 20. Time-like proton magnetic form factor vs q^2.

Their propagator is good only for $q^2 \geq m_\phi^2$ since they assume the $\delta_{\pi\pi}$ I=J=1 phase shift satisfies a generalized effective range formula which, even theoretically, can have exact validity only on the elastic cut. Their propagator results in an adequate description of the low-energy pion form factor data, but fails completely to explain the space-like data, giving an over-all $\chi_F^2=6$. Renard (110) and Bonneau and Martin (111) have included the effects of inelastic channels coupled to the ρ. Both models suffer from ad hoc assumptions about the structure of the ρ-hadron vertex and are therefore unreliable.

Deo and Parida (112) have enriched the momentum structure of the ρ-propagator through a further generalization of the effective range formula. A fit to the world data of the pion in both the space and time-like regions gives $\chi_F^2=1.32$. However, the model suffers from arbitrariness and the use of a large number (6) of free parameters to adjust for lapses in theoretical knowledge. Many other models have been proposed (113).

At the time of the original analysis (66) of the time-like form factor data, data was available only down to about -1.2 $(GeV/c)^2$. For the kaon, colliding beam experiments had given four values down to -3.20 $(GeV/c)^2$. Due to its scarcity the data therefore did not warrant fitting, but was instead predicted on the basis of universality fits to the nucleon form factor data. For Fits 2 and 3 the assumption of ρ-universality was used to related the pion form factor to the isovector form factor according to Eq. (2.54). In Fig. 21 data points are shown for the pion form factor along with the upper and lower bounds for $f^{\gamma\pi}$ con-

sistent with the ρ mass, width and coupling variances given in Tables 11 and 12. The upper curve is seen to fall noticeably below the peak experimental data points. Note the shift in the ρ-peak due to the different preferred mass values for the ρ. It is easy, of course, to fit this data by letting the ρ parameters float. However, this destroys the correlation of the parameters determined by fitting the space-like nucleon form factor data.

Augustin et al. (108) were the first to detect a contribution to the pion form factor from ρ-ω mixing. This occurs as a consequence of the G-parity violating electromagnetic $\omega \to 2\pi$ decay (114). It is thought to go through the processes shown in Fig. 22. In terms of these graphs the pion form factor becomes

$$f^{\gamma\pi}(q^2) = 1 - 2g_1^{p\rho}(m_\rho^2/2\gamma_\rho)G_\rho(q^2) - g_{\omega\pi}(m_\omega^2/2\gamma_\omega)G_\omega(q^2),$$

where ρ-ω mixing has been introduced phenomenologically by using the ω-propagator and a complex-valued coupling constant, $g_{\omega\pi}$.

In order to investigate the significance of this effect, the pion form factor is fit for values of $q^2 \leq -1.04$ $(GeV/c)^2$. This momentum range is chosen to avoid possible contributions from higher vector mesons. The results, labeled Fit 4 and compiled in Tables 23 and 24, are achieved treating the ω parameters as free values and confining the ρ parameters within the bounds set by the nucleon data (115):

$$m_\omega = 0.781 \pm 0.001 \text{ GeV}; \quad \Gamma_\omega = 0.0095 \pm 0.0003,$$

and,

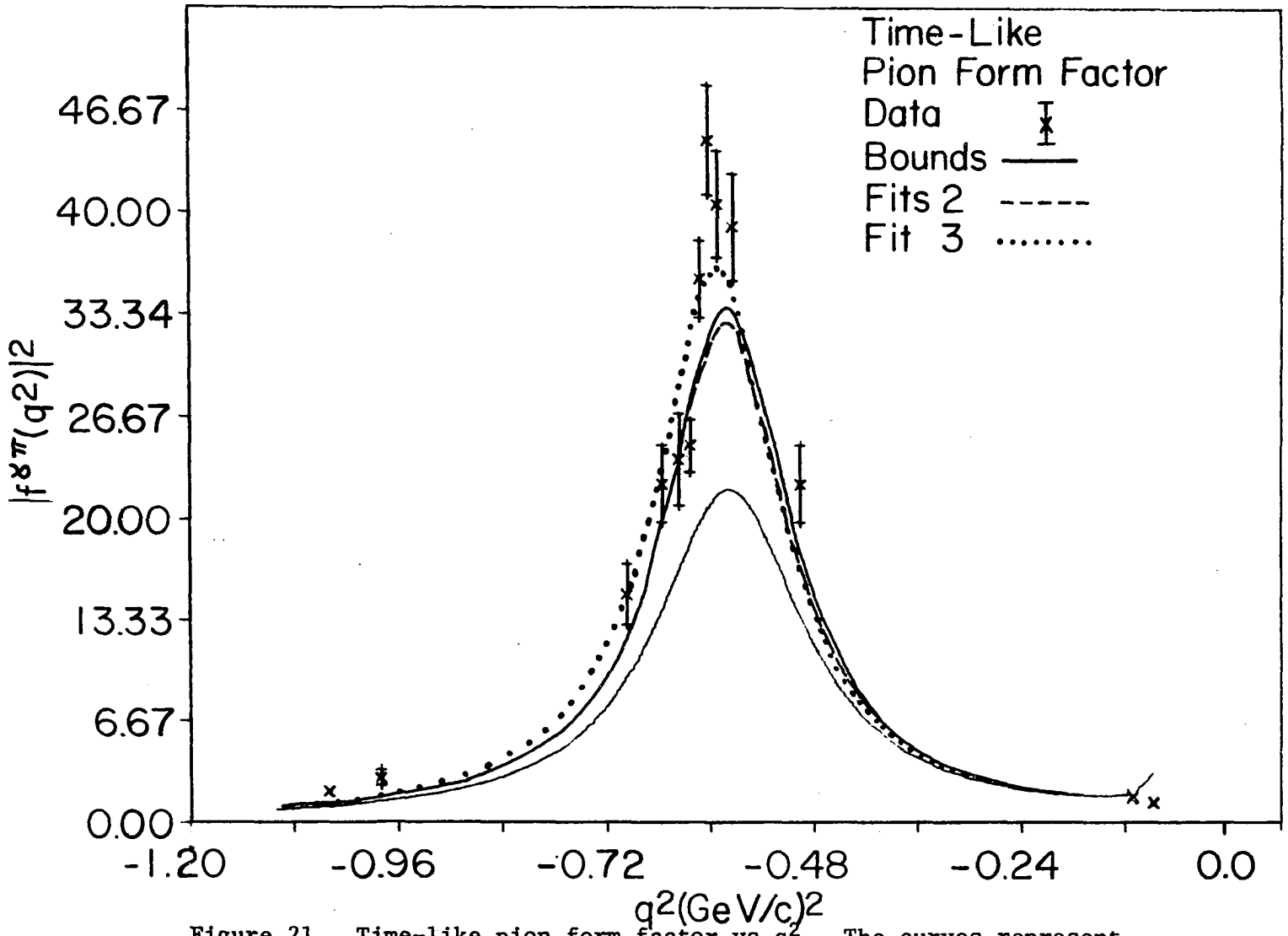

Figure 21. Time-like pion form factor vs q^2. The curves represent predictions based on fits to the nucleon form factor data.

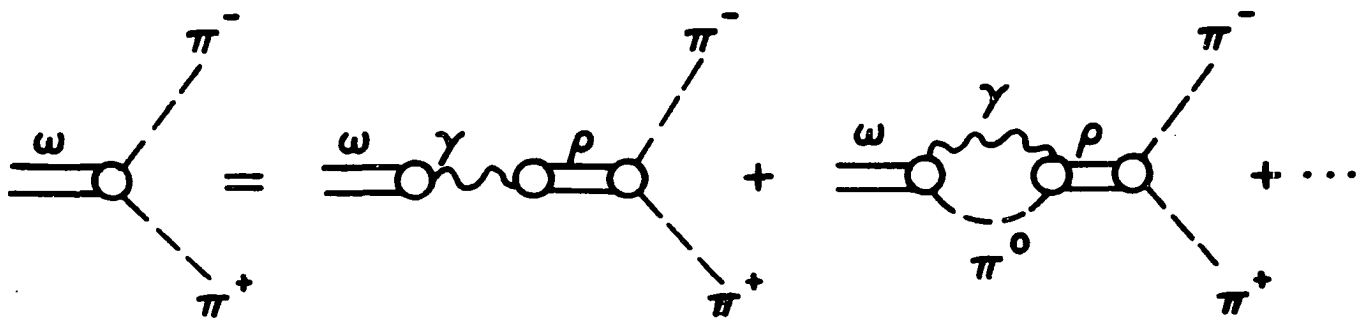

Figure 22. Feynman diagrams contributing to electromagnetic ρ-ω mixing.

Table 23. Vector Meson Masses and Widths in GeV Obtained From Fits to the Psuedoscalar Meson Form Factor Data

	Fit 4[a]	Fit 5[b]	Fit 6[c]
m_ρ	0.766	0.763	0.763
Γ_ρ	0.115	0.130	0.119
m_ω	0.781 ±0.001	0.782	0.782
Γ_ω	0.0095±0.0003	0.0090	0.0094
m_ϕ			1.049
Γ_ϕ			0.0051
$m_{\rho'}$		$1.51^{+0.3}_{-0.1}$	1.72±0.2
$\Gamma_{\rho'}$		$0.25^{+0.7}_{-0.1}$	0.32±0.1

[a]Fit 4: Fit to pion form factor peak with ρ-ω mixing.

[b]Fit 5: Fit to pion form factor data with ρ, ω, and ρ'.

[c]Fit 6: Fit to kaon form factor data with ρ, ω, ϕ, and ρ'.

Table 24. Vector Meson-Pseudoscalar Meson Coupling Constants Obtained From Pseudoscalar Meson Form Factor Fits[a]

	Fit 4	Fit 5	Fit 6
$g_{\rho\pi}$	4.6	5.2	
$\lvert g_{\omega\pi}\rvert$	0.26±0.02	0.28 ±0.01	
α	75.0 ±1.0°	96.0 ±6.0°	
$g_{\rho K}$			2.3
$g_{\omega K}$			13.6
$g_{\phi K}$			-7.0
$g_{\rho'\pi}/2\gamma_{\rho'}$		-0.071±0.03	
$g_{\rho'K}/2\gamma_{\rho'}$			-0.12±0.03

[a]For a definition of the fits, see Table 23.

$$g_{\omega\pi} = |g_{\omega\pi}|\exp(i\alpha),$$
$$|g_{\omega\pi}| = 0.26\pm0.02,\ \alpha = 75\pm1^{\circ},$$

for χ^2_F=0.8. The result for the ρ-ω mixing angle, α, is in agreement with $\alpha=86\pm14^{\circ}$ obtained from colliding beam experiments (116) based on a fit to the data using the Gounaris-Sakurai propagator. The ρ-ω mixing angle has also been measured in dipion production experiments (117), giving $\alpha=104\pm5^{\circ}$. The result is therefore model-dependent, making a comparison with experiment difficult.

The branching ratio for ω→2π can now be calculated using the formula

$$B(\omega\rightarrow2\pi) = \Gamma(\omega\rightarrow2\pi)/\Gamma_{\omega} = (m_{\omega}/12)(|g_{\omega\pi}|^2/4\pi)[1-(\mu_{\rho}/m_{\omega})^2]^{3/2}.$$

The numerical value based on the parameters of Fit 4 is

$$B(\omega\rightarrow2\pi) = 3.1\pm0.05\%.$$

Experiments involving the production of pion-antipion pairs in strong interactions (118) give branching ratios of 0.80±0.28%, whereas colliding beam experiments (116) typically give values on the order of 3.61±2% when analyzed using the Gounaris-Sakurai propagator. The result obtained using the exact propagator is seen to be consistent with the later values. If the correlation between the ρ parameters is released then χ^2_F as low as 0.1 can be achieved. In this case the real part of $g_{\omega\pi}$ changes sign, giving a ρ-ω mixing angle of 101°, more in line with the results from dipion production experiments.

It appears that the exact time-like propagator gives an adequate description of the peak data points of the pion form factor, though the description is no better than that provided by other finite-width parametrizations which include the effects of ρ-ω mixing. It is not possible, for example, to shed any light on the different results for the ρ and ω parameters obtained from colliding beam experiments and dipion production experiments.

In Fig. 23 the time-like kaon form factor obtained from the nucleon form factor fits assuming SU(4) universality is shown. Though the data is widely scattered, it appears that the theory expressions predict larger form factors than are consistent with experiment. Note the large enhancement at -9 $(GeV/c)^2$ due to the 3 GeV ρ' (this peak is shown somewhat exaggerated in width for purposes of clarity). Because the width of this ρ' is so ill-determined by the data, it is not possible to conclude whether the existence of a $\rho' \to K^+K^-$ decay mode is present in the data.

1. Fits to the pion and kaon form factor data

For time-like q^2 the electromagnetic interactions of the pseudoscalar mesons can be accounted for in the vicinity of the vector meson mass by pole-dominance using either monopole or exact propagators. In the case of the pion, universality of the ρ coupling is suggested and results in the identification $2f_1^V = f^{\gamma\pi}$. But a good fit to the data requires contributions from electromagnetic ρ-ω mixing.

The recent experiment of Bernadini et al. (102) gives values for the pion and kaon form factors to -9 $(GeV/c)^2$. This experiment has the

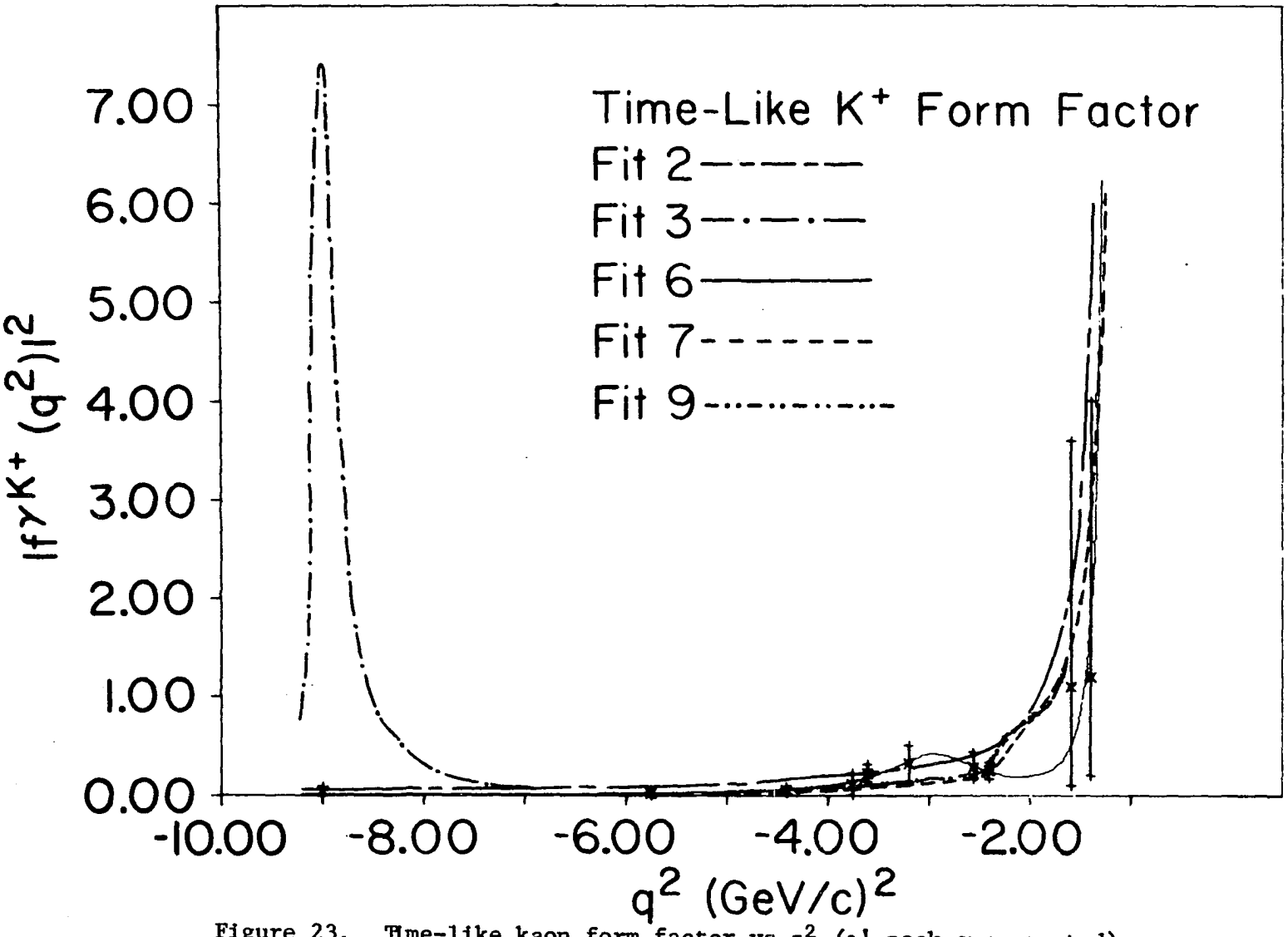

Figure 23. Time-like kaon form factor vs q^2 (ρ' peak exaggerated)

crucial merit that a separation of the pion and kaon signals is made, and shows that below -2 $(GeV/c)^2$ the form factors of the pion and kaon are much larger than is to be expected on the basis of an extrapolation of the vector meson tails and may in fact tend to unity, characteristic of a point particle.

To account for this discrepancy two major lines of thought have been developed. One is the idea that the pseudoscalar mesons are composed of point-like constituents, quarks or partons, and that at large time-like q^2 the point-like structure of the meson is being probed. The other is based on the attempt to modify vector meson dominance by including contributions from higher vector mesons or from inelastic channels that give cusp effects at their thresholds.

In this latter sense, in one type of dual resonance model (119) a fit was made to the time-like and selected values of the space-like pion form factor data using generalized vector meson dominance and the duality mass relation. A good fit to the data required the use of three hypothetical isovector resonances beyond the ρ. Zovko (120) has constructed a zero parameter simple-pole model of the pion and kaon form factors by imposing the asymptotic bounds, Eq. (2.25). A good fit required the introduction of six vector mesons, only three of which correspond to experimentally established vector mesons. The pattern that emerges again is that vector meson dominance models for electromagnetic form factors which ignore finite-width effects require the use of non-exsistent vector mesons in order to obtain acceptable fits to the data.

In this analysis a generalized vector meson dominance model with ρ and ρ' contributions is constructed in the hope of predicting vector mesons which have some experimental basis. Attempts to fit the high energy pseudoscalar meson data with ρ and ω contributions alone fail even if all the masses, widths and couplings are taken as adjustable parameters. This is due to the high energy behaviour of the data discussed previously and to the existence of an enhancement at about 1.5 GeV in the pion data and at 1.7 GeV in the kaon data. If these enhancements correspond to higher vector mesons then an analysis using the unstable vector meson propagators developed in this work may lead to important insights concerning the real mass and width parameters of the resonance.

In this extended model the pion form factor is written

$$f^{\gamma\pi}(q^2) = 1 - g_{\rho\pi}(m_\rho^2/2\gamma_\rho)G_\rho(q^2) - g_{\omega\pi}(m_\omega^2/2\gamma_\omega)G_\omega(q^2) - g_{\rho',\pi}(m_{\rho'}^2/2\gamma_{\rho'})G_{\rho'}(q^2),$$

and the kaon form factor becomes

$$f^{\gamma K}(q^2) = 1 - (g_{\rho\pi}/2)(m_\rho^2/2\gamma_\rho)G_\rho(q^2) - g_{\omega K}(m_\omega^2/2\gamma_\omega)G_\omega(q^2) - g_{\phi K}(m_\phi^2/2\gamma_\phi)G_\phi(q^2) - (g_{\rho',\pi}/2)(m_{\rho'}^2/2\gamma_{\rho'})G_{\rho'}(q^2),$$

where ρ-universality has been assumed. In the first fit to the pion data, labeled Fit 5, the ρ' parameters are allowed to float and the ρ parameters are held within the bounds determined by the nucelon data. The best fit (compiled in Tables 23 and 24) occurred for the following ρ' parameters (χ_F^2=0.6):

$$m_{\rho'} = 1.51\pm0.15 \text{ GeV}, \quad \Gamma_{\rho'} = 0.25\pm0.20 \text{ GeV},$$
$$g_1^{p\rho'}/2\gamma_{\rho'} = -0.071\pm0.03,$$

where the errors are estimated by making several runs yielding the same χ^2 for different parameter sets. This fit is shown in Figs. 24 and 25. Note the complexity of the ρ-peak due to ρ-ω mixing and the small local maximum near the two pion threshold (due to the logarithmic branch cut). At higher values of the momentum transfer there is a bump in the form factor at $-(1.51)^2$ corresponding to the virtual $\rho' \to 2\pi$ decay. The branching ratio for this process, defined by

$$B(\rho' \to 2\pi) = (m_{\rho'}/\Gamma_{\rho'})(g^2_{\rho',\pi}/48\pi)[1-(\mu_\rho/m_{\rho'})^2]^{3/2},$$

is

$$B(\rho' \to 2\pi) = 0.08\gamma^2_{\rho'},\%.$$

The values of the $\gamma_{\rho'}$ coupling are still controversial. Ceradini *et al.* report (121)

$$(2\gamma_{\rho'})^2/4\pi = 17\pm5$$

if the ρ' decays completely into $\rho\varepsilon$, and

$$(2\gamma_{\rho'})^2/4\pi = 13\pm5$$

if an $\omega\pi$ mode is also present. From a theoretical analysis of the ρ' decays, Bramon and Greco (122) conclude

$$\gamma_{\rho'} = 2\gamma_\rho.$$

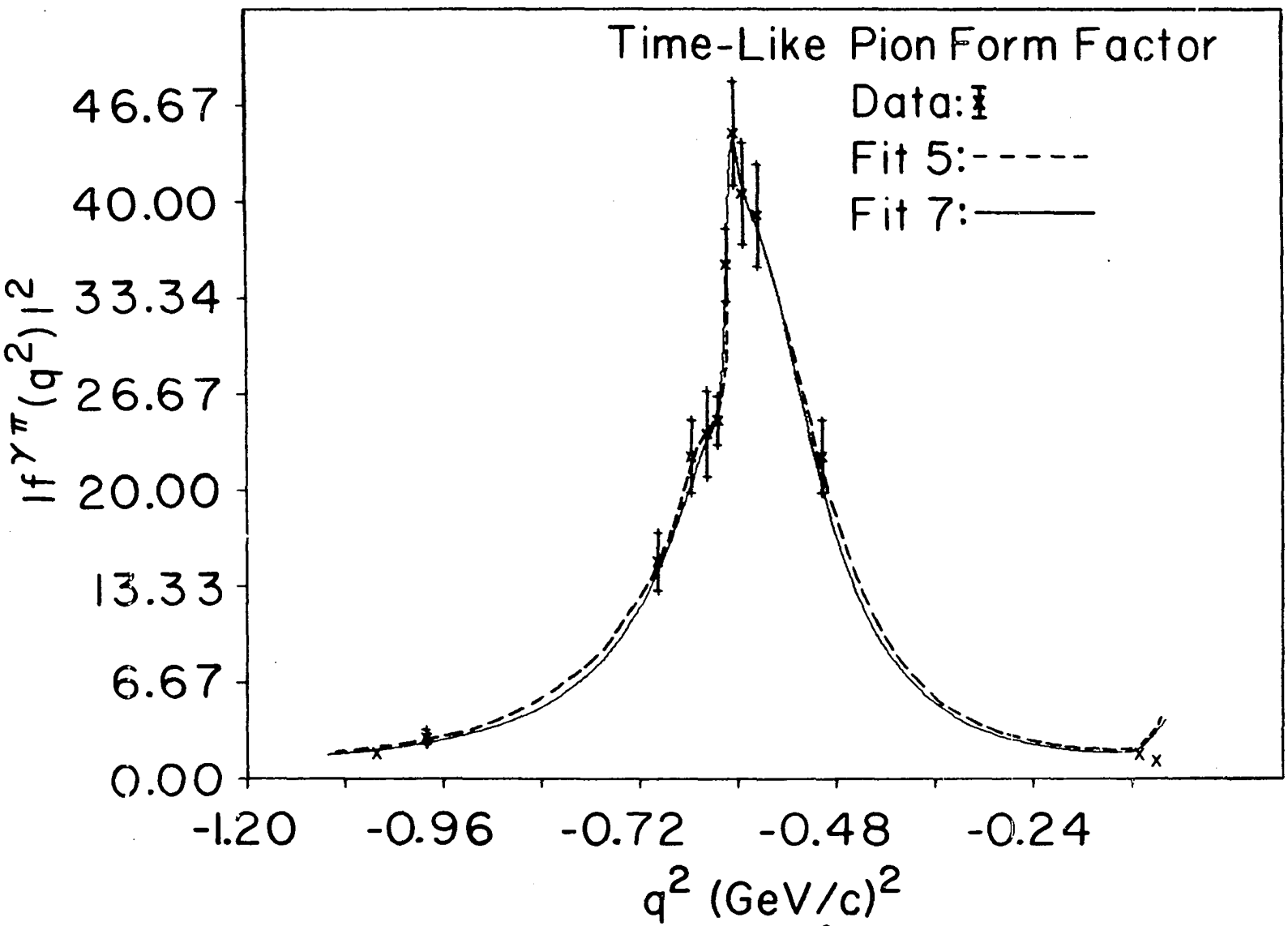

Figure 24. Time-like pion form factor vs q^2, obtained from pion form factor fits.

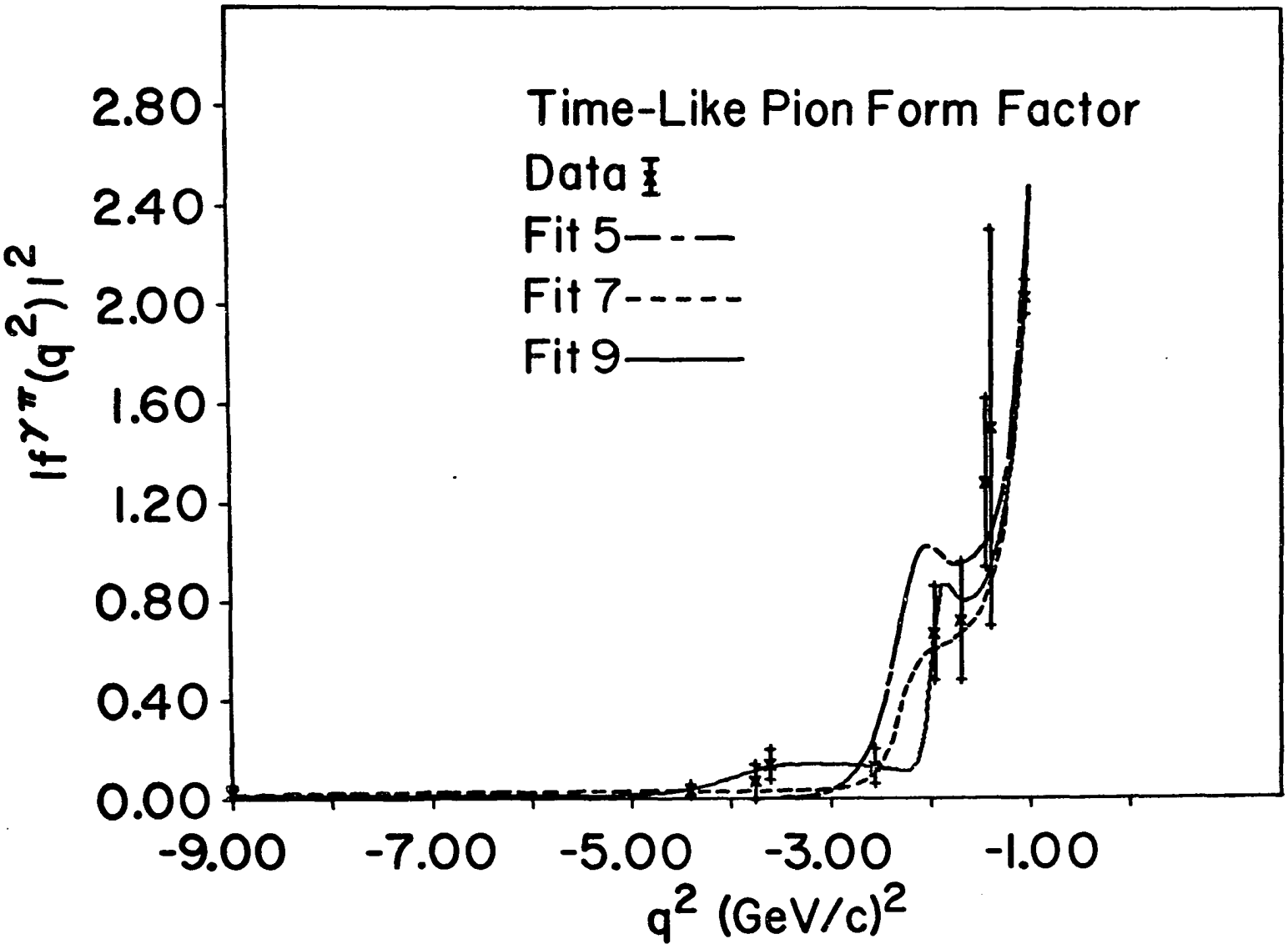

Figure 25. High-energy time-like pion form factor vs q^2.

Using the value suggested by the analysis of Bramon and Greco, it follows that

$$B(\rho' \to 2\pi) = 2.1\%$$

compared to the experimental result (123),

$$B(\rho' \to 2\pi) < 10\%.$$

Considering the available phase space, the smallness of the $\rho' \to 2\pi$ branching ratio is surprising. Explanations for this have been proposed by the quark model (124) and by gauge theories (125).

Continued into the space-like region, the pion form factor is seen to fall below the experimental points, as shown in Fig. 26. Note that the curve corresponding to Fit 4 has a zero at 1.7 $(\text{GeV/c})^2$. This is a result of fitting only the peak data points; the asymptotic behaviour of the pion form factor is not constrained by the data.

There appears to be an enhancement in the high-energy time-like kaon data, shown in Fig. 23, that may be due to the presence of a $\rho' \to 2K$ decay mode. In order to check this the kaon time-like data is fit with a contribution from the ρ'. The vector meson-kaon couplings are confined within the limits set by the nucleon data according to SU(4) universality. This fit is labeled Fit 6 and gives χ^2_F=0.9 for

$$m_{\rho'} = 1.72 \pm 0.2 \text{ GeV}, \quad \Gamma_{\rho'} = 0.32 \pm 0.1 \text{ GeV},$$
$$g_1^{p\rho'}/2\gamma_{\rho'} = 0.12 \pm 0.03.$$

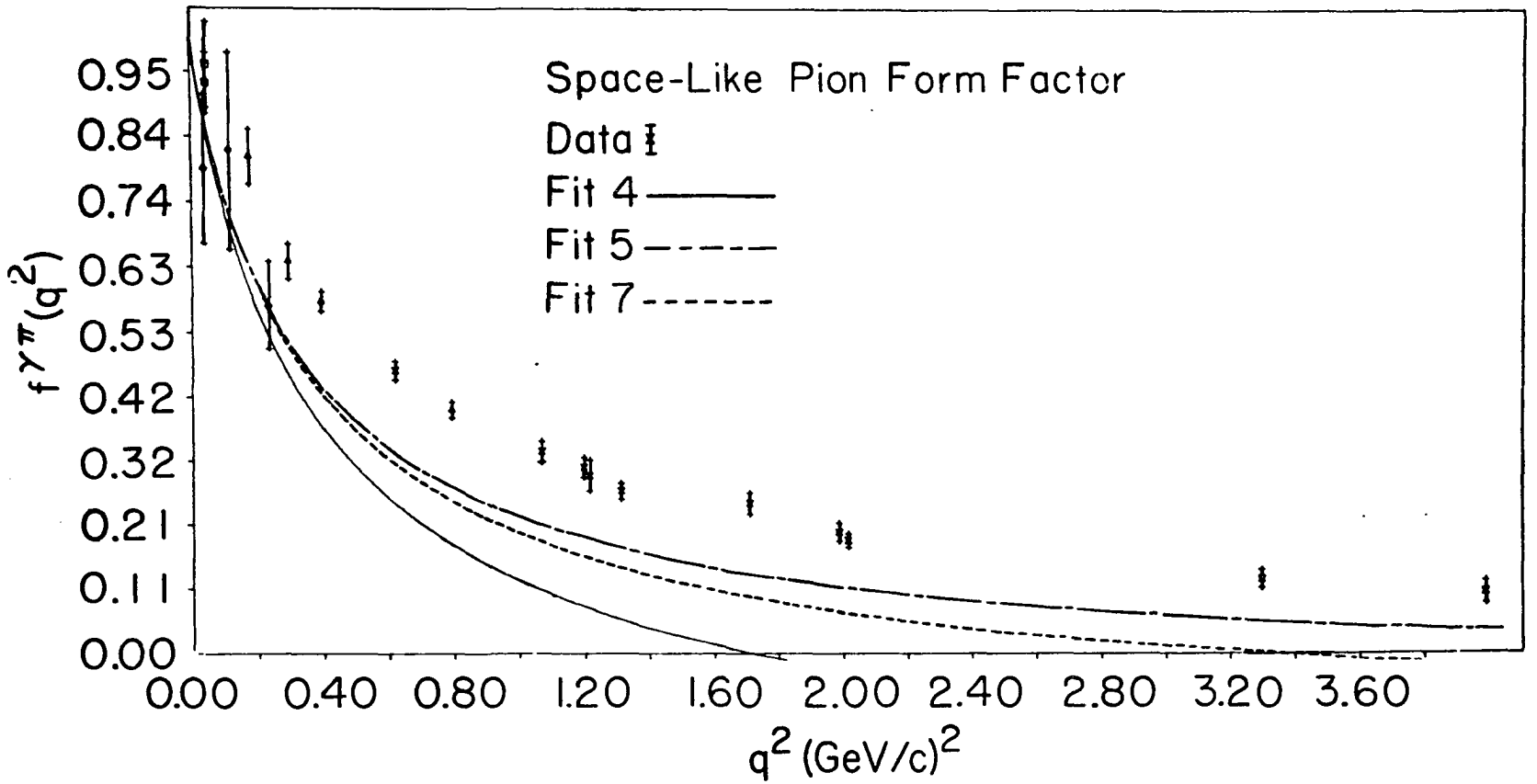

Figure 26. Space-like pion form factor vs q^2, obtained from pion form factor fits.

The calculated $\rho' \to 2K$ branching ratio is

$$B(\rho' \to 2K) = 0.10\gamma_{\rho'}^2, \%.$$

For $\gamma_{\rho'}=2\gamma_{\rho}$ this gives $B(\rho' \to 2K)=3.1\%$, in agreement with the experimental result

$$B(\rho' \to 2K) < 10\%.$$

The time-like kaon form factor obtained by fitting the kaon data is shown in Fig. 23. The extrapolation to space-like q^2 is shown in Fig. 16, and possesses the same general behaviour predicted by SU(4) universality fits 2 and 3, though the slopes of the curves at the origin are slightly different.

Considering the large errors on the ρ' mass and width (due to the paucity of data) obtained from the pion and kaon form factor data fits, these results suggest that a single vector meson in the 1.5-1.7 GeV mass region contributes to both the pion and kaon form factors. The mass and width of this meason can be pinned down better if the pion and kaon data are fit simultaneously. This will place more constraint on the parameters and should result in a better determined set of mass, width and coupling constants.

If the ρ, ω, and ϕ masses and widths are retained within the variances listed in Table 11, a good fit with $\chi_F^2=0.6$ occurs for a ρ' with a mass of 1.52 GeV and a width of 0.23 GeV. The parameters are given in Tables 25 and 26 under the heading, Fit 7. For this fit the

Table 25. Vector Meson Masses and Widths in GeV Obtained From Fits to the Pseudoscalar Meson Form Factor Data

	Fit 7[a]	Fit 8[b]	Fit 9[c]	Fit 10[d]
m_ρ	0.763	0.763	0.763	0.775
Γ_ρ	0.129	0.129	0.129	0.141
m_ω	0.782	0.782	0.782	0.783
Γ_ω	0.0101	0.0110	0.0110	0.014
m_ϕ	1.016	1.016	1.016	
Γ_ϕ	0.0057	0.0057	0.0057	
$m_{\rho'}$	1.52±0.02	1.53	1.32	
$\Gamma_{\rho'}$	0.23±0.04	0.21	0.22	
$m_{\rho''}$			1.70	
$\Gamma_{\rho''}$			0.29	

[a] Fit 7: Simultaneous fit to pion and kaon form factor data with contribution from ρ'.

[b] Fit 8: Simultaneous fit to pion and kaon form factor data with SU(3) couplings and contribution from ρ'.

[c] Fit 9: Simultaneous fit to pion and kaon form factor data with contributions from ρ' and ρ''.

[d] Fit 10: Fit to peak data points of pion form factor using the complex propagator.

Table 26. Vector Meson-Pseudoscalar Meson Coupling Constants Obtained From Pseudoscalar Meson Form Factor Fits[a]

	Fit 7	Fit 8	Fit 9	Fit 10
$g_{\rho\pi}$	5.2	5.2	5.2	5.65
$\lvert g_{\omega\pi}\rvert$	0.29±0.03	0.31		0.46
α	95.0 ±1.0°	95.0°		102.°
$g_{\rho K}$	2.6	2.6	2.6	
$g_{\omega K}$	$1.8^{+5.0}_{-1.2}$	2.6	1.9	
$g_{\phi K}$	$4.9^{+0.9}_{-3.4}$	4.1	4.9	
$g_{\rho'\pi}/2\gamma_{\rho'}$	-0.07	-0.088	-0.046	
$g_{\rho''\pi}/2\gamma_{\rho''}$			-0.02	
$g_{\rho' K}/2\gamma_{\rho'}$	-0.035	-0.029	-0.023	
$g_{\rho'' K}/2\gamma_{\rho''}$			-0.01	

[a]For a definition of the fits, see Table 25.

couplings are obtained with the isovector parts of the pion and kaon form factors related by universality. The isoscalar couplings are nearly identical to those predicted by SU(4); indeed, when the exact SU(4) couplings are used the χ^2 changes only negligibly (Fit 8). If the accepted values for the ω and ϕ mass and width are used it is also possible to obtain a good fit to the data using essentially the same couplings, so only the isovector part of the kaon form factor is of crucial importance to the fit.

As can be seen from Fig. 24 and 25, Fit 7 gives a good representation of the pion form factor in both the low and high energy regions. However, the corresponding space-like form factor has a zero at 3.4 $(GeV/c)^2$. The fitting of the isovector part of the kaon form factor with the pion form factor clearly does not lead to wholly acceptable results. The space and time-like kaon form factors for this fit are shown in Figs. 16 and 23. Note that the ρ' peak in the kaon data shifts to a region where no data is present. It is therefore not possible to conclude whether a ρ' contributes to the kaon data or not, and if it does, whether it is the same ρ' that affects the pion data.

Crossing relates the couplings determined in Fit 7 to the vector meson decay strengths so that the branching ratio for the two-pion and two-kaon decays can be calculated:

$B(\omega \to 2\pi) = 4.1\%,$

$B(\rho' \to 2\pi) = 2.3\%,$

$B(\rho' \to 2K) = 0.3\%.$

The theoretical analysis of the mesonic form factors has thus far given no evidence in favor of the existence of a vector meson resonance at 1.25 GeV, reported in some experiments (see Table 15). In order to clean this problem up, an attempt is made to determine the mass and width of two consecutive daughters of the ρ-trajectory that lead to a good fit to the pion and kaon data simultaneously. This requires the use of the duality mass and width relations,

$$m^2_{\rho_n} = m^2_n(1+an),$$

$$\Gamma_n/m_n = \Gamma_\rho/m_\rho,$$

where m_ρ=0.763 GeV, Γ_ρ/m_ρ=0.169, and a=2. It then follows that

$$m_{\rho'} = 1.3 \text{ GeV}, \ \Gamma_{\rho'} = 0.22 \text{ GeV},$$
$$m_{\rho''}=1.7 \text{ GeV}, \ \Gamma_{\rho''} = 0.29 \text{ GeV}.$$

SU(4) couplings are used for the ρ, ω, and φ. The results of the fit are given in Tables 25 and 26 under the heading of Fit 9, and the curves are shown in Fig. 23 and 25. The double peaks in the form factors cannot be taken too seriously, of course, since there is not enough data to justify their existence. If the masses, widths and couplings of the higher vector mesons are allowed to float, then the χ^2_F drops from 0.7 to 0.4. The ρ' and ρ'' masses move up to 1.4 and 1.98, respectively, and the widths to 0.10 GeV and 0.40 GeV. A good fit to the data cannot be obtained if, for example, only the odd daughters are retained. The mass spacing parameter, a, may also be allowed to float freely. The best

fit occurs for a=2.75, corresponding to masses of 1.49 GeV and 1.96 GeV. The data therefore apparently does not favor either the existence of a ρ' at 1.25 GeV or the duality mass relation with a=2.

1. Pion and kaon sum rules

If the form factors of the pseudoscalar mesons drop to zero as rapidly as given in Eqs. (2.55), then sum rules for Q_P and Z_P, defined by Eqs. (2.56), must be obeyed. The values for Q_π, Q_{K^+}, and Q_{K^0} calculated using the parameters of fits 4-9 are given in Table 27. In the cases where the high q^2 pion and kaon data is fit either independently or simultaneously, the charge sum rules are satisfied to within 5%. This suggests that the pion has no hard core and is a composite, not an elementary, particle. Likewise, the results for the kaon charges suggest that both the charged and neutral kaon is not elementary.

The values for Z_π, Z_{K^+} and Z_{K^0} are also given in Table 27. The results indicate that the form factors of the pseudoscalar mesons decrease no faster than the monopole and that there exists a hard core term in the function $q^2 f^{\gamma P}(q^2)$.

2. Pion and kaon charge radii

The pion and kaon charge radii are defined by Eq. (2.57). The values of these radii based on the parameters from fits to the pseudoscalar meson data are given in Table 18. These fits yield values for the pion charge radius on the order of 0.94 f., which is larger than the value, 0.85 f., obtained by assuming $f^{\gamma\pi}=2f_1^V$, and extrapolating from fits to the nucleon data. It is also larger than the values predicted on the basis of other models, as seen in Table 18.

Table 27. Predictions of the Pseudoscalar Meson Charges and Asymptotic Parameters Based on Fits to the Pseudoscalar Meson Form Factor Data

	Fit 4	Fit 5	Fit 6	Fit 7	Fit 9
Q_{π}	1.26	1.04		1.02	1.10
Q_{K^+}			1.00	1.05	1.05
Q_{K^0}			-0.34	-0.06	-0.04
Z_{π}	-0.58	-0.25		-0.40	-0.31
Z_{K^+}			-0.51	-0.67	-0.63
Z_{K^0}			0.66	-0.27	-0.31

The values of the kaon charge radius based on fits to the pseudoscalar meson form factor data are given in Table 19. The experimental values for these radii are not at all well-determined, so the values in Table 19 must be treated as predictions to be compared with future experiments. This model therefore predicts that the charge radius of the K^+ is 0.78±0.02 f. and the charge radius of the K^0 is 0.47±0.08 f.

3. The P-wave pion-pion phase shift

To explain the large value of the pion charge radius deduced from a recent eπ scattering experiment, Levin and Okubo (126) have concluded that the I=J=1 pion-pion phase shift must possess a large enhancement on the elastic cut. Such a behaviour has no dynamical basis in existing theory, but is not explicitly ruled out by the data. This is an important result for this study because the phase shift makes its connection to the pion form factor through the relation

$$\delta_{\pi\pi}(q^2) = \tan^{-1}\{\mathrm{Im}[f^{\gamma\pi}(q^2)]/\mathrm{Re}[f^{\gamma\pi}(q^2)]\}, \qquad (3.7)$$

where $\delta_{\pi\pi}$ is the phase shift for the scattering of two pions in the I=J=1 state, that is the isovector P-wave state. Eq. (3.7) is exact only on the elastic cut; i.e., for q^2 from $-4m_\pi^2$ to $-16m_\pi^2$, and is established by applying unitarity in the calculation of the spectral function, $\mathrm{Im}[f^{\gamma\pi}(q^2)]$, and then by making a partial wave expansion of the π-π scattering amplitude.

Data for $\delta_{\pi\pi}$ is obtained indirectly from dipion production experiments like $\pi^- p \to \pi^+ \pi^- n$. This strong interaction process is complicated by the existence of many intermediate states, just a few of which are shown in

Fig. 27. For low q^2 the process is dominated by one-pion-exchange and the analysis is simplified enough to allow a determination of the π-π scattering cross section, and thus the various π-π phase shifts.

Data from a recent experiment (127) is shown in Fig. 28. In general the data from many different experiments exhibits an appreciable spread from experiment to experiment and between different methods of analysis applied to the same experiment. This is due to the heavy theory-dependence of the data; an arbitrary extrapolation procedure is needed to go from the physical region to the pion pole. For example, in the π-π phase shift analysis of Estabrooks et al. (127) two solutions for $\delta_{\pi\pi}$ were found to fit the cross section measurements well. At the four-pion threshold one solution gave

$$\delta_{\pi\pi}(-16m_\pi^2) = 11.5\pm0.5^\circ$$

and the other gave

$$\delta_{\pi\pi}(-16m_\pi^2) = 14.6\pm0.5^\circ.$$

On the other hand, Protopopescu et al. (128) quotes a rather small value,

$$\delta_{\pi\pi}(-16m_\pi^2) = 9.4\pm0.7^\circ.$$

The $\delta_{\pi\pi}$ data is usually summarized by an effective range formula,

$$(q^2+ 4m_\pi^2)^{3/2}\cot\ \delta_{\pi\pi}(q^2) = -(\mu_\rho^2/a_1 m_\pi^3)q + fq(q^2 + m_\pi^2), \quad (3.8)$$

where $a_1 m_\pi^3=0.05$ and $f=-2.21$ so that $\delta_{\pi\pi}(-16m_\pi^2)=11^\circ$. This formula follows from the Chew-Low extrapolation theory.

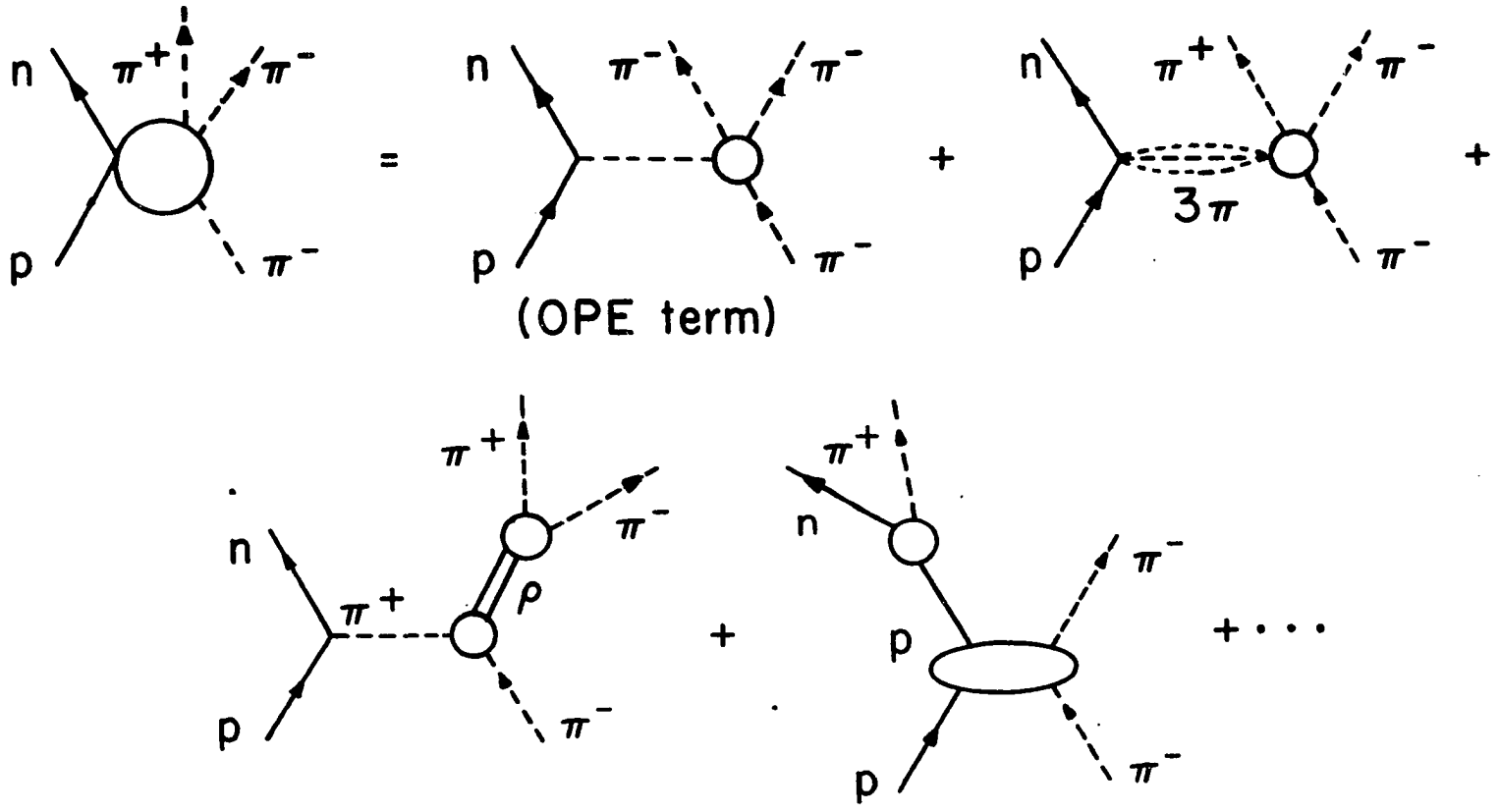

Figure 27. Feynman diagrams for the reaction $\pi^- p \to \pi^+\pi^- n$.

Since the model constructed in this work leads to a large pion charge radius, the question arises as to whether the predicted π-π phase shift behaves according to the Levin-Okubo conjecture. This phase shift is plotted in Fig. 28 for Fits 2 and 3 (the other fits lead to very similar results). The curves for these fits swells way above the effective range formula and takes the value $24\pm3^{\circ}$ at the inelastic (i.e., four-pion) threshold, as compared to the experimental result, which is on the order of 11°. This step-function-like behaviour is due to the presence of the logarithmic cut in the propagator and to mathematical interplay between various terms at q^2 values near the two-pion threshold. This in turn is due to the specific nature of the approximation made for $\mathrm{Im}[R_V(m')]$, Eq. (2.36).

The curves labeled B, C and D in Fig. 28 are taken from the Levin-Okubo paper and represent phase shifts which give radii at least as large as the anomalous result from direct eπ scattering, $\langle r^2\rangle^{\frac{1}{2}}=0.78\pm0.10$ f. (98). In order to improve the unphysical threshold behaviour of the propagator used thus far in the analysis, and to investigate the relevance of the Levin-Okubo conjecture to this method of attack, a second ρ-propagator was derived assuming

$$\mathrm{Im}[R_\rho(m')] = (\Gamma_\rho/m_\rho)[1-(\mu_\rho/m_\rho)^2]^{-3/2}[1-(\mu_\rho/m')^2]^{3/2}\theta(m'-\mu_\rho),$$

in keeping with the dynamical assumption, Eq. (2.32). In this equation $\theta(m'-\mu_\rho)$ is the usual unit step-function. The simple propagator, derived from Eq. (2.37), is thus the limit of this new propagator for $m'>>\mu_\rho$.

The new propagator then takes the form

$$\alpha_V^{-1}\pi D_V(m') = \{ [\pi i + L(m^*_{1V})]R(m^*_{1V},m') - [\pi i + L(m_{1V})]R(m_{1V},m')$$

$$+ [\pi i - L(m')]\frac{(m'^2-\mu_V^2)^{3/2}}{m'^2}$$

$$-\mu_V^2 \frac{(m'-m_{1V})(m'-m^*_{1V})}{m'|m_{1V}|^2}\left[1+\tfrac{1}{2}\pi\mu_V\left(\frac{1}{m'}+\frac{1}{m_{1V}}+\frac{1}{m^*_{1V}}\right)\right] \}$$

where

$$\alpha_V = (\Gamma_V/2m_V)[\,1 - (\mu_V/m_V)^2]^{-3/2},$$

$$L(m') = \log_e \frac{(m'+\mu_V)^{\frac{1}{2}} + (m'-\mu_V)^{\frac{1}{2}}}{(m'+\mu_V)^{\frac{1}{2}} - (m'-\mu_V)^{\frac{1}{2}}},$$

and

$$R(m,m') = \frac{(m^2-\mu_V^2)^{3/2}(m'-m^*_{1V})}{m_V^2(m^*_{1V}-m_{1V})},$$

A fit to the pion form factor data for $q^2 \geq -1$ $(\mathrm{GeV/c})^2$ (to avoid effects of the ρ') gives $\chi^2_F = 0.8$ for the parameters

$$m_\rho = 0.775 \pm 0.005 \text{ GeV}, \quad \Gamma_\rho = 0.141 \pm 0.005 \text{ GeV},$$

$$g_{\rho\pi} = 5.65.$$

The relevant data for this fit, called Fit 10, is given in Tables 25-27.

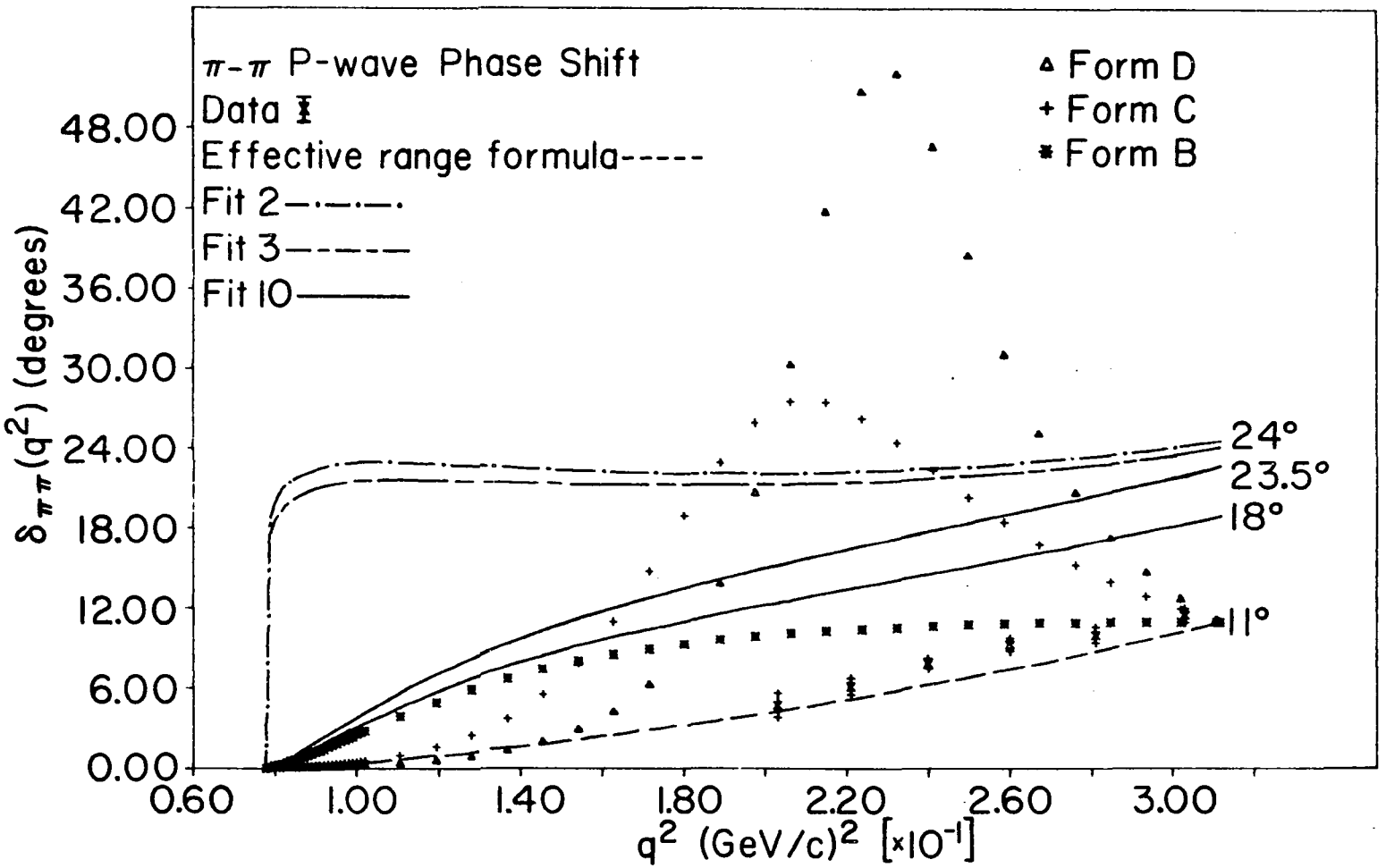

Figure 28. Pion-pion P-wave phase shift vs q^2.

The pion charge radius evaluated for the parameters and the propagator of Fit 10 is

$$\langle r^2 \rangle_\pi^{\frac{1}{2}} = 0.75 \pm 0.05 \text{ f.},$$

even in better agreement with the latest result from electron-pion scattering (98). Note, however, that this value is substantially smaller than the other values compiled in Table 18 calculated using the simple propagator.

The phase shift calculated using this propagator is plotted in Fig. 28. The two curves correspond to the bounds allowed by different equally-good fits to the low energy pion form factor data. Note that the step-function-like behaviour is absent and that at the inelastic threshold,

$$\delta_{\pi\pi}(-16m_\pi^2) = 18 \pm 3^\circ$$

more in keeping with the experimental result, though the predicted value is still too large.

It appears that the use of the exact ρ-propagator leads to large radii and large phase shifts that do not behave like those posited by Levin and Okubo. The Gounaris-Sakurai propagator, on the other hand, leads to a small charge radius and a small phase shift (8°). Yet both fit the time-like pion form factor data well for low q^2.

The difference between these propagators in this respect may be traced to the fact that the pion charge radius calculated using the exact ρ-propagator has terms proportional to Γ_ρ^2/μ_ρ^2, $\mu_\rho m_\rho/\Gamma_\rho^2$, and m_ρ^2/μ_ρ^2

(see Appendix C), none of which are small numbers for the ρ. These terms do not appear in the Gounaris-Sakurai propagator due to the manner in which the branch cut is mathematically put in. Thus the large π-π P-wave phase shift seems to be irrelevant to the conjecture of Levin and Okubo that the pion charge radius therfore be large.

To further investigate this question, the ρ-propagator has been modified to include the possibility of structure in the $\rho\pi\pi$ vertex. The results of this analysis are preliminary and are contained in Appendix E.

IV. DISCUSSION AND CONCLUSIONS

A. Status

The use of unstable particle propagators in the description of the electromagnetic form factors of hadrons has led to some notable results. First of all, a good fit to the low-energy nucleon form form factor data has been obtained using just ρ, ω, and ϕ dominance, and has led to a determination of the vector meson resonance parameters in good agreement with experiment. This result must be contrasted with the simple-pole model, which requires the ρ mass to be very low, or requires the existence of experimentally unconfirmed higher isovector vector mesons if the known ρ resonance parameters are retained. The fit obtained on the basis of the theory presented in this work is especially good considering all the constraints placed on the analysis: the accuracy of the data and the high correlation between the four form factors due to their common dependence on only three vector meson propagators. Moreover, no ad hoc assumptions about the momentum dependence of the strong vector meson-nucleon form factors is made. The coupling constants are shown to be interrelated by sum rules and to give good predictions for the vector meson decay constants. Since the experimental values of the vector meson-nucleon couplings could have been imposed by the experimental data at the outset, effectively a two-parameter fit to the data has been achieved.

Due to the step-function-like behaviour of the simple propagator near threshold, the initial slopes of the nucleon form factors come out somewhat large as compared to experiment. In particular, the initial slope

of the electric form factor of the neutron is too large by about 60%. This same effect leads to an enhancement in the values of the nucleon radii as compared to experiment.

The low energy form factors of the pion and kaon have been shown to be related to those of the nucleon on the basis of ρ-universality. A more general vector meson universality based on SU(4) does not seem to give adequate fits to the data, though in most cases the data itself is uncertain so a good test is not possible. The predictions for both the time-like pion and kaon form factor data are in excellent agreement with experiment if due account for the existence of electromagnetic ρ-ω mixing is made. For the space-like form factors of the pseudoscalar mesons, the experimental data is model-dependent so no direct comparison with experiment can be made. However, for the pion the predicted space-like form factor is consistent with the earliest model-dependent experimental values, and brackets the most recent high-energy measurements.

At higher energies, new vector mesons like the heavy ρ's at 1.5 and 3.0 GeV are required to obtain good fits to the pseudoscalar meson and nucleon data, respectively. The heavy ρ at 1.5 GeV may be identified with the experimental ρ' at 1.6 ± 0.2 GeV reported in some experiments. There is no obvious candidate for the heavy ρ at 3.0 GeV, though the recent discovery of a heavy vector meson, $\psi(3105)$, at 3.1 GeV may be a possibility. Until the isospin of the ψ is measured nothing can be said with any certainty. In general the high energy form factor data is too sparse to uniquely determine a given vector meson, so the theoretical errors in the resonance parameters are quite large and can be decreased

only by more accurate measurements performed over small q^2 intervals above 3 $(GeV/c)^2$. In particular, the data on the neutron form factors is in dire need of improvement.

The most recent measurements of the pion charge radius have prompted a reanalysis of the pion form factor using an unstable particle propagator with the correct P-wave threshold behaviour. The result is that the predicted value for the pion charge radius decreases from its former large value, 0.94 f., to the value 0.75 f., in very good agreement with the direct measurement in $e\pi$ scattering. The predicted P-wave phase shift is much larger than the experimental result, however. For example, at the four-pion threshold, the phase shift is around 18° compared to the experimental value of 11°. It is not clear whether this discrepancy is due to the theory-dependence of the data or to some more fundamental consideration.

In the hope of bringing the phase shift prediction into line with experiment, structure in the $\rho\pi\pi$ vertex has been posited. This leads to the introduction of a new free parameter, a, which complicates the momentum-dependence of the ρ-propagator considerably. Preliminary results, given in Appendix E, indicate that values of a leading to an experimentally consistent value for the P-wave phase shift also lead to predictions for the charge radius close to those of the vector meson dominance model. It therefore appears that, if the recent measurements of the pion charge radius are correct, some mechanism other than vector meson instability is needed to account for its large value.

Vector meson dominance was first suggested by the behaviour of the nucleon electromagnetic form factors. It is known to work well in the time-like region near the vector meson resonance peaks when the effects of vector meson instability can be ignored. This work suggests it is also a viable description of the interaction of space-like photons with hadrons if the role of vector meson instability is not ignored.

In a wider theoretical context, pole dominance has recently been raised from its original status as a low-energy phenomenology to a basic description of photons, vector mesons and intermediate vector bosons in gauge field theories incorporating spontaneous symmetry breaking (129). It has been suggested, for example, that the weak interactions owe their origin to vector and axial-vector dominance (130) in which (so far hypothetical) intermediate vector bosons couple to the ρ and the A_1, and that gravitation is due to dominance by f-mesons (131) in which the graviton couples to massive 2^+ f-mesons which interact universally with hadrons through the conserved energy-momentum tensor. In fact, unified gauge theories of weak, electromagnetic and strong interactions have been proposed (132) in which vector meson dominance plays a leading role.

B. Improvements

There are several ways in which the proposed model for the electromagnetic form factors may be modified or refined:

(1.) A careful analysis and compilation of all the available nucleon form factor and ep total elastic cross section data should be made. In this way questionable data points can be eliminated. Since systematic errors between different data sets can seriously affect χ^2,

the number of variable parameters in the fit should be increased to include normalization parameters (133).

(2.) The model for the form factors should be improved. The assumption of dominant two-body decay modes should be dropped for the ω. Even though the Γ_ω/m_ω ratio is small, suggesting that the exact form of the ω-propagator is irrelevant as long as analyticity is assumed, an ω-propagator which includes the dominance of three-body decay modes may result in a set of ω-hadron couplings more in line with universality predictions. Looking ahead to the future, the difference between various parametrizations of the ω peak will become especially crucial as the precision of the colliding beam experiments is increased. There is basically no other model for the ω-propagator in existence because alternate parametrizations rely on effective range formulas and dispersion relations, and a phase shift analysis of three-body decays is very difficult.

The nucleon form factor data should be re-fit using the complex propagators. The nucleon radii calculated using the parameters of the fit are expected to give better agreement with the data due to the absence of anomalous threshold effects. It might be expected, therefore, that the theoretical value of the slope of the neutron electric form factor at $q^2=0$ will be in better agreement with experiment.

(3.) The charge, magnetic moment and asymptotic sum rules obtained in this analysis can be solved simultaneously for the coupling-ratios if only four vector meson contributions are included and the masses and widths are fed in as input. It would be interesting to know how well these parameters fit the data.

(4.) Finally, the high-energy nucleon form factor data should be re-fit using only the known (or most probable) higher vector mesons; that is, $\rho'(1.6)$, $\psi(3105)$ and $\psi'(3695)$. According to the quark model, the ϕ decays dominantly only into states with non-zero strangeness. In particular, $g_{1,2}^{\phi N} \simeq 0$. Experimentally it is known, for example, that the cross section for photoproduction of ϕ mesons is very small relative to that for the photoproduction of the ρ and ω (134). Yet good fits to the nucleon electromagnetic form factor data cannot be obtained unless a contribution from an isoscalar vector meson other than the ω is utilized. This is a consequence of the dipole behaviour of the isoscalar form factor. To achieve consistency with the quark model, it is judicious, therefore, to re-fit the nucleon form factor data utilizing contributions from only the ρ and ρ' in the isovector part of the form factor, and from ω and ψ (and perhaps ψ') in the isoscalar part of the form factor.

V. APPENDIX A: PHYSICAL INTERPRETATION OF ELECTROMAGNETIC FORM FACTORS

It is tempting to conceive the elementary particle as a rigid three-dimensional structure possessing a more or less definite radius. However, it is difficult to maintain this idea due to requirements imposed by the special theory of relativity. If an elementary particle is extended in space then the spatially separated parts of it must be connected like the parts of an absolutely rigid body. The special theory of relativity requires, on the other hand, that deformations in a solid object propagate no faster than the speed of light. But for a solid object to behave like a rigid body deformations would have to propagate instantaneously to all parts of the body. Thus an elementary particle cannot be spatially distributed, and therefore must be a point-like object. This argument, of course, does not exclude the possibility that an elementary particle might consist of some kind of impenetrable fluid.

At one time it was hoped that non-local field theories (135) would lead to a representation of space-time extension and to the elimination of the divergences in the quantum theory of interacting fields. These hopes have been frustrated by the difficulty in making non-local theories simultaneously causal and Lorentz-invariant (136).

From the discussions in Sec. IA and IB, $f_1^{\gamma N}(q^2)$ and $f_2^{\gamma N}(q^2)$ are seen to include all possible effects due to virtual particle fields around the nucleon which interact with the photon and do not violate Lorentz or gauge invariance. This cloud of virtual particles surrounding the nucleon

is usually not regarded as representing a real static spatial structure because it consists of particles not identified with real entities: i.e., with virtual particles (137). What do the form factors have to do, then, with the "form" of the particle; i.e., with the actual charge and magnetization density of the particle in coordinate space? As will be made clear below, they have nothing to do with it at all in a rigorous sense- they actually represent only theoretically defined functions which can be measured in the laboratory and thus by which a theory can be tested. The relativistic form factors allow a relativistic scattering amplitude for point-particle scattering to be parametrized in such a way as to express deviations from non-relativistic results.

The whole package to terms like "particle", "core", and "structure" actually represent euphemisms. A "particle" in the context of this analysis is simply a pole of the S-matrix. If the pole lies on the real axis below the threshold of its interactions, the particle is stable; and if it is on an unphysical sheet it is unstable. The "structure" of a particle is defined wholly in terms of its form factors. If $f(q^2)\neq 0$ over some range of q^2, the particle is said to possess structure. This structure has a radius only if the initial slope of the form factor does not vanish. The structure has a "core" if the form factor goes to some non-zero asymptotic value.

This terminology is motivated by the common usuage of non-relativistic nuclear physics (138) where the form factors are meaningfully defined as Fourier transforms of the nuclear charge and magnetic moment density. Then

the classical kind of image of a particle as a static charge and magnetic moment distribution with a well-defined surface, radius and core makes sense.

In the relativistic case, the relation between form factors and static charge and magnetic moment distributions has only an intuitive meaning. A number of difficulties arise which make it difficult to assign a literal meaning to the concept of spatial structure. If information concerning the static structure of a hadron, for example, is desired for small distances, the uncertainty principle requires that a photon probe of large three-momentum be involved. For real photons this corresponds to large recoil energy changes in the hadron, leaving it in an excited state and disrupting its static structure. Real photons of smaller momentum would diminish recoil effects, but would also wash-out the details of the hadronic structure.

To avoid these difficulties, virtual space-like photons can be used to probe the electromagnetic structure of hadrons in elastic electron-hadron scattering experiments. In this case the photon is off the mass shell, so the amount of recoil energy transferred to the nucleon can be considerably reduced and its ground state structure can be explored. In fact, in the Breit frame, where the energy transferred by a virtual photon vanishes, the electric and magnetic form factors can be used to define static charge and current densities in the classical sense. Since $q=p'-p$, the fourth component of q vanishes and current conservation is expressed by

$$q_\mu j_\mu^{\gamma N}(q) = 0,$$

which implies that $j_\mu^{\gamma N}(q)$ consists of a scalar and a transverse vector in this frame. A calculation then shows that in the Breit frame the nucleon matrix elements take the form

$$\bar{j}^{\gamma N}(\bar{q}) = i\bar{\sigma}\times\bar{q}G_M^N(\bar{q}^2),$$
$$j_4^{\gamma N}(\bar{q}) = iG_E^N(\bar{q}^2),$$

where both the nucleon spin states are up or down due to the selection rules on angular momentum and parity ($N\bar{N}$ must be $^3S_1$ or $^3D_1$). This same result occurs in a non-relativistic theory for the interaction of a momentum space charge density, $G_E^N(\bar{q}^2)$, with a scalar potential and a magnetic dipole interaction with $G_M^N(\bar{q}^2)$.

The Fourier transforms of the current matrix elements can now be used to define time-independent (i.e., static) charge and magnetic moment distributions according to the equations,

$$\rho^{\gamma N}(\bar{x}) = (2\pi)^{-3}\int d^3q G_E^N(\bar{q}^2)\exp(i\bar{q}\cdot\bar{x}),$$
$$\bar{J}^{\gamma N}(\bar{x}) = i(2\pi)^{-3}\int d^3q\bar{\sigma}\times\bar{q}G_M^N(\bar{q}^2)\exp(i\bar{q}\cdot\bar{x}). \qquad (A.1)$$

No such interpretation holds for the Dirac and Pauli form factors and it is important to note that the analysis in terms of the Breit frame system is specialized and valuable mainly because it produces the same result as a non-relativistic treatment.

The inverse transformations of Eq. (A.1) are

$$G_E^N(\bar{q}^2) = \int d^3x\rho^{\gamma N}(\bar{x})\exp(-i\bar{q}\cdot\bar{x}),$$
$$i\bar{\sigma}\times\bar{q}G_M^N(\bar{q}^2) = \int d^3x\bar{J}^{\gamma N}(\bar{x})\exp(-i\bar{q}\cdot\bar{x}), \qquad (A.2)$$

and the normalization condition gives

$$G_E^N(0) = Q_N = \int d^3x \rho^{\gamma N}(\bar{x}),$$

as expected. If $\rho^{\gamma N}(\bar{x})$ is assumed to be purely radial, then by Eq. (A.2) the electric form factor becomes

$$G_E^N(\bar{q}^2) = \int \rho^{\gamma N}(r)[|\bar{q}|r]^{-1}\sin(|\bar{q}|r)4\pi r^2 dr.$$

In Table 28 pertinent examples of $G_E^N(\bar{q}^2)$ and their corresponding Fourier transforms are displayed assuming the charge distribution is spherically symmetric. As can be seen from this table, a monopole form factor (Form 2) gives a Yukawa-type, e^{-r}/r, charge density. The dipole form factor, on the other hand, corresponds to a decaying exponential charge density.

The dipole and scaling laws, Eq. (1.1) and Eq. (2.11), are known to give a fit to the nucleon form factor data which removes the major part of the q^2-dependence. Thus, in the loose conceptual sense of Eq. (A.1), the charge and magnetization density of the nucleon are spread out in space and drop-off exponentially with distance. This is quite different from the behaviour of nuclear charge densities, which present sharp drops in charge density corresponding to surface features.

The net charge of the neutron is zero, so its charge density must change sign at some definite point. The scaling law for G_E^n, Form 4 in Table 28, is seen to describe just such a detail. The Fourier transform gives a charge density which is negative for $r<2b$, vanishes for $r=2b$, and changes sign for $r>2b$.

Table 28. Spatial Charge Distributions for Given Form Factors

Form	$G_E^N(q^2)$	$\rho_E^N(r)$
1.	1	$\delta(r)$
2.	$[1+(q^2/b^2)]^{-1}$	$(b^2/4\pi r)\exp(-br)$
3.	$[1+(q^2/b^2)]^{-2}$	$(b^3/8\pi)\exp(-br)$
4.	$[q^2/a^2][1+(q^2/a^2)]^{-2}$	$[b^4/8\pi a^2][1-(2b/r)]\exp(-br)$

The justification for this interpretation of the Fourier transform of the Breit-frame current matrix elements has been given by Ernst et al. (139). They show that the interaction of a nucleon wave packet with a static external electromagnetic field is described by an interaction energy identical in form to the classical self-energy of a distribution of charge and magnetic moment. The analogs of the classical charge and magnetic moment density in this interaction energy are just Eq. (A.1).

As suggestive as this interpretation is, it is flawed in at least four ways (140):

(1.) To measure the charge and magnetic moment distributions defined by Eqs. (A.1) the form factor in the Breit frame must first be measured. But a given Breit frame is reached by a boost from a rest frame that varies with the momentum transferred to the nucleon. Thus it is not clear in what frame the charge and magnetic moment densities defined by Eq. (A.1) are expected to apply. The ambiguity is removed in the non-relativistic limit where the Breit and Lab frames are identical.

(2.) Static charge and magnetic moment distributions are ruled out by special relativity, which does not allow the existence of rigid distributions of charge (or mass).

(3.) For time-like form factors, a completely different definition of spatial charge and magnetic moment densities would be necessary because the Breit-frame does not exist and the form factors are complex-valued.

(4.) The electromagnetic form factors are defined only in first order electromagnetic interactions. At high momentum transfer, or

small distances, inelasticity sets in and the meaning of a static charge density becomes obscure.

Despite these difficulties, it is common to formulate theories of nucleon structure in terms of Eq. (A.2) by making some assumption about the electromagnetic current density and to make predictions for the electric and magnetic rather than the Dirac and Pauli form factors. The reasons for doing so are related to the operational meanings of the electric and magnetic form factors (141). The use of G_E^N and G_M^N rather than $f_1^{\gamma N}$ and $f_2^{\gamma N}$ eliminates the interference term in the differential cross section. This makes it easier to determine the form factors from the data and reduces their correlated error. Secondly, the expectation value of the magnetic moment operator taken between nucleon wave packet rest states is proportional to the total magnetic moment, $G_M^N(0)$, and of the charge operator to the total charge, $G_E^N(0)$, as required. By contrast, the Pauli form factor normalizes to the anomalous moment.

A. Electromagnetic Radii

Even though it does not make good physical sense, in the context of quantum field theory, to speak of static charge and magnetic moment distributions, it is permissible to define root-mean-square electromagnetic radii in terms of the form factors directly and bypass the question as to whether they correspond to anything real or not. Such a definition can be made as an analogy to the definition of the expectation value of r^2 for a hadron described by a radial wave function. First expand the exponentials in Eq. (A.2) to lowest order in q^2. This gives

$$G_E^H(\bar{q}^2) = G_E^H(0) - \tfrac{1}{2}\int d^3x(\bar{q}\cdot\bar{x})^2\rho^{\gamma H}(\bar{x}),$$

where the $\bar{q}\cdot\bar{x}$ term integrates to zero by symmetry considerations. Here G_E^H may be taken to represent either the electric form factor of a spin ½ baryon or the charge form factor of a pseudoscalar meson. Next, assume $\rho^{\gamma H}(\bar{x})$ describes a spherically-symmetric charge distribution. Then it follows that

$$G_E^H(\bar{q}^2) = G_E^H(0) - (1/6)\bar{q}^2\langle r^2\rangle_E^H G_E^H(0), \tag{A.3}$$

where the charge radius squared is defined by

$$\langle r^2\rangle_E^H = G_E^H(0)^{-1}\int \rho^{\gamma H}(r) r^2 d^3x. \tag{A.4}$$

Unfortunately, there is no guarantee that the radius defined in this way will be positive-definite. The radius may be expressed in terms of the form factor by differentiating Eq. (A.3). This leads to

$$\langle r^2\rangle_E^H = -6G_E^H(0)^{-1}[dG_E^H(\bar{q}^2)/d\bar{q}^2]_0 \tag{A.5}$$

if $G_E^H(0)\neq 0$. If $G_E^H(0)=0$, it is conventional to drop the term in the denominator of Eq. (A.5). The subscript, $_0$, indicates that the derivative is to be evaluated at $q^2=0$.

For the magnetic form factor (if it exists), one may start with Eq. (A.1) and write

$$\bar{j}^{\gamma H}(\bar{x}) = \bar{\sigma} \times \bar{j}_M^{\gamma H}(\bar{x}),$$

where the hadronic spin magnetization, $\bar{j}_M^{\gamma H}$, is defined by

$$\bar{j}_M^{\gamma H}(\bar{x}) = i(2\pi)^{-3}\int d^3q G_M^H(\bar{q}^2)\bar{q}\exp(i\bar{q}\cdot\bar{x}).$$

This equation may be re-expressed in terms of a magnetic scalar potential, $\phi_M(\bar{x})$, defined by

$$\phi_M(\bar{x}) = -(2\pi)^{-3}\int d^3q G_M^H(\bar{q}^2)\exp(i\bar{q}\cdot\bar{x}).$$

Then,

$$\bar{j}_M^{\gamma H}(\bar{x}) = -\nabla\phi_M(\bar{x}).$$

The Fourier transform then gives

$$G_M^H(\bar{q}^2) = \int d^3x\phi_M(\bar{x})\exp(i\bar{q}\cdot\bar{x}).$$

The radius of the magnetic moment distribution is defined by analogy to Eq. (A.5) as

$$\langle r^2\rangle_M^H = -6G_M^H(0)^{-1}[dG_M^H(\bar{q}^2)/d\bar{q}^2]_0, \qquad (A.6)$$

where ϕ_M is assumed to be radial.

B. Compositeness

Reductionism of the large to smaller constituents has dominated science for centuries. In physics, the concept of compositeness usually entails the idea that the composite entity may be taken apart and put together with no drastic alteration of its constituents during the process. This concept breaks down in the elementary particle domain when the mass defect is of the same order as the mass of the "complex" entity. For a hydrogen atom, $\Delta m/m=10^{-5}$, so it makes sense to speak of the hydrogen atom as a composite system. But for the nucleon built from quarks, for example, $\Delta m/m=3f-1$, where $f>1$ is the ratio of the quark and nucleon masses.

The quarks presumably loose their identity in the nucleon, and it is more accurate to think of the nucleon as composed of quarks in the abstract group-theoretical sense of irreducible representations, especially since quarks do not experimentally appear to exist as free particles.

In relativistic quantum field theory, on the other hand, the nucleon is conceived as a dynamic structure. At any moment the physical nucleon may consist of a bare point-like nucleon and any number of virtual mesons allowed by the conserved quantum numbers of the strong interaction. The existence of such a bare nucleon implies the existence of a hard core term in the nucleon electromagnetic form factor. The simplest way to justify this result is through a consideration of the ground state atomic charge structure of the hydrogen atom. If the hydrogen atom is treated as a composite particle, then its non-relativistic ground state wave function is easily shown to be

$$\psi_0(\bar{x}) = (1/\pi a_0^3)^{\frac{1}{2}} \times \exp(-|\bar{x}|/a_0),$$

where

$$a_0 = \hbar^2/\mu e^2.$$

The atomic form factor of the hydrogen atom is determined by the charge density,

$$\rho(\bar{x}) = |\psi_0(\bar{x})|^2,$$

and can be written as

$$f(\bar{q}^2) = \int d^3x \rho(\bar{x}) \exp(i\bar{q}\cdot\bar{x}).$$

If the Fourier transform is performed, the form factor is seen to obey a dipole equation,

$$f(\bar{q}^2) = (16/a_0^4)[\bar{q}^2+(4/a_0^2)]^{-2},$$

which has an asymptotic q^{-4} behaviour. Had the hydrogen atom been treated as an elementary particle, its charge density would have been written as a delta function so its atomic form factor would be

$$f(\bar{q}^2) = 1.$$

This difference in the asymptotic behaviour of an elementary and composite particle applies in the relativistic case as well, though the proof is complicated by relativity and requires the use of the Bethe-Salpeter equation. Amati and collaborators (142) have shown that the functional form of the form factors at high q^2 allows one to distinguish between a finitely and an infinitely composite particle. The more composite a particle is, the more rapidly its form factor decreases (the fastest decrease consistent with dispersion relations is the exponential). Models of hadrons with N constituents predict that (143)

$$G(q^2) \sim q^{2-2N}$$

as q^2 goes to infinity. In the classical quark model for the nucleon, N=3, so it follows that the nucleon form factors obey

$$G^N_{E,M}(q^2) \sim q^{-4},$$

which is consistent with the dipole formula. For the pion and kaon, N=2, so a monopole form is predicted:

$$f^{\gamma P}(q^2) \sim q^{-2}.$$

VI. APPENDIX B: VECTOR MESON UNIVERSALITY

In order to complete the analogy between vector and axial-vector forces in electromagnetic and weak interactions, in 1960 J.J. Sakurai proposed (8) that the strong interactions are vector in nature, that the neutral vector mesons are coupled to the conserved currents of the strong interaction in a minimal way, and that there exists universal vector meson coupling constants. In particular, he proposed that the ρ is coupled to the isospin, the ϕ to the hypercharge and the ω to the baryon number currents of the hadrons. The nucleonic, pionic and kaonic terms of the effective Lagrangian density for the vector meson-charge interactions are thus

$$\begin{aligned} L_{VHH} = \bar{\rho}_\mu \cdot [2g_{\rho N}\bar{N}\gamma_\mu N + ig_{\rho\pi}\bar{\pi}\times\partial_\mu\bar{\pi} + ig_{\rho K}(K^+ \overleftrightarrow{\partial_\mu} K^-)\ ] \\ + \omega_\mu[ig_{\omega N}\bar{N}\gamma_\mu N + ig_{\omega K}K^+ \overleftrightarrow{\partial_\mu} K^-] \\ + \phi_\mu[ig_{\phi N}\bar{N}\gamma_\mu N + ig_{\phi K}K^+ \overleftrightarrow{\partial_\mu} K^-]. \end{aligned}$$

The universality condition (144) is then written

$$\begin{aligned} g_{\rho\pi} &= 2g_{\rho N} = 2g_{\rho K}, \\ g_{\omega N} &= g_{\omega K}, \\ g_{\phi N} &= g_{\phi K}. \end{aligned} \qquad \text{(B.1)}$$

In terms of vector meson dominance of the electromagnetic form factors the universality relations take the form

$$f^{\gamma\pi}(q^2) = 2f_1^V(q^2) = 2f^{VK}(q^2),$$

$$f_1^{\gamma p}(q^2) = f^{\gamma K^+}(q^2),$$
$$f_1^{\gamma n}(q^2) = f^{\gamma K^0}(q^2). \qquad \text{(B.2)}$$

In SU(3) the $J^{PC}=1^{--}$ vector mesons form a nonet; i.e., an octet and a singlet. In the limit of pure SU(3) symmetry the nine vector mesons are mass-degenerate. But since the physical masses range from 0.770 to 1.02 GeV, it is clear that SU(3) is badly broken by the medium strong and electromagnetic interactions. Consequently, there is no a priori reason why SU(3) should be a good symmetry for the description of the electromagnetic properties of the vector mesons. In fact, in order to explain the failure of simple SU(3) symmetry breaking to identify the masses of V_0 and V_8 (the pure isosinglet and the pure eighth component of the vector meson octet) with the known ω and ϕ, the auxiliary concept of ω-ϕ mixing (145) had to be introduced. In this scheme the physical ω and ϕ are treated as superpositions of the pure SU(3) states as follows:

$$|\omega\rangle = |V_0\rangle\cos\theta + |V_8\rangle\sin\theta,$$
$$|\phi\rangle = |V_8\rangle\cos\theta - |V_0\rangle\sin\theta.$$

Using second order perturbation theory it is possible to show that the mixing angle, θ, has the value 40.2°, determined by the masses of the ω and ϕ. Other forms of mixing theory have been proposed and lead to different predictions for the mixing angle. In all of these predictions the effects of mixing between different nonets in different states of angular momentum excitation is ignored; for example, between nonets containing the ρ and the ρ' (146).

The massive $\psi(3105)$ and $\psi(3695)$ are believed to require a higher internal symmetry group, SU(4), for a complete description. In this scheme the $J^{PC}=1^{--}$ vector meson nonet is contained in a larger $15 \oplus 1$ dimensional representation. The other members include $\psi(3105)$ and three other so far unconfirmed charmed vector mesons and their anti-particles, with masses on the order of 2.2 GeV. This more complicated symmetry results in mixing between the ω, ϕ, and ψ, but the former results are not affected. The ρ', $K^{*'}$, $\psi(3695)$,... are radial excitations of the ρ, K^{*}, $\psi(3105)$,... and form another $15 \oplus 1$ dimensional representation. Hence the notation $\psi'=\psi(3695)$ in Table 1.

In SU(3) there are two ways the vector mesons may be coupled to the baryons and only one way they can be coupled to the pseudoscalar mesons. The SU(3) baryon-vector meson couplings are determined by positing the interaction Lagrangian density,

$$L_{VBB} = f\mathrm{Tr}([\bar{B},B]V) + d\mathrm{Tr}(\{\bar{B},B\}V), \qquad (B.3)$$

where f and d are undetermined coupling constants, and B and V are 3x3 matrices. These matrices are built from the SU(3) generators, λ_i, and from the baryon and vector meson fields, B_i and V_i, according to the equations

$$B = \sqrt{\tfrac{1}{2}} \sum_{i=1}^{8} \lambda_i B_i,$$

$$V = \sqrt{\tfrac{1}{2}} \sum_{i=1}^{8} \lambda_i V_i.$$

Note that the d-type couplings bear no resemblance to Sakurai's vector current theory, but the f-type coupling is identical to his conjecture except that the physical ω and ϕ fields do not occur in Eq. (B.3), but the pure SU(3) fields, V_0 and V_8.

For the vector meson-pseudoscalar meson interaction only the f-type coupling,

$$L_{VPP} = g_P \mathrm{Tr}(V_\mu [P, \overleftrightarrow{\partial_\mu} P]),$$

is possible due to charge conjugation invariance. The Sakurai universality assumption is thus exact in the pure SU(3) limit.

The coupling constants in Eq. (B.1) are related to the SU(3) coupling, g_P, by

$$\begin{aligned} g_{\rho\pi} &= \sqrt{2} g_P, \\ g_{\rho K} &= \sqrt{\tfrac{1}{2}} g_P, \\ g_{\omega K} &= \sqrt{3/2} g_P \sin\theta, \\ g_{\phi K} &= \sqrt{3/2} g_P \cos\theta. \end{aligned} \qquad \text{(B.4)}$$

If the pion form factor is completely dominated by the ρ, then

$$g_P / \sqrt{2} \gamma_\rho = 1.$$

This relation, and the quark model prediction for the mixing angle, $\theta = 35.2^\circ$ (or $\cos\theta = \sqrt{2/3}$, $\sin\theta = \sqrt{1/3}$), then gives

$$\begin{aligned} g_{\rho\pi} / 2\gamma_\rho &= 1, \\ g_{\rho K} / 2\gamma_\rho &= 1/2, \end{aligned}$$

$$g_{\omega K}/2\gamma_{\omega} = 1/6,$$
$$g_{\phi K}/2\gamma_{\phi} = 1/3. \qquad \text{(B.5)}$$

In the field theory of Kroll, Lee and Zumino (16), the vector mesons are coupled to the conserved currents of the strong interaction in a way that results in the hadronic current operator being composed of a simple linear combination of the known neutral vector meson fields, as follows

$$J_{\mu}^{\gamma H} = -(m_{\rho}^2/2\gamma_{\rho})\rho_{\mu} - (m_{\omega}^2/2\gamma_{\omega})\omega_{\mu} - (m_{\phi}^2/2\gamma_{\phi})\phi_{\mu}.$$

The source currents, J_{μ}^{V}, for the vector mesons are defined

$$J_{\mu}^{\rho} = g_{\rho} I_{\mu},$$
$$J_{\mu}^{\omega} = [\cos(\theta_Y - \theta_B)^{-1}][-g_Y Y_{\mu} \sin\theta_B + g_B B_{\mu} \cos\theta_Y],$$
$$J_{\mu}^{\phi} = [\cos(\theta_Y - \theta_B)^{-1}][\, g_Y Y_{\mu} \cos\theta_B + g_B B_{\mu} \sin\theta_Y], \qquad \text{(B.6)}$$

where I_{μ}, Y_{μ}, B_{μ} are the conserved isospin, hypercharge and baryon number currents, and g_Y, g_B, θ_Y, θ_B are undetermined parameters whose values depend on some model for SU(3) symmetry-breaking.

The assumption of SU(4) symmetry allows a reduction of the number of these parameters and imposes a universal coupling on the vector mesons. Banerjee and Levinson (95) have shown that in this case

$$J_{\mu}^{\rho} = g_{\rho} I_{\mu},$$
$$J_{\mu}^{\omega} = (g_{\omega}/2)[2B_{\mu} + Y_{\mu}],$$
$$J_{\mu}^{\phi} = (g_{\phi}/\sqrt{2})[Y_{\mu} - B_{\mu}]. \qquad \text{(B.7)}$$

These equations can be used to relate the vector meson-hadron couplings as follows. For the pseudoscalar mesons, which possess only one form factor, take the matrix element of Eq. (B.7) between single P-states. This leads to

$$
\begin{aligned}
g_{\rho P} &= g_{\rho} I_3(P), \\
g_{\omega P} &= (g_{\omega}/2)[2B(P)+Y(P)], \\
g_{\phi P} &= (g_{\phi}/\sqrt{2})[Y(P)-B(P)],
\end{aligned}
\tag{B.8}
$$

where $I_3(P)$, $B(P)$ and $Y(P)$ are the isospin, baryon number and hypercharge of P. The vector meson-baryon couplings have a similar representation with P replaced by B.

Specialized to the case of the pion, kaon and nucleon, Eq. (B.8) becomes

$$
\begin{aligned}
g_{\rho} &= g_{\rho\pi} = 2g_1^{pp} = 2g_{\rho K}, \\
g_{\omega} &= 2g_{\omega K} = (2/3)g_1^{p\omega}; \; g_{\omega\pi} = 0, \\
g_{\phi} &= \sqrt{2}g_{\phi K}; \; g_1^{p\phi} = g_{\phi\pi} = 0.
\end{aligned}
\tag{B.9}
$$

Sakurai (147) has compared the relevant experiments which give the ρ-hadron coupling constant and has found that the universality of the ρ coupling is strongly supported by the data. Banerjee and Levinson (95) have considered some of the experimental data bearing on the question of ω-universality and have found that it supports a universal coupling.

There are reasons for believing that universality cannot be an exact relation between the vector meson charges, namely, because the assumption of ρ-dominance of the pion form factor, for example, is a

drastic assumption far from the ρ pole, say at $q^2=0$. On the other hand, if the ρ mass vanished, universality would be natural, just as it is for the photon. Since the vector mesons have a large mass, universality can only be an approximate relation.

VII. APPENDIX C: CALCULATIONS OF $I_V(0)$, $I_V'(0)$ AND $I_V''(0)$

The functions $I_V(0)$, $I_V'(0)$ and $I_V''(0)$ are defined as the zeroth, first and second derivatives of $I_V(q^2)$ evaluated at $q^2=0$. They may be written in terms of the derivatives of $D_V(q)$ by making a power series expansion of both sides of Eq. (2.38) and equating the coefficients of equal powers of q^2. This gives

$$\begin{aligned} I_V(0) &= m_V^2[D_V^{-1}(0)]', \\ I_V'(0) &= (m_V^2/6)[D_V^{-1}(0)]''', \\ I_V''(0) &= (m_V^2/60)[D_V^{-1}(0)]^{v}. \end{aligned} \tag{C.1}$$

It is convenient to write $D_V(q)$ in the general form

$$D_V(q) = [\ -(m_V/C) + (A/C)q + (BF_V(q^2)/Cm_V)q^2\ ], \tag{C.2}$$

where

$$F_V(q^2) = 1 + [D_V'''(0)/3D_V''(0)]q + [D_V^{iv}(0)/12D_V''(0)]q^2 + \ldots$$

and where A, B, and C are defined in terms of the derivatives of $D_V(q)$ by

$$\begin{aligned} C &= -m_V/D_V(0), \\ A &= D_V'(0)C, \\ B &= (m_VC/2)D_V''(0). \end{aligned} \tag{C.3}$$

It is then straightforward, but tedious, to shown that by expanding the inverse of Eq. (C.2), the derivatives can be expressed in terms of A, B, and C and the other derivatives of $D_V(q)$ through the relations

$$I_V(0) = -AC,$$

$$I_V'(0) = (C/m_V^2)[A^3+2AB+(m_VB/3)\{D_V'''(0)/D_V''(0)\}],$$

$$I_V''(0) = -(2C/m_V^4)[A^5+4BA^3+3AB^2+m_VBA^2\{D_V'''(0)/D_V''(0)\}$$
$$+ (2m_VB^2/3)\{D_V'''(0)/D_V''(0)\} + (ABm_V^2/6)\{D_V^{iv}(0)/D_V''(0)\}$$
$$+ (m_V^3B/60)\{D_V^{v}(0)/D_V''(0)\}]. \qquad (C.4)$$

The values of the derivatives of $D_V(q)$ for the two propagators used in this analysis are as follows:

(1.) For the simple propagator,

$$D_V'(0) = [1+(1/\pi)\tan^{-1}(\Gamma_V/2\{m_V-\mu_V\})]-(\Gamma_V/4\pi m_V)\log_e(\mu_V^2/|m_{1V}-\mu_V|^2),$$

$$D_V''(0) = \Gamma_V/\pi m_V\mu_V,$$

$$D_V'''(0) = 3\Gamma_V/2\pi m_V\mu_V^2,$$

$$D_V^{iv}(0) = 4\Gamma_V/\pi m_V\mu_V^3,$$

$$D_V^{v}(0) = 15\Gamma_V/\pi m_V\mu_V^4.$$

(2.) For the complex propagator,

$$\alpha_V^{-1}\pi D_V(0) = 2Re\{ [\pi i+L(m_{1V}^*)]R(m_{1V}^*,0) \} + (3\pi\mu_V/4)$$
$$-(\mu_V^2/|m_{1V}|^2)[(\pi\mu_V/2)+2Re\{m_{1V}+(\pi\mu_V m_{1V}/2m_{1V}^*)\}],$$

$$\alpha_V^{-1}\pi D_V'(0) = 2Re\{ [i+L(m_{1V}^*)]R(m_{1V}^*,0)/m_{1V} \} - (4/3)$$
$$-(\mu_V^2/|m_{1V}|^2) - (\pi\mu_V^3/|m_{1V}|^2)Re(1/m_{1V}),$$

$$\alpha_V^{-1}\pi D_V''(0) = 3\pi/8\mu_V,$$

$$\alpha_V^{-1}\pi D_V'''(0) = 6/5\mu_V^2,$$

$$\alpha_V^{-1}\pi D_V^{iv}(0) = 3\pi/4\mu_V^3,$$

$$\alpha_V^{-1}\pi D_V^{v}(0) = 48/7\mu_V^4.$$

To lowest order in Γ_V/m_V, μ_V/m_V, and $\mu_V\Gamma_V/m_V^2$, for the simple propagator the initial derivatives of I_V may be written

$$I_V(0) = -1 + (\Gamma_V/2\pi m_V)[1+(2\mu_V/m_V)+\log_e(\mu_V/m_V)],$$

$$I_V'(0) = (1/m_V^2)[1+(\Gamma_V/2\pi m_V)-(4\Gamma_V\mu_V/2\pi m_V^2)-(3\Gamma_V/2\pi m_V)\log_e(\mu_V/m_V)$$
$$+(\Gamma_V/\mu_V)\{1-(\Gamma_V/2\pi m_V)-(\Gamma_V\mu_V/2\pi m_V^2)\}].$$

VIII. APPENDIX D: THE COMPUTER PROGRAMS

A number of computer programs were utilized in the analysis of the hadronic electromagnetic form factors in order to minimize the total χ^2. The most efficient of these is based on the gradient expansion algorithm of Marquardt (148). A brief description of the theory underlying this program follows.

Let the data points be (x_i,y_i) and let σ_i represent the standard deviation for each measurement, which is assumed to be equal to the experimental error. Ignore errors in x_i. Let the theory function be represented by $y(x,a_k)$, where a_k represents a set of NTERM parameters to be determined by fitting the data; k=1,2,3,...NTERM.

The theory function may be expanded about its value at the initial parameters, a_{ok}, as follows:

$$y(x,a) = y(x,a_o) + \sum_{j=1}^{NTERM} (\partial y/\partial a_j)_{a_{oj}} \delta a_{oj}, \qquad (D.1)$$

where $\delta a_j = a_j - a_{oj}$. The deviation from the ith experimental value is

$$(DEV)_i = y_i - y(x_i,a) = y_i - y(x_i,a_o) - \sum_j (\partial y(x_i)/\partial a_j)_{a_{oj}} \delta a_j.$$

The chi-square function is now defined as the sum of the squares of the deviations from the observed values weighted by the mean standard deviations; that is,

$$\chi^2 = \sum_i \frac{(DEV)_i^2}{\sigma_i^2}, \qquad (D.2)$$

and is a measure of the goodness of the fit of the theory function to the data. The goal is to determine the set of parameters which minimizes the difference between theory and experiment. In the method of least squares, this is the same as finding the smallest value for the calculated chi-square. Thus minima are sought in χ^2 for values of δa_k that are simultaneous solutions to

$$\partial\chi^2/\partial\delta a_k = 0. \tag{D.3}$$

If the curvature matrix element, α_{jk}, is defined by the equation

$$\alpha_{jk} = \sum_i (1/\sigma_i^2)[\partial y(x_i)/\partial a_k]_{a_{ok}} [\partial y(x_i)/\partial a_k]_{a_{ok}} \tag{D.4}$$

and the column vector, β_k, by

$$\beta_k = \sum_i (1/\sigma_i^2)[y_i - y(x_i)][\partial y(x_i)/\partial a_k]_{a_{ok}}, \tag{D.5}$$

then the condition for a minimum in χ^2 can be re-written more compactly as the matrix equation

$$\bar{\beta} = \alpha\delta\bar{a}. \tag{D.6}$$

This equation is a condition for a minimum in χ^2 only if the initial values of the parameters are very close to the minimum in order for the Taylor series expansion, Eq. (D.1), to apply. The $\delta\bar{a}$ calculated by inverting Eq. (D.6) may not correspond to those of the minimum. Thus the need for an iteration procedure to search for the true minimum.

It is not mathematically convenient to solve these equations analytically when the theory functions are complicated. Instead, χ^2 is

considered to be a continuous function of NTERM parameters describing a hypersurface in an NTERM-dimensional space. This space is then searched for the appropriate minimum of χ^2. Since local minima usually interfere with the search it is necessary to estimate the values of the unknown parameters so that the initial chi-square lies close to the absolute minimum. This can be implemented by performing a grid mapping to identify the desired range of parameters and by using as much physical insight as possible to set their initial values.

The gradient-expansion algorithm is designed to optimize the searching procedure even far from the minimum χ^2. The algorithm begins by increasing the diagonal elements of the curvature matrix by an amount λ. Then,

$$\alpha'_{jk} = \begin{cases} \alpha_{jk}(1+\lambda); & j=k \\ \alpha_{jk} & ; \; j\neq k. \end{cases}$$

If λ is very small, the solution to this equation is essentially the same as that of Eq.(D.6). If λ is very large, the equations decouple because the diagonal terms dominate,

$$\beta_j = \lambda \delta a_j \alpha_{jj}.$$

The increments, δa_j, are now in the same direction as the gradients, β_j. The complete algorithm reads

1. Compute $\chi^2(a)$.
2. Let $\lambda=0.001$.
3. Calculate $\delta\bar{a}$ and $\chi^2(a+\delta a)$ from Eq. (D.6) for $\lambda=0.001$.

4. If $\chi^2(a+\delta a)>\chi^2(a)$, increase λ by a factor of 10 and go to 3.

5. If $\chi^2(a+\delta a)<\chi^2(a)$, decrease λ by a factor of 10. Take $a+\delta a$ as the new starting point and go to 3.

Thus, far from the minimum the algorithm gives solutions characteristic of a gradient-search, in which the direction of search is along the direction of maximum decrease of χ^2. Close to the mimimum, as can be seen from Eq. (D.6), the algorithm yields solutions characteristic of an analytical expansion method in which it is assumed that χ^2 is parabolic near the minimum. The Fortran-coded program used to minimize χ^2 and fit the pion form factor data is given at the end of the discussion.

All of the expressions derived in this Appendix are slightly modified when several different sets of data and corresponding theory functions are fit simultaneously using the same set of free parameters. In this case χ^2 is composed of a sum of chi-squares defined by the separate theory functions,

$$\chi^2 = \sum_{k=1}^{NTF} \chi_k^2,$$

where

$$\chi_k^2 = \sum_{i=1}^{NDP_k} (1/\sigma_i^2)[y_i^k - y^k(x_i^k,a) - \sum_{j=1}^{NTERM} (\partial y^k(x_i^k,a_o)/\partial a_j)_{a_{oj}} \delta a_j]^2$$

and where the superscript k represents the kth theory function, and the sum over i is over the total number of theory functions, NTF. It is then straightforward to see that the curvature matrix element and the β vector become

$$\beta_h = \sum_{k=1}^{NTF} \sum_{i=1}^{NDP_k} (1/\sigma_i^{k2})[y_i^k - y^k(x_i^k, a_o)][\partial y^k(x_i^k)/\partial a_h]_{a_{oh}},$$

$$\alpha_{jh} = \sum_{k=1}^{NTF} \sum_{i=1}^{NDP_k} (1/\sigma_i^{k2})[\partial y^k(x_i^k)/\partial a_j]_{a_{oj}} [\partial y^k(x_i^k)/\partial a_h]_{a_{oh}}.$$

The goodness of fit is measured by the chi-square per degree of freedom, χ_F^2, also called the reduced chi-square. This quantity is determined by the total number of data points,

$$NDP = \sum_{k=1}^{NTF} NDP_k,$$

and by the number of variable parameters in the fit (NVPAR) according to the equation

$$\chi_F^2 = \chi^2/(NDP-NVPAR).$$

A good fit is defined by a set of parameters for which the theory function falls within the errors of all the data points, $\chi_F^2 \leq 1.0$. A value of χ_F^2 less than one does not necessarily indicate an improvement of the fit because the data represents a limited sample and the chi-square is expected to fluctuate from experiment to experiment.

Assuming the deviations obey a Gaussian distribution, the probability that a random set of NDP measurements will yield a value of χ^2 as large or larger than that obtained is expressed by the confidence level, $P(\chi^2, NDP)$, which is tabulated and easily accessible in books on statistics. A reduced chi-square of one corresponds to a confidence level of approximately 50%. In general, the confidence level is useful as a tool for rejecting theory functions, not for validating the correctness of two theory functions giving similar confidence levels.

```
C
C       CURFIT:  A MINIMIZATICN PROGRAM UTILIZING THE
C       GRADIENT EXPANSION ALGORITHM OF MARQUARDT
C       TO FIT THE TIME-LIKE PION FORM FACTOR
C
C       DESCRIPTION OF PARAMETERS
C       X: ARRAY OF DATA POINTS FOR INDEPENDENT VARIABLE
C       Y:  ARRAY OF DATA POINTS FOR DEPENDENT VARIABLE
        SIGMAY:  ARRAY OF STANDARD DEVIATIONS FOR
C       Y DATA POINTS
C       NDP:  NUMBER OF PAIRS OF DATA POINTS
C       NTERMS: NUMBER OF PARAMETERS
C       NVPAR:  NUMBER OF VARIABLE PARAMETERS
C       A:  ARRAY OF PARAMETERS
C       THEORY:  THE THEORY FUNCTION; CALCULATED VALUES
C       OF Y
C       CHISQ1:  CHI SQUARE
C
C       CCMMENTS:
C       DIMENSION STATEMENTS ALLOW NTERMS UP TO 8
C       FLAMDA=0.001 AT BEGINNING OF SEARCH
C
        REAL BETA(8),ALPHA(8,8),FLAMDA,A(8),B(8)
        REAL BET(8),WT(8),ARRAY(8,8),ALPH(8,8),C(8)
        INTEGER COUNT(25),C1(8),C2(8)
        COMMON /BBB/ NDP,NVPAR
        CCMMCN/CCC/ WT
        COMMON/EEE/NQ
        CATA FLAMDA/0.001/
        CALL ASSIGN(5,'CR:',3,IERR)
        CALL ASSIGN(6,'LP:',3,IERR)
        CEFALT=.00000000000001
C
C   DEFALT SHOULD BE <<(EPS)**2
C
        READ(5,111) EPS,NTERMS,NSTEPS
  111   FORMAT(F10.3,8X,I2,8X,I2)
        WRITE(6,111) EPS,NTERMS,NSTEPS
      5 DO 12 I=1,NSTEPS
     12 COUNT(I)=0
        NSTEPS=0
        FLAMDA=.001
C
C       INPUT DATA:  INITIAL PARAMETER VALUES AND WEIGHTS
C
        READ(5,10,END=90)(C1(I),C2(I),A(I),WT(I),I=1,NTERMS)
   10   FORMAT(9X,A4,6X,A4,5X,F12.7,F10.4)
        WRITE(6,11)
   11   FORMAT(5X,'INPUT PARAMETERS:')
        WRITE(6,13)(I,C1(I),C2(I),A(I),WT(I),I=1,NTERMS)
```

```
 13    FORMAT(4X,I2,3X,A4,2X,A4,4X,F10.4,F7.1)
       READ(5,321) NQ
 321   FORMAT(9X,I1)
C
       NVPAR=0
       DO 17 I=1,NTERMS
       C(I)=A(I)
    17 NVPAR=NVPAR+WT(I)
C
C   CALCULATE CHISQ,ALPHA, BETA
C
       CALL FCN(NTERMS,  CHISQ1,A,1,ALPHA,BETA)
    35 ARRAY(J,K)=ALPHA(J,K)/ SQRT(ABS(ALPHA(J,J)
       CHISQ3=CHISQ1/(NDP-NVPAR)
       WRITE(6,104) CHISQ1,CHISQ3
 104   FORMAT('0',/,1X,9X,'CHISQUARE',5X,'CHISQUARE/(NDP-
      1NVPAR)',3X, NDF',3X,'NVPAR',2X,'STEPS',3X,'COUNT',
      1/,1X,2F20.10)
       IF(NQ .EQ. 0) GO TO 91
C
C   COUNT THE ITERATIONS
C
    70 NSTEPS=NSTEPS+1
C
C   DEFINE ARRAY ACCORDING TO FORMULA,
C      NORMALIZING IT TO THE DIAGONAL
C
    55 DO 30 J=1,NTERMS
       DO 34 K=1,J
      1*ALPHA(K,K))+DEFALT)*WT(K)*WT(J)
    34 ARRAY(K,J)=ARRAY(J,K)
       ARRAY(J,J)=(1. + FLAMDA  )*WT(J)
    30 CONTINUE
C
C   INVERT ARRAY
C
       CALL MATINV (ARRAY,NTERMS,DET)
C
C    INCREMENT A, AND CALCULATE NEW VALUES OF CHISQ, ALPHA,
C      AND BETA
C
       DO 40 J=1,NTERMS
       B(J)=A(J)
       DO 40 K=1,NTERMS
    40 B(J)=B(J)+ BETA(K)*ARRAY(J,K)/SQRT(ABS(ALPHA(J,J)*
      1ALPHA(K,K))+DEFALT)
       CALL FCN(NTERMS,CHISQ2,B,4,ALPH,BET)
       IF(CHISQ1-CHISQ2) 45,50,50
    45 FLAMDA=10*FLAMDA
       COUNT(NSTEPS)=COUNT(NSTEPS)+1
```

```
C
C  IF SEQUENCE IS NOT CONVERGING, ABORT
C
      IF(FLAMDA.GT.10000) GO TO 61
      GO TO 55
C
C  CHECK TO SEE IF DELTA CHISQ IS LESS THAN EPS
C
 50   WRITE(6,76) CHISQ2
 76   FORMAT('0',/,10X,'INTERMEDIATE CHISQ=',F20.10)
      WRITE(6,1131)
 1131 FORMAT('0',T13,'PARAMETER',T25,'WEIGHT',T36,
     1'INITIAL VALUE',T58,'FINAL VALUE')
      WRITE(6,1121)(I,C1(I),C2(I),WT(I),C(I),B(I)
     |,I=1,NTERMS)
 1121 FORMAT(1X,3X,I2,5X,A5,A5,5X,F2.0,2F20.10)
      IF(CHISQ1-CHISQ2-EPS  ) 65,60,60
   65 CHISQ1=CHISQ2
C
C  IF SEQUENCE IS NOT CONVERGING, ABORT
C
      IF(NSTEPS.GT.24) GO TO 61
      DO 75 J=1,NTERMS
      BETA(J)=BET(J)
      A(J)=B(J)
      DO 75 I=1,NTERMS
   75 ALPHA(I,J)= ALPH(I,J)
      FLAMDA=FLAMDA/10.
C
C  SINCE DELTA CHISQ WAS TOO LARGE, BUT CHISQ DECREASED,
C     REITERATE
C
      GO TO 70
   61 WRITE(6,153)
  153 FORMAT('    THE SEQUENCE IS NOT CONVERGING')
      DO 699 J=1,NTERMS
  699 BETA(J)=B(J)-A(J)
      WRITE(6,651)(A(J),BETA(J),J=1,NTERMS)
  651 FORMAT(1X,'THE COMPARISON SET OF PARAMETERS AND THE
     1LAST SET OF INCREMENTS WERE',/,10(2F20.10,/))
      WRITE(6,124) CHISQ1
  124 FORMAT(1X,'THE COMPARISON CHISQUARE WAS  ',F20.10)
   60 CHISQ3=CHISQ2/(NDP-NVPAR)
      WRITE(6,102) CHISQ2,CHISQ3,NDP,NVPAR,NSTEPS,
     1(COUNT(I),I=1,NSTEPS)
  102 FORMAT(    2F20.10,7X,3(I3,4X),20(I2,1X))
C
C     OUTPUT INITIAL AND FINAL VALUES OF PARAMETERS
C
      WRITE(6,113)
```

```
 113  FORMAT(T13,'PARAMETER',T25,'WEIGHT',T36,
     1'INITIAL VALUE',T58,'FINAL VALUE')
      WRITE(6,112)(I,C1(I),C2(I),WT(I),C(I),B(I),
     1I=1,NTERMS)
 112  FORMAT(1X,3X,I2,5X,A5,A5,5X,F2.0,2F20.10)
C  CALL FCN FOR THE LAST TIME, IFLAG = 3
C
      CALL FCN(NTERMS, CHISQ2,B,3, ALPHA, BETA)
 91   CONTINUE
C
C  GO ON TO NEXT DATA SET
C
      GO TO 5
   90 STOP
      END




      SUBROUTINE MATINV(ARRAY,NORDER,DET)
      REAL   ARRAY,DET
      DIMENSION ARRAY(8,8),IK(8),JK(8)
      NSTEPS=0
      DET=1.
      DO 100 K=1,NORDER
      AMAX=0.
   21 DO 30 I=K,NORDER
      DO 30 J=K,NORDER
      IF(ABS(AMAX)- ABS(ARRAY(I,J))) 24,24,30
   24 AMAX=ARRAY(I,J)
      IK(K)=I
      JK(K)=J
   30 CONTINUE
      IF(AMAX) 41,32,41
 41   I=IK(K)
      IF(I-K) 21,51,43
   43 DO 50 J=1,NORDER
      SAVE=ARRAY(K,J)
      ARRAY(K,J)=ARRAY(I,J)
   50 ARRAY(I,J)=-SAVE
   51 J=JK(K)
      IF(J-K) 21,61,53
   53 DO 60 I=1,NORDER
      SAVE=ARRAY(I,K)
      ARRAY(I,K)=ARRAY(I,J)
   60 ARRAY(I,J)=-SAVE
   61 DO 70 I=1,NORDER
      IF(I-K) 63,70,63
   63 ARRAY(I,K)=-ARRAY(I,K)/AMAX
```

```
   70 CONTINUE
      DO 80 I=1,NORDER
      DO 80 J=1,NORDER
      IF(I-K) 74,80,74
   74 IF(J-K) 75,80,75
   75 ARRAY(I,J)=ARRAY(I,J)+ARRAY(I,K)*ARRAY(K,J)
   80 CONTINUE
      DO 90 J=1,NORDER
      IF(J-K) 83,90,83
83    ARRAY(K,J)=ARRAY(K,J)/AMAX
90    CONTINUE
      ARRAY(K,K)=1./AMAX
      NSTEPS=NSTEPS+1
  100 DET=DET*AMAX
   32 DO 130 L=1,NSTEPS
      K=NSTEPS+1-L
      J=IK(K)
      IF(J-K) 111,111,105
  105 DO 110 I=1,NORDER
      SAVE=ARRAY(I,K)
      ARRAY(I,K)=-ARRAY(I,J)
  110 ARRAY(I,J)=SAVE
  111 I=JK(K)
      IF(I-K) 130,130,113
  113 DO 120 J=1,NORDER
      SAVE=ARRAY(K,J)
      ARRAY(K,J)=-ARRAY(I,J)
  120 ARRAY(I,J)=SAVE
  130 CONTINUE
  140 RETURN
      END
```

```
      FUNCTION THEORY(T,X,J,K)
      REAL*4 I0,I1,T(2,13),   PHASE1,SNGL,LQ
      COMPLEX DV10,DV20,IV,GV(5),DV1,DV2,FPI,Q1
      REAL*4 ALOG,SQRT,ATAN,REAL,CABS
      REAL*8 W0,DATAN,DLOG,CDABS,D1,D2,I2(2),DBLE
      COMPLEX M1,M2,  L1,S1,RS,CMPLX,CONJG
      COMPLEX CSQRT,CLOG,A1,A2,M3,M4,CEXP
      COMPLEX M5,A3,A4,A5,M6
      REAL*4 ALPHR(5),ABS,ALPHA(5),GAMA(5)
      REAL*4 PI,MU(5),X(8),WT(8)
      DATA PI/3.141593/
      DATA    GAMA   /2.6,7.7,6.2,5.2,5.2/
      DATA    MU/0.2792,0.2792,0.9877,0.5584,0.5584/
      DATA ALPHR/0.08824,0.0064,0.0022,0.1094,0.1094/
```

```
      DO 9 I=1,2
      M1=CMPLX(X(I), X(I+2)/2.)
      M2=CONJG(M1)
      THETA=SNGL(DATAN(X(I+2)/(2.D0*(DBLE(X(I))-
     1DBLE(MU(I))))))
      PHI   =SNGL(DATAN(X(I+2)/(2.D0*(DBLE(X(I))+
     1DBLE(MU(I))))))
      B1=CABS(M1-CMPLX(MU(I),0.0))
      B2=CABS(M1+CMPLX(MU(I),0.0))
      A1=CMPLX(0.0,THETA)
      A3=CMPLX(0.0,PHI)
      A4=(A1-A3)/2.
      ANGLE=(THETA-PHI)/2.
      M3=B1*CEXP(A1)
      M5=B2*CEXP(A3)
      Z=SQRT(B1/B2)
      BETA=ATAN((2.*Z*SIN(ANGLE))/(1.-(Z**2)))
      A5=CMPLX(0.0,BETA)
      B3=1.+(Z**2)-(2.*Z*COS(ANGLE))
      B4=1.-(Z**2)
      B5=2.*Z*SIN(ANGLE)
      M4=CMPLX(B4/B3,B5/B3)
      L1=CMPLX(ALOG(CABS(M4)),BETA)
      GAMMA=3.*(THETA+PHI)/2.
      S1=((SQRT(B1*B2))**3)*CEXP(CMPLX(0.0,GAMMA))
      RS=(((CMPLX(0.0,PI)+L1)*S1)/((M1-M2)*M1**2))
      RV=REAL(M2+((PI*MU(I)*M2)/(2.*M1)))
      D00=(-2.*REAL(RS*M2)/1.)-(3.*PI*MU(I)/4.)+
     1((((PI*MU(I)/2.)+(2.*RV))*MU(I)**2)/(CABS(M1)**2))
      C10=((2.*1.0   *REAL(RS))/1.)-(4./3.)-((MU(I)**2)/
     1(CABS(M1)**2))- ((PI*REAL(1./M2)*MU(I)**3)/
     1(CABS(M1)**2))
      ALPHA(I) =(X(I+2)/(2.*X(I)))/(SQRT(1.-((MU(I)/X(I))
     1**2))**3)
      C0=D00*ALPHA(I)/PI
      D1=D10*ALPHA(I)/PI
      D2=((3.*PI)/(8.*MU(I)))*ALPHA(I)/PI
      D3=(6./(5.*MU(I)**2))*ALPHA(I)/PI
      C=-X(I)/D0
      A=D1*C
      B=((X(I)*C)/2.)*D2
      I0=-A*C
      I1=(A**3)+(2.*A*B)
      I1=I1+((B*X(I)/3.)*(D3/D2))
      I1= (C/(X(I)**2))*I1
      Q=SQRT(-T(J,K))
      Q1=CMPLX(Q,0.0)
      SQ=(Q**2)-(MU(I)**2)
      LQ=ALOG((Q+SQRT(SQ))/MU(I))
100   CONTINUE
```

```
      DV10=(1./Q)+(1./M1)+(1./M2)
      CV10=DV10*(PI*MU(I)/2.)
      DV10=1.+DV10
      CV10=DV10*(CABS(Q1-M2))**2
      CV10=-DV10*( (MU(I)**2)/(Q*CABS(M1)**2))
      DV10=DV10+2.*REAL(RS*(Q1-M2))
      IF(G .LT. 0) GO TO 101
      DV1 =DV10+(((CMPLX(0.0,PI)-LQ)*SQRT(SQ)**3)/(Q**2))
      Q=-Q
      Q1=-Q1
      GO TO 100
101   CONTINUE
      DV20=DV10+((LQ*SQRT(SQ)**3)/(Q**2))
      DV1=DV1 *ALPHA(I)/PI
      CV2=DV20*ALPHA(I)/PI
      IV=((X(I)**2)/(2.*(-Q)))*((1./DV1)-(1./DV2))
      GV(I)  =I1+((I0-IV)/T(J,K))
9     CONTINUE
      GO TO (10,20),J
10    FPI=1.-((2.*X(5)*GV(1)*X(1)**2)/(2.*GAMA(1)))
     1-CMPLX(X(6),X(7))*GV(2)*((X(2)**2)/(2.*GAMA(2)))
      THEORY=(CABS(FPI))**2
20    CONTINUE
      GO TO 50
50    CONTINUE
      RETURN
      END



      SUBROUTINE FDTH(NTERMS,X,A,I,J)
      REAL X(2,13),A(8),WT(8),DERIV(8)
      COMMON/CCC/WT
      COMMON/DDD/DERIV
      DO 18 K=1,NTERMS
      A(K)=A(K)+.0005
      F2=THEORY(X,A,I,J)
      A(K)=A(K)-.001
      F1=THEORY(X,A,I,J)
      DERIV(K)=(F2-F1)/.001
18    A(K)=A(K)+.0005
      RETURN
      END
```

```
      SUBROUTINE FCN(NTERMS,CHISQ1,A,IFLAG,ALPHA,BETA)
      REAL ALPHA(8,8),BETA(8),DERIV(8),A(8),WT(8)
      REAL X(2,13),Y(2,13),SUM(2),SIGMAY(2,13)
      INTEGER N(4),Z
      COMMON/BBB/ NDP,NVPAR
      COMMON/CCC/WT
      COMMON/DDD/DERIV
      COMMON/EEE/NQ
      GO TO (10,20,30,40),IFLAG
 10   CONTINUE
      READ(5,1400) N1,N2
 1400 FORMAT(8X,I2,8X,I2)
C     READ IN PION DATA
      READ(5,1301)(X(1,K),Y(1,K),SIGMAY(1,K),K=1,N1)
 1301 FORMAT(3F13.4)
      WRITE(6,1360)
 1360 FORMAT('0',5X,' TIME-LIKE PION DATA:',/,T4,
     1'MOMENTUM**2',T18,'FORM FACTOR**2',T34,'ERROR')
      WRITE(6,1301)(X(1,K),Y(1,K),SIGMAY(1,K),K=1,N1)
      N(1)=N1
      N(2)=N2
      NDF=N(1)
 40   CONTINUE
      DO 12 K=1,2
 12   SUM(K)=0.0
C***DO 11 J=1,2; DO 50 M=1,2 *********
      J=1
      Z=N(J)
      DO 11 K=1,Z
 11   SUM(J)=SUM(J)+((THEORY(X,A,J,K)-Y(J,K))/
     1(SIGMAY(J,K))
     1)**2
      CHISQ1=SUM(1)
      IF(NQ .EQ. 0) GO TO 30
C
C     INITIALIZE CURVATURE MATRIX
      DO 34 J=1,NTERMS
      BETA(J)=0.
      DO 34 K=1,J
 34   ALPHA(J,K)=0.
C
C     DEFINE UPPER ECHELON OF CURVATURE MATRIX
      M=1
      Z=N(M)
      DO 50 I=1,Z
      CALL FDTH(NTERMS,X,A,M,I)
      DO 46 J=1,NTERMS
      BETA(J)=BETA(J)+((Y(M,I)-THEORY(X,A,M,I))/
     1((SIGMAY(M,I))**2))
     1*DERIV(J)*WT(J)
```

```
      DO  46 K=1,J
 46   ALPHA(J,K)=ALPHA(J,K)+((DERIV(J)*DERIV(K))/
     1((SIGMAY(M,I))**2))
     1*WT(J)*WT(K)
 50   CONTINUE
C
C     DEFINE LOWER ECHELON OF CURVATURE MATRIX
      DO 53 J=1,NTERMS
      DO 53 K=1,J
 53   ALPHA(K,J)=ALPHA(J,K)
      GO TO 20
 30   CONTINUE
 20   CONTINUE
      RETURN
      END
```

IX. APPENDIX E: RESEARCH IN PROGRESS

To further investigate the P-wave pion-pion phase shift problem associated with the unstable particle propagators presented in this discussion, the ρ-propagator is modified by introducing a parameter, a_ρ, and writing

$$\mathrm{Im}[R_\rho(m')] = \alpha_\rho m'[1-(\mu_\rho/m')^2]^{3/2} f(m')\theta(m'-\mu_\rho),$$

where

$$f(m') = (m'/m_\rho)^2[(m_\rho^2 + a_\rho^2)/(m'^2 + a_\rho^2)].$$

This parametrization, giving $f(m_\rho)=1$, is a phenomenological way of introducing structure into the $\rho\pi\pi$ vertex.

The parameter, a_ρ, is treated as an adjustable parameter and its value is to be determined by a least squares fit to the pion form factor and simultaneously to the phase shift data. This parametrization will introduce a degree of freedom that hopefully will allow the P-wave phase shift to be fit. This gives the theory the option of controlling discordant data until the values of the pion phase shift at the inelastic threshold are known with more certainty.

Preliminary work utilizing this propagator leads to the following results. A plot of the pion radius against the parameter a_ρ for fixed values of the ρ resonance parameters (Fit 10) shows that for $a_\rho=0$ the pion charge radius is 0.75 f., as required for consistency, the radius then decreases uniformly with increasing a_ρ until for $a_\rho=1.0$ the radius is

quite close to the standard vector meson dominance result using monopole propagators, 0.60 f. Over this same region, the P-wave phase shift varies from 24° at $a_{\rho}=0$ to 12° at $a_{\rho}=1.0$.

The correlation between the parameters m_{ρ}, Γ_{ρ}, $g_{\rho\pi}$, and a_{ρ} can only be determined by a fit to the data, which has not yet been performed. The indications are, however, that if the least square fit chooses a value for a_{ρ} much larger than 1.0, as will probably be required in order to simultaneously fit the pion form factor and the phase shift data, then the corresponding pion charge radius will not be much different from the standard vector meson dominance result. This suggests that if the measurements leading to a large pion charge radius are correct (as well as the highly model-dependent phase shift measurements), some mechanism other than vector meson instability will be needed to account for it; for example, the inclusion of inelastic channels coupled to the ρ.

X. ACKNOWLEDGEMENTS

The author is deeply indebted to Dr. C.L. Hammer for his thought and guidance throughout this work, and to Dr. B. DeFacio and Dr. B.L. Young for many rewarding discussions.

XI. REFERENCES

1. J.E. Augustin, A.M. Boyarski, M. Breidenback et al., Phys. Rev. Lett. 34, 233(1975).

2. R.G. Sachs, Phys. Rev. 87, 1100(1952); F. Zachariasen, Phys. Rev. 102, 295(1956); S. Fubini, Nuovo Cimento 3, 1425(1956); G. Salzman, Phys. Rev. 105, 1076(1957).

3. R. Hofstadter, F. Bumiller and M.R. Yearian, Rev. Mod. Phys. 30, 482(1958).

4. A recent calculation has improved this situation, however. See B.B. Deo and L.P. Singh, Phys. Rev. D10, 308(1974).

5. G.F. Chew, R. Karplus, S. Gasiorowicz and F. Zachariasen, Phys. Rev. 110, 265(1958); W.R. Frazer and J.R. Fulco, Phys. Rev. Lett. 2, 365(1959).

6. There are two ambiguities in the dispersion relation approach. First it is unclear to which form factors, the Pauli and Dirac, or the electric and magnetic, the method is to apply. Secondly, there is no way in the context of dispersion theory alone to determine whether subtracted or unsubtracted dispersion relations are required.

7. J.W. Moffat, Phys. Rev. 177, 2456(1969); N. Zovko, Nuovo Cimento Lett. 4, 1278(1970).

8. J.J. Sakurai, Ann. Phys. (N.Y.) 11, 1(1960).

9. L.H. Chan, K.W. Chen, J.R. Dunning et al., Phys. Rev. 141, 1298(1966).

10. L.N. Hand, D.G. Miller and R. Wilson, Rev. Mod. Phys. 35, 335(1958); M.W. Kirson, Phys. Rev. 132, 1249(1963); A.P. Balachandran, P.G.O. Freund and C.R. Schumacher, Phys. Rev. Lett. 12, 209(1964).

11. J.S. Levinger, Nuovo Cimento 26, 813(1962); G.L. Kane and R.A. Zdanis, Phys. Rev. 151, 1239(1966).

12. J.S. Ball and M. Parkinson, Phys. Rev. 162, 1509(1967).

13. J.S. Ball and D.Y. Wong, Phys. Rev. 130, 2112(1963); S. Furichi and K. Watanabe, Prog. Theor. Phys. 35, 174(1966); P. Signell and J.W. Durso, Phys. Rev. Lett. 18, 185(1967).

14. G. Cocho, Nuovo Cimento 42A, 421(1966).

15. T. Massam and A. Zichichi, Nuovo Cimento 43A, 1137(1966); T. Massam and A. Zichichi, Nuovo Cimento Lett. 1, 387(1969).

16. N.M. Kroll, T.D. Lee and B. Zumino, Phys. Rev. 157, 1376(1967).

17. K.Y. Ng, Phys. Rev. 170, 1435(1968).

18. R.F. Meyer, Nuovo Cimento Lett. 2, 76(1969); K. Fujimura, Prog. Theor. Phys. 43, 73(1970).

19. R.E. Krepps and J.W. Moffat, Phys. Rev. 175, 1945(1972).

20. P. DiVecchia and F. Drago, Nuovo Cimento Lett. 1, 917(1969); P.H. Frampton, Phys. Rev. 186, 1419(1969); M. Kobayashi, Prog. Theor. Phys. 42, 1319(1969).

21. R. Jengo and E. Remiddi, Nuovo Cimento Lett. 1, 922(1969).

22. V. Wataghin, Nuovo Cimento 54A, 805(1968); V. Wataghin, Nucl. Phys. B10, 107(1969).

23. B.B. Deo and M.K. Parida, Phys. Rev. D9, 2939(1973).

24. G.F. Chew and S. Mandelstam, Phys. Rev. 119, 467(1960).

25. F.M. Renard, Phys. Lett. B47, 361(1973).

26. D.R. Yennie, M.M. Levy and D.G. Ravenhall, Rev. Mod. Phys. 29, 144(1957); M. Gourdin, Nuovo Cimento 36, 129(1965).

27. Let $C=C^{+}=C^{-1}$ be the charge conjugation operator for the strong interactions. Then

$$CJ_{\mu}^{Y}C^{-1} = -J_{\mu}^{Y}.$$

From these properties note that if $|a\rangle$ is a single-particle state, and $|\bar{a}\rangle$ the single-antiparticle state,

$$\langle a|CJ_{\mu}^{Y}C^{-1}|a\rangle = \langle\bar{a}|J_{\mu}^{Y}|\bar{a}\rangle = -\langle a|J_{\mu}^{Y}|a\rangle.$$

Consequently, for a particle that is identical to its antiparticle, it follows that

$$\langle a|J_{\mu}^{Y}|a\rangle = 0;$$

that is, self-conjugate fields have no form factor.

28. M.N. Rosenbluth, Phys. Rev. 79, 615(1950).

29. This result is inconclusive, however, because under certain circumstances two-photon contributions can still give the Rosenbluth formula. Details may be found in D. Flamm and W. Kummer, Nuovo Cimento 28, 33(1963). Direct experimental measurements show that two-photon contributions are negligible below 5 $(GeV/c)^2$. See J. Mar, Phys. Rev. Lett. 21, 482(1968).

30. E. Reya and K. Schilcker, University of Mainz preprint MZ-TH74/2, 1974.

31. E. Lohrmann, in Proceedings of the Fifth International Conference on Elementary Particles, Lund, 1969, edited by G. von Dardel (Berlingska Boktryckeriet, Lund, Sweden, 1970), p. 21.)

32. V. Z. Jankus, Phys. Rev. 102, 1586(1956); M. Gourdin, Nuovo Cimento 33, 1391(1964).

33. There is also a deuteron quadrupole form factor (there are three deuteron form factors since the deuteron is spin 1). The theoretical analysis shows it is proportional to the isoscalar electric form factor, so it has been ignored in the discussion.

34. S. Galster, H. Klein, J. Moritz et al., DESY preprint 71/7, 1971.

35. T. Hamada, Nucl. Phys. 34, 382(1962); I. McGee, Phys. Rev. 151, 772 (1966); H. Feshbach and E. Lomon, Rev. Mod. Phys. 36, 611(1967).

36. F. Gross, Phys. Rev. 155, 1607(1967), and references mentioned therein.

37. D. Harrington, Phys. Rev. 133, 142(1964); R.J. Adler and S.D. Drell, Phys. Rev. Lett. 13, 249(1964); R.J. Adler, Phys. Rev. 141, 1499 (1966); Y. Fugi and M. Kawaguchi, Prog. Theor. Phys. 26, 519(1971).

38. L. Durand, Phys. Rev. 115, 1020(1959); I.J. McGee, Phys. Rev. 158, 1500(1967); D. Braess, Z. Phys. 198, 527(1967).

39. R. Wilson, in XV International Conference on High Energy Physics, edited by V. Shelest (Naukova Dumka, Kiev, U.S.S.R., 1972), p. 85.

40. W. Bartel, F.W. Busser, W.R. Dix et al., DESY preprint 73/5, 1973.

41. C.N. Brown, C.R. Canizares, W.E. Cooper et al., Phys. Rev. Lett. 26, 991(1971).

42. C. Akerlof, W.W. Ash, K. Berkleman et al., Phys. Rev. 163, 1482(1967).

43. C. Mistretta, J.A. Appel, R.J. Budnitz et al., Phys. Rev. 184, 1487(1969).

44. C.J. Bebek, C.N. Brown, M. Herzlinger et al., Phys. Rev. D9, 1229 (1974); C.J. Bebek, C.N. Brown, M. Herzlinger et al., Harvard University preprint, 1975.

45. N. Zagury, Phys. Rev. 145, 1112(1966); B. DeTollis and F. Nicob, Nuovo Cimento 48A, 281(1967); S.L. Adler, Ann. Phys. (N.Y.) 50, 189(1968); G. Von Gehlen and M.G. Schmidt, Nucl. Phys. B20, 102 (1970); F.A. Berends, Phys. Rev. D1, 2590(1970).

46. B.H. Kellet and C. Verzegnassi, Nuovo Cimento A13, 185(1973).

47. N. Dombey and B.J. Read, Nucl. Phys. B60, 65(1973).

48. A. Bartland and W. Majerotto, Nucl. Phys. B90, 285(1975).

49. R.E. Mickens and J.E. Rush, Phys. Rev. D3, 784(1971).

50. T.T. Wu and C.N. Yang, Phys. Rev. 137B, 708(1965); T.T. Chou and C.N. Yang, Phys. Rev. 170, 1591(1968).

51. For further studies along this line see G. Mack, Phys. Rev. 154, 1617(1967); M. Greco, Phys. Lett. B27, 578(1968); M. Kac, Nucl. Phys. B62, 402(1973).

52. Attempts to explain the dipole behaviour include: J.S. Ball and F. Zachariasen, Phys. Rev. 170, 1541(1968); M. Ciagaloni and P. Menotti, Phys. Rev. 173, 1575(1968); D. Amati, L. Caneschi and R. Jengo, Nuovo Cimento 58, 783(1968); D. Amati, R. Jengo, H.R. Rubinstein et al., Phys. Lett. B27, 38(1968);A.O. Barut, D. Corrigan and H. Kleinert, Phys. Rev. Lett. 20, 167(1968);Y. Shimizu, Phys. Rev. D6, 188(1972); P. Yodzis, Phys. Rev. D6, 929(1972); C.L. Hammer and T.A. Weber, Phys. Rev. Lett. 28, 1675(1972); M. Blagojevic and D. Lalovic, Prog. Theor. Phys. 51, 1152(1974).

53. I. Bars and K. Lane, Phys. Rev. D8, 1169(1973); I. Bars, M.B. Halpern and K.D. Lane, Nucl. Phys. B65, 518(1973).

54. W. Bartel, Phys. Lett. B33, 245(1970); C. Berger, V. Burkert, G. Knop et al., Phys. Lett. B35, 87(1971); L.E. Price, J.R. Dunning, M. Goitein et al., Phys. Rev. D4, 45(1971).

55. D.R. Botterill, D.W. Braben, A. Del Guerra et al., DESY preprint DNPL/P162, 1973.

56. K. J. Barnes, P. Carruthers and F. von Hippel, Phys. Rev. Lett. 14, 82(1965); S. Fenster and Y. Nambu, Prog. Theor. Phys. Supplement,

250(1965); S. Ishida, J. Otokozawa and H. Shimodaira, Prog. Theor. Phys. 34, 1000(1965); I.T. Drummond, Phys. Rev. 168, 1550 (1968). SU(6) also predicts that

$$1+\mu_p/\mu_n = -3/2,$$

which is well-satisfied. See G. Morpurgo, Physics 2, 95(1965).

57. D. Drickey and L.N. Hand, Phys. Rev. Lett. 9, 521(1962).

58. C.R. Schumaker and H.A. Bethe, Cornell University preprint CLNS-180(1972).

59. As a consequence of this standard quark models of the nucleon are claimed to be ruled out. Quark models which are constructed to match the initial slope of the neutron electric form factor have to include a complicated $q\bar{q}$ structure or exhibit unexpected symmetry states. This upsets the spectrum of known excited states or robs the model of simplicity. See P.M. Fishbane, J.S. McCarthy, J.V. Noble and J.S. Trefil, "Quark-Parton Models and the Neutron Charge Radius", State University of New York, Stony Brook, 1974.

60. R. Budnitz, J. Appel, L. Carroll et al., Phys. Rev. 19, 809(1967).

61. There have been several theoretical studies of the breakdown of the scaling law. See, for example, G. Morpurgo, Phys. Lett. B27, 378 (1968); T. Narita, Prog. Theor. Phys. 42, 1336(1969); V. Singh, Phys. Rev. Lett. 28, 859(1972); C.R. Schumacher and I.M. Engle, Argonne Preprint, ANL/HEP 7023, 1972.

62. T. Massam and A. Zichichi, Nuovo Cimento Lett. 1, 387(1969); P.N. Kirk, M. Breidenbach and J.I. Friedman et al., Phys. Rev. D8, 63(1973).

63. H. Pilkuhn, W. Schmidt, A.D. Martin et al., Nucl. Phys. B65, 460(1973).

64. C.L. Hammer and T.A. Weber, Phys. Rev. D5, 3069(1972); C.L. Hammer and T.A. Weber, Phys. Rev. Lett. 28, 1675(1972).

65. E. Clementel and C. Villi, Nuovo Cimento 4, 1207(1956).

66. C.L. Hammer, T.A. Weber and V.S. Zidell, Phys. Rev. D9, 158(1974).

67. The electromagnetic radii can always be defined in this way independent of the theoretical analysis given in Appendix A. But the procedure is ambiguous because no recipe for deciding which form factors (the Pauli and Dirac, or the electric and magnetic) to use to define the radii is given.

68. J.B. Filho and R.F. Meyer, DESY preprint 73/8, 1973.

69. F. Borkowski, P. Peuser, G.G. Simon et al., Nucl. Phys. A222, 269(1974).

70. T.D. Lee and G.C. Wick, Nucl. Phys. B9, 209(1969).

71. M.S. Chanowitz and S.D. Drell, Phys. Rev. Lett. 30, 807(1973).

72. J.G. Cordes and P.J. O'Donnell, Phys. Rev. 185, 1858(1969).

73. J.G. Cordes and P.J. O'Donnell, Phys. Rev. Lett. 20, 1462(1968).

74. N. Zovko, Acta Phys. Austriaca 36, 354(1972).

75. R. Felst, DESY preprint 73/56, 1973.

76. S.I. Bilenkaya, S.M. Bilenkii, Y.M. Kazarinov and L.I. Lapidus, JETP Lett. 19, 317(1974).

77. M. Bohm, Acta Phys. Austriaca 38, 123(1973).

78. G. Veneziano, Nuovo Cimento 57A, 190(1966).

79. G.J. Gounaris, Nucl. Phys. B68, 574(1974).

80. M.M. Islam and J. Rosen, Phys. Rev. 178, 2135(1969); M.M. Islam and K.V. Vasavada, Phys. Rev. 178, 2140(1969).

81. V. Barger and R.J.N. Phillips, Phys. Rev. 187, 2210(1969).

82. S.K. Bose, Nuovo Cimento A46, 419(1966).

83. B.A. Loiseau and B. Nicolescu, Nuovo Cimento Lett. 1, 1031(1971).

84. M. Davier , in Proceedings of the XVI International Conference on High Energy Physics, edited by J.D. Jackson and A. Roberts (National Accelerator Laboratory, Batavia, Illinois, 1972), p.104.

85. G. Barbarino, M. Grilli, E. Iarocci et al., Nuovo Cimento Lett. 3, 689(1972); C. Bacci, G. Penso, G. Salvini et al., Phys. Lett. B38, 551(1972).

86. H. Alvensleben, V. J. Becker, W.K. Bertram et al., Phys. Rev. Lett. 26, 273(1971).

87. In addition to experiments reporting positive results, there are experiments looking for resonances in the dipion system that report no find. See G. McClellan, N. Mistry, P. Mostek et al., Phys. Rev. Lett. 23, 718(1969).

88. J.E. Augustin, A.M. Boyarski, M. Breidenbach et al., Phys. Rev. Lett. 33, 1406(1974); G.S. Abrams, D. Briggs, W. Chinowsky et al., Phys. Rev. Lett. 33, 1453(1974).

89. J.J. Aubert, V. Becker, P.J. Biggs et al., Phys. Rev. Lett. 33, 1404(1974).

90. A.M. Boyarski, M. Breidenbach, F. Bulos et al., Phys. Rev. Lett. 34, 762(1975).

91. J.E. Augustin, A.M. Boyarski, M. Breidenbach et al., Phys. Rev. Lett. 34, 764(1975).

92. S. Borchardt, V.S. Mather and S. Okubo, Phys. Rev. Lett. 34, 38(1975); S. Okubo, V.S. Mather and S. Borchardt, Phys. Rev. Lett. 34, 236(1975).

93. A.S. Goldhaber and M. Goldhaber, Phys. Rev. Lett. 34, 36(1975).

94. J. Schwinger, Phys. Rev. Lett. 34, 37(1975).

95. M.K. Banerjee and C.A. Levinson, Phys. Rev. 176, 2140(1968).

96. B.H. Kellet and C. Verzegnassi, Nuovo Cimento A13, 185(1973).

97. B.H. Kellet and C. Verzegnassi, Nuovo Cimento A20, 194(1974).

98. G.T. Adylov, F.K. Aliev, D. YuBardin, et al., Phys. Lett. B51, 402(1974).

99. The data from this experiment has been reanalyzed using a different parametrization of the pion form factor to give

$$\langle r^2 \rangle_\pi^{\frac{1}{2}} = 0.71 \pm 0.05 \text{ f.},$$

more in agreement with standard vector meson dominance models. See S. Dubnicka and O.V. Dumbrajs, Phys. Lett. B53, 285(1974).

100. M. Conversi, T. Massam, TH. Mullier, et al., Nuovo Cimento A40, 690(1965); D.L. Hartill, B.C. Barish, D.G. Fong et al., Phys. Rev. 184, 1415(1969); M. Castellano, G. diGiugno, J.W. Humphrey et al., Nuovo Cimento A14, 1(1973).

101. A. Bietti and S. Petrarca, Nuovo Cimento A22, 595(1974).

102. M. Bernadini, F. Rimond, A. Zichichi et al., Phys. Lett. B46, 261(1973).

103. Y. Lepetre and F.M. Renard, CNRS preprint, PM/72/4, 1972.

104. J. LeFrancois, in Proceedings of the 1971 International Symposium on Electron and Photon Interactions at High Energies, edited by N.B. Mistry (Cornell University, New York, 1972), p.52; V.A. Sidorov, in Proceedings of the 1971 International Symposium on Electron and Photon Interactions at High Energies, edited by N.B. Mistry (Cornell University, New York, 1972), p. 65.

105. S.F. Berezhnev, Sov. J. Nucl. Phys. 16, 99(1973).

106. M. Bernadini, F. Rimondi, A. Zichichi et al., Phys. Lett. B44, 393(1973); R. Wilson, in Proceedings of the 1971 International Symposium on Electron and Photon Interactions at High Energies, edited by N.B. Mistry (Cornell University, New York, 1972), p. 97.

107. V.E. Balakin, G.I. Bodker, V.A. Sidorov et al., Phys. Lett. B41, 205(1972).

108. J.E. Augustin, D. Benaksas, J. Buon et al., Nuovo Cimento Lett. 2, 214(1969). The accuracy of this data has been questioned by D. Benaksas, G. Cosme, J.P. Repellin et al., Phys. Lett. B39, 289(1972).

109. G.J. Gounaris and J.J. Sakurai, Phys. Rev. Lett. 21, 244(1968).

110. F.M. Renard, Phys. Lett. B47, 361(1973).

111. G. Bonneau and F. Martin, Nuovo Cimento A13, 413(1973).

112. B.B. Deo and M.K. Parida, Phys. Rev. D9, 2068(1974).

113. Some of the other models of the pion form factor include: Y. Oyanagi, Prog. Theor. Phys. 42, 898(1969); H. Surra, Phys. Rev. Lett. 23, 551(1969); R. Jengo and E. Remiddi, Nucl. Phys. B15, 1(1970); W.S. Lam, Nucl. Phys. B17, 237(1970); S.J. Brodsky and G.R. Farrar, Phys. Rev. Lett. 31, 1153(1973); F.M. Renard, CNRS preprint PM/73/3, 1973; M. Bohm and M. Krammer, Phys. Lett. B50, 457(1974); F. Gutbrod and U. Weiss, Nucl. Phys. B90, 52(1975).

114. Theoretical studies of ρ-ω mixing have been made by R.G. Sachs and J.F. Willemsen, Phys. Rev. D2, 133(1970); A. Burnell, Nucl. Phys. B25, 471(1971).

115. The errors on these and other parameters discussed in this section are determined only for variable parameters if enough runs were made to make a reasonable estimate.

116. J. LeFrancois, in Proceedings of the 1971 International Symposium on Electron and Photon Interactions at High Energies, edited by N.B. Mistry (Cornell University, New York, 1972), p.52.

117. P.J. Biggs, R.W. Clift, E. Gabathuler et al., Phys. Rev. Lett. 24, 1201(1970).

118. G. Goldhaber, B.H. Hall, G.H. Trilling, et al., Phys. Rev. Lett. 23, 1351(1969).

119. L.F. Urrutia, Phys. Rev. D9, 3213(1974).

120. N. Zovko, Phys. Lett. B51, 54(1974).

121. F. Ceradini, M. Conversi, L. Paoluzi et al., Phys. Lett. B43, 341(1973).

122. A. Bramon and M. Greco, Nuovo Cimento Lett. 1, 739(1971).

123. G. Smadja, H.H. Bingham, W.B. Fretter et al., in Experimental Meson Spectroscopy-1972, edited by A.H. Rosenfeld and K.W. Lai (American Institute of Physics, New York, 1972), p. 349.

124. W.B. Kaufmann and R.J. Jacob, Phys. Rev. D10, 1051(1974).

125. K. Fujikawa and P.J. O'Donnell, DAMTP preprint 73/17, 1973.

126. D.N. Levin and S. Okubo, Phys. Rev. D6, 3149(1972).

127. P. Estabrooks, A.D. Martin, G. Grayer, et al., in π-π Scattering-1973, edited by P.K. Williams and V. Hagopian (American Institute of Physics, New York, 1973), p. 37.

128. S.D. Protopopescu, M. Alston-Garnjost, A. Babaro-Galtieri, et al., in Experimental Meson Spectroscopy-1972, edited by A.H. Rosenfeld and K.W. Lai (American Institute of Physics, New York, 1972), p. 17.

129. T. Dass, Phys. Rev. Lett. 21, 242(1968); K. Fujikawa, DAMTP preprint 73/11, 1973.

130. T. Suzuki and H. Senju, Prog. Theor. Phys. 45, 1185(1971); J. Leite Lopes, Nucl. Phys. B38, 555(1972).

131. C.J. Isham, A. Salam and J. Strathdee, Trieste preprint, IC/70/108, 1970.

132. I. Bars, M.B. Halpern and M. Yoshimura, Phys. Rev. D7, 1233(1973).

133. In many cases, the absolute normalization of a set of form factor measurements may be in error. This is a correlated error applying to a whole data set. For any given q^2, several sets of data may be used originating from different labs with different normalization errors. To account for this, normalization parameters, λ_n, are introduced into the χ^2 as follows:

$$\chi^2 = \sum_{q^2}\sum_{n}\left[\frac{\lambda_n G_n(q^2) - G_{n,exp}(q^2)}{\sigma_n(q^2)}\right]^2 + \sum_{n}\left[\frac{\lambda_n - 1}{\Delta_n}\right]^2$$

where Δ_n is the experimental normalization error of the nth data set.

134. B.L. Young and K.E. Lassila, Ames Laboratory preprint, "Photoproduction of J(ψ) Particles and Predictions for Proton Compton Scattering", 1975.

135. M. Chretien and R.E. Pierls, Proc. R. Soc. A223, 468(1954); E. Arnous and W. Heitler, Nuovo Cimento 11, 443(1959); E. Arnous, W. Heitler and Y. Takahashi, Nuovo Cimento 16, 671(1960); L. O'Raifeartaigh and Y. Takahashi, Helv. Phys. Acta 34, 554(1960).

136. Recently, A. Chodos, R.L. Jaffe, K. Johnson, C.B. Thorn and V.F. Weisskopf, Phys. Rev. D9, 3471(1975), have constructed an extended model of hadrons in which the strongly interacting particle is imagined to consist of quark or parton fields confined to a finite region of space in a Lorentz-invariant way. The model apparently is not solvable in three dimensions.

137. Generically, virtual particles arise simply from the attempt to give every Feynman diagram a physical meaning in terms of the exchange of "particles". See the article by M. Bunge, Int. J. Theor. Phys. 3, 507(1970).

138. See, for example, R.C. Barrett, Rep. Prog. Phys. 37, 1(1974).

139. F.J. Ernst, R.G. Sachs and K.C. Wali, Phys. Rev. 119, 1105(1960); R.G. Sachs, Phys. Rev. 126, 1256(1962).

140. See also the comments by G. Breit, in XII International Conference on High Energy Physics, edited by Y.A. Smorodinsky (Atomizdat, Moscow, 1966), p. 985.

141. K.J. Barnes, Phys. Lett. 1, 166(1962).

142. D. Amati, R. Jengo, H.R. Rubinstein, et al., Phys. Lett. B27, 38(1968).

143. A. Martin, Nuovo Cimento 37, 671(1965); A.M. Jaffe, Phys. Rev. Lett. 17, 661(1966); J.D. Stack, Phys. Rev. 164, 1904(1967); J. Harte, Phys. Rev. 165, 1557(1969); F.E. Close, Nucl. Phys. B71, 217(1974).

144. M. Gell-Mann and F. Zachariasen, Phys. Rev. 124, 953(1961).

145. J.J. Sakurai, Phys. Rev. Lett. 9, 472(1962).

146. T. Laankan, S. Oneda and S. Matsuda, University of Maryland preprint, 73-147, 1973.

147. J.J. Sakurai, Phys. Rev. Lett. 17, 1021(1966).

148. See the discussion of the Marquardt algorithm in P.R. Bevington, Data Reduction and Error Analysis for the Physical Sciences (McGraw-Hill, New York, 1969), p. 235.

149. V.E. Krohn and G.R. Ringo, Phys. Rev. 148, 1303(1966).

150. E. Melkonian, B.M. Rustad and W. Wittavens, Phys. Rev. 114, 1571 (1959).

151. D.J. Hughes, J.A. Harvey, M.D. Goldberg and M.J. Stafne, Phys. Rev. 90, 497(1953).

152. J.J. Murphy, Y.M. Shin and D.M. Skopik, Phys. Rev. C9, 2125(1974).

153. J. Ballam, G.B. Chadwick, Y. Eisenberg et al., Nucl. Phys. B76, 375(1974).

154. C. Bacci, G. Penso, G. Salvini et al., Phys. Lett. B38, 551(1972).

155. M. Conversi, L. Paoluzi, F. Ceradini et al., Phys. Lett. B52, 493(1974).

156. P. Frenkiel, Nucl. Phys. B47, 61(1972).

157. H. Alvensleben, U.J. Becker and W.K. Bertram et al., Phys. Rev. Lett. 26, 273(1971).

158. H.H. Bingham, W.B. Fretter, W.J. Podolsky et al, SLAC preprint, SLAC-PUB-1113, 1972.

159. M. Davier, SLAC preprint, SLAC-PUB-666(1969).

160. G. Barbarino, M. Grilli, E. Iarocci et al., Nuovo Cimento Lett., 3, 689(1972).

161. M. Davier, SLAC preprint, 1971.

162. A. Benvenuti, D. Cline, R. Rutz et al., Phys. Rev. Lett. 27, 283(1971).

163. A. DelGuerra, C. Verzegnassi, B.H. Kellet et al., Phys. Lett. B50, 487(1974).

164. C.F. Cho and J.J. Sakurai, Nuovo Cimento Lett. 2, 7(1971).

165. G. Hohler and E. Pietarinen, Phys. Lett. B53, 471(1975).

166. H. Foeth, M. Holder, E. Radermacher et al., Phys. Lett. B30, 276(1969).